HYBRID MAGNETIC POLYMERIC NANOPARTICLES FOR THE ENVIRONMENTAL REMEDIATION OF CRUDE OIL AND PERFLUOROOCTANOIC ACID FROM AQUEOUS SYSTEMS

A Dissertation

by

ADRIANA PAVIA SANDERS

Submitted to the Office of Graduate and Professional Studies of
Texas A&M University
in partial fulfillment of the requirements for the degree of

DOCTOR OF PHILOSOPHY

Chair of Committee,	Karen L. Wooley
Committee Members,	Daniel A. Singleton
	Lei Fang
	Jodie L. Lutkenhaus
Head of Department,	François P. Gabbaï

December 2015

Major Subject: Chemistry

ABSTRACT

Environmental remediation of pollutants from water systems is an expanding billion dollar industry. Recently, engineered nanoparticles (ENPs) have been of particular interest to this field as they hold promise in improving existing remediation technologies. Hybrid well-defined magnetic shell crosslinked knedel-like (MSCK) nanoparticles comprised of iron oxide nanoparticles encapsulated in amphiphilic block copolymer micellar assemblies and selectively crosslinked throughout the hydrophilic shell domain of the assembly have been investigated for their pollutant uptake capabilities. The main focus of this dissertation is to design, develop, and investigate tailored MSCK nanoparticle systems for specific environmental pollutants and applications.

Alterations of the polymeric components of the nanoparticle systems allow for the development of fine-tuned materials by providing control over the composition, shape, and size of the nanoparticles produced. The polymeric components utilized for the co-assemblies of the MSCK systems presented here were produced through two types of controlled living radical polymerizations, atom transfer radical polymerization (ATRP) and reversible addition-fragmentation chain-transfer (RAFT) polymerization. The non-covalent incorporation of iron oxide nanoparticles into the cores of the systems was performed in order to afford magnetically active materials that can be controlled and/or recovered after deployment through the use of an external magnetic field. In order to achieve a high magnetic response, the co-assemblies of these systems were

achieved with equal mass feed ratios of the polymers and iron oxide nanoparticles during the micellization process. MSCKs designed for their utilization following the bulk recovery stage at oil spill sites to recover oil at low concentrations, or sheen, were composed of poly(acrylic acid)$_{20}$-*b*-polystyrene$_{280}$ (PAA$_{20}$-*b*-PS$_{280}$) and demonstrated superb sheen recovery of ten-fold by weight. Fluorinated MSCK (MSCK-F$_9$) nanoparticles were also investigated for the remediation of perfluorooctanoic acid (PFAO) from water. A library of four fluorinated systems was developed in order to probe the effect size/fluorine content and shell charge would have on the recovery efficiency of these materials. A fluorinated monomer was incorporated into the polymer during polymerization in order to increase the solvation of PFOA within the core during loading. The results of this dissertation suggest that MSCKs are a viable option and ENPs for environmental remediation.

DEDICATION

To my mother, Alejandra Jiménez Lastra, my father, Jose Alfonso Frias, and my husband, Jonathan Sanders

ACKNOWLEDGEMENTS

I would first like to thank my advisor, Professor Karen L. Wooley, for all of her support, advice, and care for the last five years. She has not only been a great mentor, but a great role model and example for what a strong woman in the sciences can truly accomplish. I would also like to thank my committee members Dr. Daniel A. Singleton, Dr. Lei Fang, and Dr. Jodie L, Lutkenhaus for their invaluable time and advice.

I would like to extend a heartfelt gratitude to the Wooley Team. In particular to my great friend and colleague, Jennifer S. Zigmond, for motivating me and pushing me to succeed when even I did not think I could. I would also like to thank Jeniree A. Flores for her aid and critical advice. Although she only spent a short year with us, a special thanks is needed for a great undergraduate researcher, Sarah M. Ward, for all of her time and effort in the development of a new hybrid magnetic system. I would also like to thank Dr. Ashlee A. Jahnke and Joel D. Russell for all of their help in lab, and their help outside of lab in helping me keep my sanity. Dr. Guorong “da shu” Sun has also been a great friend and constant source of inspiration; thank you for all that you have done for me. A lot of my personal and professional development is owed to several previous Wooley lab members, in particular Dr. Solène Caüet Fidge, Dr. Shiyi Zhang, Dr. Jiong Zou, Dr, Tiffany P. Gustafson, and Dr. Jeffery E. Raymond. I know that the friendships I developed during my time here will last a life-time, and for that I am forever glad for the experiences and opportunity to have worked with a group of amazing scientists.

Although he is no longer with us, my passion for chemistry and my coming to graduate school to pursue my doctorate degree would not have been possible without my undergraduate mentor, Dr .J. D. Lewis. He was my motivation, my guide, my Papa Bear, and he is greatly missed. I will be forever in his debt for his advice and love.

Last, but not least, I would like to thank my family for all of their love and support. My parents, Alejandra Jiménez Lastra and Jose Alfonso Frias, are the best parents I could have ever asked for, and I am eternally thankful for all of the opportunities they have provided for me. My siblings, Andrea Pavia Jiménez, Marco Frias, and Daniel O'Dwyer have been instrumental in my growth. Los amo, feos! Finally, my husband, Jonathan E. Sanders has been my rock, collaborator, colleague, and best friend; thank you for all of your patience and love.

NOMENCLATURE

ACHN	azobis(cyclohexanenitrile)
AFM	Atomic force microscopy
ATRP	Atom transfer radical polymerization
CNT	Carbon nanotube
CuBr	Cuprous bromide
DCM	Dichloromethane
DI	Deionized
DLS	Dynamic light scattering
DMF	*N, N*-dimethylformamide
DSC	Dynamic scanning calorimetry
EDCI	1-(3-(dimethylamino)propyl)-3-ethyl-carbodiimide methiodide
EDDA	2,2'-(ethylenedioxy)bis(ethylamine)
ENHP	N-ethylpiperidine hypophosphite
ENP	Engineered nanoparticle
FPT	Freeze-pump-thaw
GC-MS	Gas chromatography-mass spectrometry
GPC	Gel permeation chromatography
IR	Infrared
MSCK	Magnetic shell crosslinked knedel-like
MSCK-F9	Fluorinated magnetic shell crosslinked knedel-like

MW	Molecular weight
MWCO	Molecular weight cutoff
PAA	Poly(acrylic acid)
PAEA	Poly(acrylamideoethylamine)
PDI	Polydispersity index
PFOA	Perfluorooctanoic acid
PFS	2,3,4,5,6-pentafluorostyrene
PMDETA	*N, N, N′, N′, N″* pentamethyldiethylenetriamine
PS	Polystyrene
PtBA	Poly(*tert*-butyl acylate)
RAFT	Reversible addition-fragmentation chain-transfer
RI	Refractive index
TEM	Transmission electrom microscopy
TFA	Trifluoroacetic acid
TFS-F9	1,2,4,5-tetrafluoro-3-((3,3,4,4,5,5,6,6,6-nonafluorohexyl)oxy)-6-vinylbenzene
TGA	Thermogravimetric analysis
THF	Tetrahydrofuran
TLC	Thin layer chromatography
USEPA	United States Environmental Protection Agency

TABLE OF CONTENTS

Page

LIST OF FIGURES

LIST OF SCHEMES

LIST OF TABLES

CHAPTER I

INTRODUCTION AND LITERATURE REVIEW

1.1 Nanotechnology and Nanoremediation

Nanotechnology encompasses the design, characterization, production, and application of structures with dimensions of less than 100 nm. The concept of nanotechnology was first introduced to the world in 1959 by physicist Richard Feynman through the lecture *There's Plenty of Room at the Bottom*.[1] However, it was almost another two decades before nanotechnology truly emerged through the invention of the scanning tunneling microscope, the discovery of fullerenes,[2] and K. Eric Drexler's *Engines of Creating: The Coming Era of Nanotechnology*.[3] Since these fundamental steps, the development and application of nanotechnologies has expanded into medicine, materials, and electronics, among other emerging fields.

In the past 15 years, the field of nanoremediation has emerged as a means to employ nanotechnology for the purpose of environmental remediation. Engineered nanoparticles (ENPs) have been of particular interest in the field of nanoremediation due to their colloidal properties, size, and surface area to volume ratios. ENPs are typically classified into three categories: polymeric/micelle, carbon-based, and metal/metal oxide nanoparticles. The vast majority of research in this field has been performed in testing nanoscale zerovalent iron (nZVI),[4-6] bimetallic particles[7,8], colloidal activated carbon,[9] and other carbon-based materials.[10-14] Of the materials mentioned, primary focus has been given to nZVI due to its potential use for both pump-and-treat and for permeable

reactive barriers. However, the mobility of these nanoparticles in aqueous and groundwater systems is limited due to their quick agglomeration thus requiring the aid surface modification and coatings.[15-17]

Carbon based materials such as fullerenes and nanotubes have also been investigated for their use in nanoremediation because of their shape, size, surface area, sorption properties, molecular interactions, *etc*.[11] Owing in great part to their large surface area, carbon nanotubes (CNTs) have been proposed as hydrophobic pollutant sorbents in the field of nanoremediation. Sun *et al*. fabricated *p*-phenylenediamine modified CNTs for the removal of hydrophobic pollutants from water.[13] These nanotubes were capable of sorbing almost 120× by weight pump oil from water. CNTs have also shown great promise for the removal of toxic chemicals, notably, Luo and co-workers demonstrated the successful capture of mercury through the use of a CNT-silver composite.[18] Additionally, nanoscale-C_{60} has also shown promise as a remediation tool for hydrophobic materials such as naphthalene and 1,2-dichlorobenzene. However, more specialized materials have been developed in the past few years with specific contaminant remediation in mind.

1.2 Oil Spill Remediation

There exists a wide range of materials that is commonly used for oil spill remediation. These include booms, skimmers, dispersants, absorbents and solidifiers.[19] Of particular interest are absorbent materials, as these give promise of complete removal of the pollutant with relatively low waste production. Commonly used polymeric

materials at oil spill sites are comprised of polypropylene; these polymer fibers have shown superior absorbing capabilities over other natural and synthetic fibers with an absorbing ratio of 1:4 by mass.[20] Some issues with these polymer fibers extend from the difficulty in their recovery; to compensate for this, these materials are often entrapped within netting prior to deployment. This issue is common among many of the absorbent materials currently in use.[21]

In recent years, much interest in nanotechnology for sheen removal has led to the development of various materials for this application including fabrics,[22,23] sponges,[24-26] fibers,[27] gels,[28] nanoparticles,[29-32] and nanowires,[33] among other materials.[34] A notable example of a sponge is Chen *et al*.'s ultralight magnetic foam which is capable of removing over 100 times its weight in oil pollutants (ca. 90× of crude oil). Additionally, the incorporation of a magnetic component allowed for these foams to be magnetically driven over the surface of the water.[24] Other hybrid materials containing carbon nanotubes have also been explored for this environmental application.[35,36] Gui and coworkers developed a magnetic carbon nanotube sponge with a maximum loading capacity of over 50× when tested against different types of oils.[36]

On the other hand, amphiphilic systems allow for a broader application of the material for recovery and loading. However, they suffer the drawback of lower loading capabilities when compared to larger materials such as those previously mentioned. Li and co-workers developed a library of hybrid mesoporous materials and tested their loading capabilities against 4-heptylphenol; the material labeled 4C20@1Z10 demonstrated a maximum loading of 49 mg of the organic compound per g of material

used (ca. 0.05× by weight).[37] Another example is that of Nayab *et al*.'s polyethyleneimine-coated mesoporous silica which was tested for its loading of anionic dyes; these particles were able to load Alizarin red S at 2× their weight. However, this loading is hypothesized to have been aided by the electrostatic interactions between the positively charged particle shell and the negatively charged dye.[38] Furthermore, magnetically active amphiphilic systems have also been investigated; Huang and co-workers developed magnetic permanently confined micelle arrays (Mag-PCMAs) and tested them against various contaminants. Although the extent of loading was not fully explored, they were able to achieve a loading of 0.5 mg/mg (0.5× by weight) of atenolol as the maximum loading reported.[39]

1.3 PFOA Remediation

Perfluorooctanoic acid (PFOA) is a man-made pollutant that has permeated our global environment through its release as a byproduct from fluorochemical facilities.[40] This contaminant's high water solubility, 9.5 g/L, and moderate sorption to solids present a particular threat to aqueous systems. PFOA is found in blood samples of the general population, and although its effects are still not fully understood, it has been linked to developmental defects and diseases,[41,42] and other health issues.[43] PFOA's low bio-degradability and moderate sorption to solids has led to its presence in human-desolate areas and has shown to have negative effects on animal species, including polar bears, sea otters, fish-eating birds, *etc*.[44-47] Additionally, PFOA has been found in groundwater, wastewater, and drinking water throughout the Unites States.[48-50] In 2006,

the United States Environmental Protection Agency (US EPA) began its PFOA Stewardship Program with the reduction of PFOA emissions as an immediate objective, and the phasing-out of this toxic chemical by the end of 2015.[51]

PFOA, like many other polyfluorinated compounds (PFCs), does not hydrolyze photolyze, or biodegrade under typical environmental conditions and has a half-life in water of over 92 years.[52] The unique properties of PFOA allow it to resist conventional *in situ* remediation techniques such as oxidation, nano-filtration, and reverse osmosis among others and render them ineffective; this has limited its treatment to *ex situ* methods,[40] with incineration as the primary method for complete removal.[53]

Recent advances for the removal or decomposition of PFOA include the use of activated carbon fil-ters,[54],[55] nanofiltration,[23] photochemical decomposi-tion,[56-59] and adsorption.[60] As a notable example, Giri and coworkers demonstrated the full decomposition (*ca*. 1.78 E-3 mg) of PFOA using low-pressure UV lamps and potassium iodide in a 3 h period.[56]. However, this technique is restricted to surface and contained water due to the penetration limits of UV light, and additional issues may be encountered from the production of smaller-chained perfluorinated byproducts whose transport and other environmental effects are not well-known. The adsorption of perfluorinated pollutants, including PFOA, has also been of particular interest due to the technique's efficiency.[61] For example, work by Nassi *et al*. testing different mesoporous silica materials showed significant PFOA adsorption. Of the materials tested, solvent extracted hexagonal mesoporous silica (HMSe) demonstrated the highest PFOA adsorption (almost 6.2 E 3 mg of PFOA mg per mg of HMSe) across a pH range of 5-

9.[60] An intricately designed polymeric system for PFOA removal is that of Koda *et al*.'s fluorous microgel star polymers. This crosslinked system is comprised of a fluorinated core for enhanced solubility and stabilization of the perfluorinated pollutant and has shown to selectively separate perfluorinated pollutants from aqueous systems. However, this system is limited by its maximum uptake capabilities, which was determined to be *ca*. 4 E-3 mg/mg.[62]

1.4 Controlled Radical Polymerizations

Uncontrolled radical polymerizations result in ill-defined polymer products that suffer from poor homogeneity due to chain transfer reactions and unwanted chain termination. Living radical polymerization techniques such as ATPR and RAFT have attracted attention due to their tolerance for different functional groups and control over the polymer architecture. ATRP is a form of controlled radical polymerization first introduced independently by Sawamoto *et al.*[63] and Matyjaszewski *et al.*[64] in 1995. ATRP relies on transition metal mediation of a halogen atom transfer through redox chemistry. In this polymerization technique, a transition metal complex (Mt^n-L) is utilized to generate an organic radical originating from an alkyl halogen bond in the dormant initiator species (R-X). The organic radical species formed after this cleavage (R^*) propagates by reacting with a monomeric unit prior to reversible termination. The dormant halogen-capped species is vastly preferred in this equilibrium, and thus side reactions from radical species are minimized. A representative scheme of this equilibrium is shown in scheme 1.1. Copper-based ATRP is the most widely researched

type of this polymerization technique due to the low cost of the copper catalyst and the commercial availability of the initiators and ligands.[65] Additional advances on ATRP as a polymerization technique include electrochemically mediated ATRP (eATRP),[66] metal-free photoinduced ATRP,[67] initiators for continuous activator regeneration (ICAR) ATRP,[68] and activators regenerated by electron-transfer (ARGET) ATRP,[69,70]

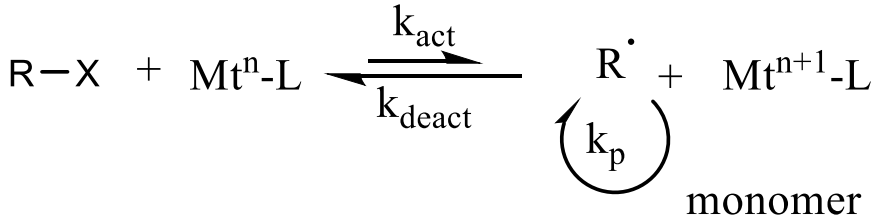

Scheme 1.1. ATRP equilibrium between dormant and active species.

Unlike ATRP, RAFT polymerization is dependent on chain transfer processes in order to establish an equilibrium between dormant and active species. The first reports of RAFT chemistry can be traced back to the early 1970s,[71,72] with its introduction into polymer chemistry beginning less than a decade later.[73] The primary component of RAFT polymerization is the chain transfer agent (CTA) which contains trithiocarbonates, dithioesters, xanthates, *etc.* This CTA reacts with propagating radicals

to generate a macroinitiator that can then react with a monomer molecule to propagate; an additional product of this radical reaction is a non-radical species that can itself react with a radical species in order to reversibly terminate the chain. The general mechanism of RAFT is shown in scheme 1.2.

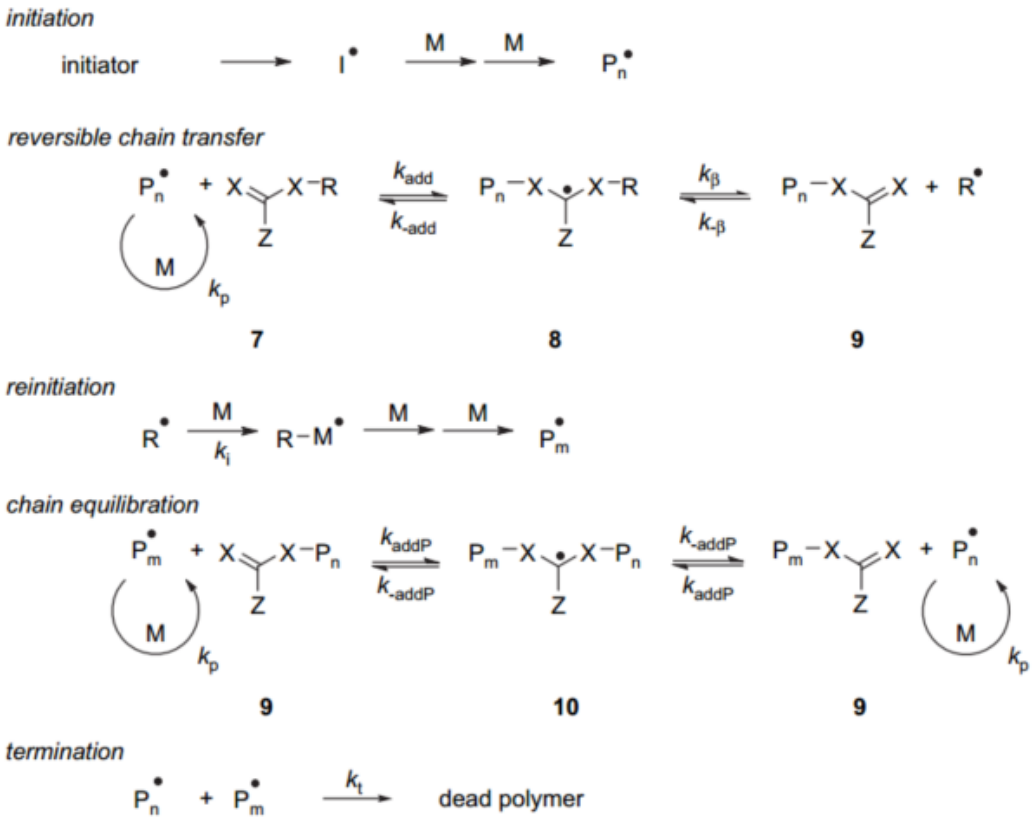

Scheme 1.2. Mechanism of RAFT Polymerization.[74]

1.5 Scope of Thesis

This dissertation is focused on the design, development, and investigation of magnetic shell crosslinked knedel-like (MSCK) nanoparticles for their application in environmental remediation. These well-defined hybrid organic-inorganic ENPs were produced through the co-assembly of hydrophobic, oleic acid stabilized iron oxide nanoparticles and amphiphilic block copolymers that were synthesized through controlled radical polymerization techniques (ATRP and RAFT). Stable vessels able to withstand infinite dilution were achieved by crosslinking selectively in the hydrophilic segment of the polymeric components. Materials tailored for specific pollutants were produced by manipulating the polymer composition through the selection of monomeric building blocks.

In Chapter II, the first generation of MSCKs was developed for the remediation of crude oil sheen at oil spill sites. Elegantly designed MSCK nanoparticles had PAA_{20}-*b*-PS_{280} as the polymeric building block for the hybrid system. The hydrophobic:hydrophilic ratio of the block copolymer was chosen as such, with a long hydrophic segment relative to the hydrophilic segment in order to achieve the desired micellar morphology. Altering the hydrophobic:hydrophilic ratio of the blocks encompassing the polymeric structure, leads to development of other morphologies such as magneto-polymersomes and magneto-core shell assemblies.[75] The magneto micelles produced contained a large number (a minimum of 75) of iron oxide nanoparticles non-covalently incorporated in the core; this number is set as a minimum due to the two-dimensional nature of transmission electron microscopy (TEM). Following the

development of a quantification method for the recovery of the crude oil, these MSCKs were evaluated for their crude oil uptake capabilities in a simulated fresh water environment. A range of initial oil:MSCK ratios were utilized in order to calculate a maximum loading capacity of 10× their initial dry weight. This superb unanticipated loading was further intensified by the finding that all fractions of this complex pollutant were removed by this simple PAA-*b*-PS hybrid system. Testing of the recyclability of this system was performed. However, it was observed that the washing procedure to unload the crude oil from the particles was altering the composition of the nanostructures.

In Chapter III, following the grad success of MSCKs for crude oil remediation, further studies on their behavior in different solvents and environments were performed. The stability and behavior of these MSCK nanoparticles in chloroform, ethanol, artificial saltwater, and saltwater were investigated through TEM, qualitative light scattering, and contact angle. MSCK nanoparticles exhibited small contact angles (less than 45°) indicating strong interactions with these solvents. Visual observation and TEM analysis showed that the sample resuspended in chloroform was actually dissolved and the MSCKs had disassociated into its organic and inorganic components. The samples resuspended in ethanol, artificial saltwater, and saltwater showed the persistence of MSCK nanoparticles. Additional oil sequestration tests were performed in artificial saltwater and saltwater environments; it was demonstrated that MSCK nanoparticles maintained their oil loading capabilities in these salty environments. Finally, the possibility of onsite production of MSCKs was also explored.

Chapter IV explores a new generation of fluorinated MSCK (MSCK-F_9) nanoparticles. A library of MSCK-F_9 nanoparticles was developed for the remediation of PFOA from aqueous environments and their deployment in PFOA-polluted D_2O was monitored. The incorporation of the fluorinated monomer 1,2,4,5-tetrafluoro-3-((3,3,4,4,5,5,6,6,6-nonafluorohexyl)oxy)-6-vinylbenzene (TFS-F9) into the core domain of these novel MSCKs was performed in order to maximize the solubility of PFOA by these nanoparticles and therefore drive this persistent, soluble pollutant out of the aqueous phase. Four nanoparticle systems comprised of PAA-*b*-P(S-*co*-TFS-F_9) and P(S-*co*-TFS-F_9)-*b*-PAEA block copolymers were explored. Kinetic studies of the removal of PFOA showed fast removal, making these particles prime candidate for use in pump-and-treat technologies for groundwater remediation. Additionally, their continued and steady long-term removal opens the possibility for use in applications such as permeable reactive barriers. Preliminary studies in bovine serum were also performed; PFOA is a toxic chemical found in the bloodstream of the general human population, and these preliminary studies aimed to test the feasibility of MSCKs for future *in vivo* use.

CHAPTER II

ROBUST MAGNETIC/POLYMER HYBRID NANOPARTICLES DESIGNED FOR CRUDE OIL ENTRAPMENT AND RECOVERY IN AQUEOUS ENVIRONMENTS*

2.1 Introduction

Petroleum and other oils are an essential part of our society and daily lives, however, they also pose contamination problems. Notably, over 20,000 oil spills are reported to the U.S. government each year.[76] Although the severity of these cases varies widely, the effects of oil spills in the environment are permeating, as demonstrated recently by the Deepwater Horizon spill in the Gulf of Mexico.[77, 78] Moreover, unwanted release of hydrocarbons during its extraction, processing and distribution contributes to additional sources requiring remediation. During the initial stages of large-scale oil spill remediation from water, standard practices of collection and containment, such as booms, skimmers and removal through suction are effective for high levels of oil present. After this initial bulk recovery stage, low oil concentration in the aqueous environment appears as sheen of 0.04 to 50 micrometers thickness on the surface of the water.[79] Sorbent materials and bioremediation are often used for the removal of this residual oil, however, these techniques are often impractical, due to cost, time, and feasibility constraints.[78, 80]

---

*Reprinted with permission from Adriana Pavía-Sanders, Shiyi Zhang, Jeniree A. Flores, Jonathan E. Sanders, Jeffery E. Raymond, and Karen L. Wooley, *ACS Nano*, **2013**, *7*, 7552-7561, Copyright 2013 American Chemical Society.

In recent years, innovative nanotechnology approaches have been developed to address oil spill remediation. For instance, much research has been performed in the development of nanomaterials for oil-water separation, from hydrogels,[81-83] sponges,[25, 84-85]nanowires,[86, 33] nanoparticles,[32, 31] among other materials.[34] Of particular interest are magnetic nanocomposites,[87] because the added magnetic component allows for recovery of the deployed nanomaterials. Predominantly, hydrophobic, magnetic materials have been studied for pollutant recovery in aqueous environments, largely due to advances in hydrophobic and superhydrophobic materials and surfaces.[88, 89] Calcagnile *et al*. have recently shown the successful removal of mineral oil from the surface of an aqueous solution by using a modified polyurethane foam, infused with iron oxide nanoparticles and functionalized with superhydrophobic polytetrafluoroethylene microparticles.[85] Similarly, highly hydrophobic hybrid nanoparticles coated with vinyl triethoxysilane have also proven to be an efficient method for oil separation and removal, as demonstrated by Zhu *et al*.[31] Although these materials were shown to selectively absorb hydrophobic pollutants in aqueous environments, experiments have been conducted against contaminants of limited complexity, such as lubricating oil, mineral oil, and other homogeneous oils, without the broad range of components that would be experienced in a crude oil spill.[81, 84, 85] Although the hydrophobic nature of these materials provide sequestration advantage, these materials neglect a crucial issue found at many spill sites, submerged oil. This particular problem continues to cause great strife, for instance, recently at the Kalamazoo River oil spill of 2010.[90] The use of amphiphilic materials is expected to be able to benefit the recovery of submerged oil and

oils of varying densities, as they could traverse along the entire water column of a system. However, few well-defined, amphiphilic, hybrid materials have been investigated for pollutant entrapment and recovery. Perhaps the most intricately-designed amphiphilic pollutant recovery vessel is the mesoporous silica-coated iron oxide nanoparticle system having small molecule surfactant-based micelles confined within the silica pores, which was shown to exhibit high hydrocarbon capture efficiencies, but with a limited capacity of 3.9 mg hydrocarbon/g nanoparticle material.[91] We anticipated that a hybrid nanomaterial that is comprised of inorganic magnetic nanoparticles and amphiphilic polymer layers would possess increased capacity for hydrocarbon pollutant packaging while maintaining aqueous phase dispersion stability and magnetic recovery properties. Moreover, in order to practically demonstrate that nanotechnology has a place in oil spill clean-up, the materials presented here were tested against a complex crude oil pollutant provided by Enbridge Energy Partners, L.P. (Fig. 2.1).

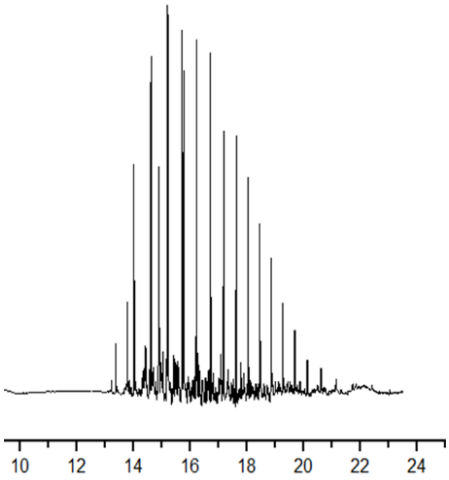

Figure 2.1. Gas chromatography-mass spectrometry (GC-MS) chromatogram of weathered crude oil.

2.2 Results and Discussion

Design of MSCKs. In order to design novel materials for oil sequestering based on state-of-the-art nanotechnology, we first assessed the needs and requirements to deal with this type of environmental pollutant. The organic-inorganic hybrid, core-shell nanoparticles were specifically designed, as shown in Scheme 2.1, for oil extraction. The inorganic magnetic component was incorporated for a means of convenient recovery in an aqueous environment. Iron oxide nanoparticles were chosen, instead of *e.g.* nickel or cobalt magnetic nanoparticles, due to their lower potential of toxicity.[92, 93] For the organic component, amphiphilic poly(acrylic acid)-*block*-polystyrene (PAA-*b*-PS) diblock copolymer was selected for the chemical stability of its backbone, the chemical

reactivity of its side chain functionalities, and its ability to self-assemble into different morphologies.[94, 95] The system was further crosslinked not only to protect it from disassembly during infinite dilution in the aqueous environment for which it was designed, but also to increase its loading potential by creating a stable vessel that could undergo reversible expansion and contraction. The self-assembly process we adopted here, allowed for a large number of magnetic nanoparticles to be non-covalently incorporated within each hybrid nanoparticle core. Multiple, small nanoparticles in the same hybrid nanostructure allow for core swelling during pollutant entrapment as this inorganic component is not covalently bound to the organic polymer, and also increase the magnetic response of the material. Crude oil contains both aliphatic and aromatic fractions; the styrene groups within the PS-based core targets the aromatic components, while the backbone of the polymer allows for the increased solubility of the aliphatic fraction.

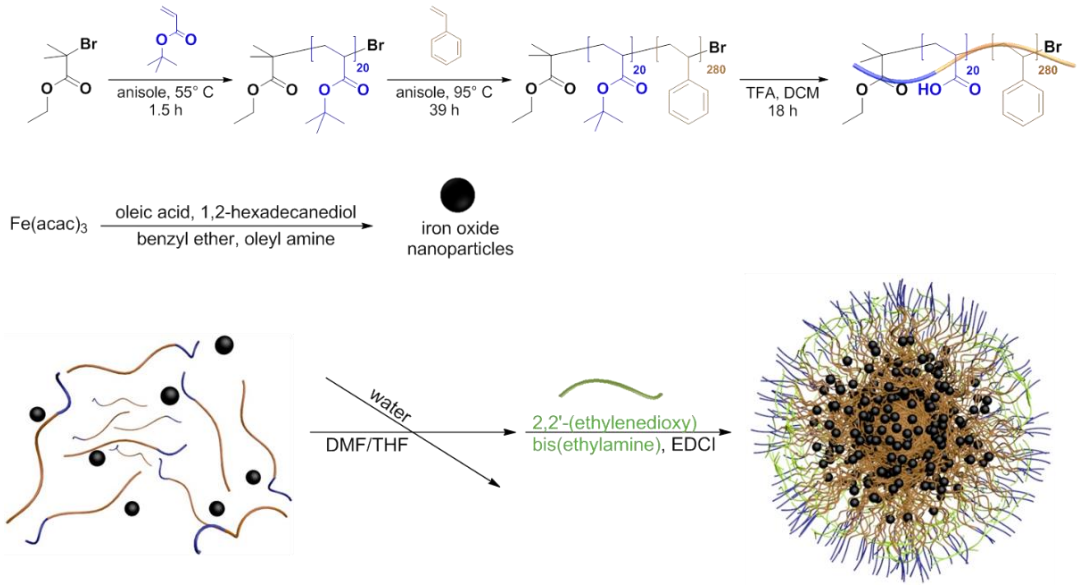

Scheme 2.1 Schematic representation of the construction of magnetic shell cross-linked (MSCK) nanoparticles.

Thermal synthesis of iron oxide nanoparticles. Synthesis of iron oxide nanoparticles was conducted by following the thermal decomposition method.[96, 97] Oleic acid and oleyl amine were used as the surfactant and co-surfactant, respectively, in benzyl ether as the solvent, while 1,2-hexadecanediol served as a reducing agent for the iron (III) acetylacetonate. The reaction was conducted in three 1-h periods at temperatures of 140 °C, 200 °C, and 250 °C, consecutively. The resulting nanoparticles were precipitated in ethanol and characterized by transmission electron microscopy (TEM), superconducting quantum interference device (SQUID), and infra-red (IR) spectroscopy. TEM showed nanoparticles of 8 ± 2 nm diameter (after analysis of over

100 nanoparticles) (Fig. 2.2). SQUID confirmed the magnetic character and determined the particle size to be 9.2 nm, in agreement with the TEM data.

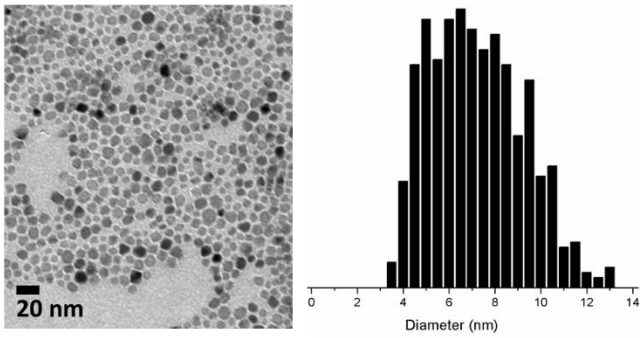

Figure 2.2. Characterization of iron oxide nanoparticles. (a) Transmission electron microscopy (TEM) of iron oxide nanoparticles. (b) Histogram of iron oxide nanoparticle population showing average diameter of 8 ±2 nm.

Synthesis of amphiphilic block copolymer. The amphiphilic diblock copolymer PAA_{20}-*b*-PS_{280} was synthesized according to conditions previously reported.[98] In brief, sequential atom transfer radical polymerizations (ATRP) of *tert*-butyl acrylate and styrene were conducted in anisole with the presence of CuBr and *N,N,N′,N′,N″*-pentamethyldiethylenetriamine (PMDETA) at 55 °C and 95 °C, respectively, to afford a diblock copolymer precursor. The polydispersity indices (PDI)

of the initial poly(*tert*-butyl acrylate)$_{20}$ homopolymer and the subsequent poly(*tert*-butyl acrylate)$_{20}$-*block*-polystyrene$_{280}$ diblock copolymer were below 1.2 (Fig. 2.3). The final PAA$_{20}$-*b*-PS$_{280}$ amphiphilic block copolymer was produced by subsequent removal of the *tert*-butyl groups through acidolysis with the aid of trifluoroacetic acid (TFA) in dichloromethane. Full characterization data for the polymers can be found in the materials and methods.

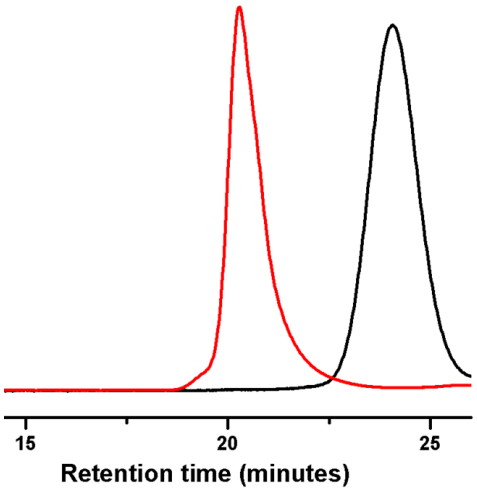

Figure 2.3. Gel permeation chromatography (GPC) trace of poly(*tert*-butyl acrylate) in black and poly(*tert*-butyl acrylate-*block*-polystyrene) in red.

Co-assembly of hybrid micelles. The co-assembly of the amphiphilic diblock copolymers and hydrophobic magnetic nanoparticles was performed by a modified process of a previously established method.[99] Magneto-micelles were chosen over other hybrid morphologies, such as magneto-polymersomes and magneto-core shell assemblies, due to their higher uniformity.[75] The PAA:PS mole ratio was tuned to 20:280 for its selectivity towards micellar structures; increasing this ratio results in a morphological change from magneto micelles to magneto-polymersomes.[75] The PAA_{20}-*b*-PS_{280} and iron oxide nanoparticles were dissolved into a solvent mixture (vol ratio 1:1) of *N*,*N*-dimethylformamide (DMF) and tetrahydrofuran (THF) at a concentration of 0.33 mg/mL for both inorganic and organic components. The mixture was added dropwise, coincidentally with 1× volume of water, *via* two separate syringe pumps at 20 mL/h, into a vessel containing an initial 0.33× volume of nanopure water (a selective solvent for PAA) to afford the desired magnet containing block copolymer micelles. Finally, the excess organic solvents were removed by extensive dialysis (tubing having MWCO 6-8 kDa) against nanopure water for 24 h. The resulting nanoparticles were characterized by TEM, dynamic light scattering (DLS), and IR spectroscopy. TEM analysis showed nanoparticles of 70 ± 12 nm diameter (after counting over 35 micelles). Within the core of these structures, multiple iron oxide nanoparticles were observed (average of 75 after counting over 20 micelles; this average number is considered to be a lower limit, due to the two-dimensionality of TEM creating difficulty to observe all iron oxide nanoparticles within a micellar assembly) (Fig. 2.4). The packaging of the iron oxide nanoparticles

within the core of the MSCKs was confirmed by tomographic TEM studies, as illustrated in a series of still and video images in the supporting information (Fig. 2.5).

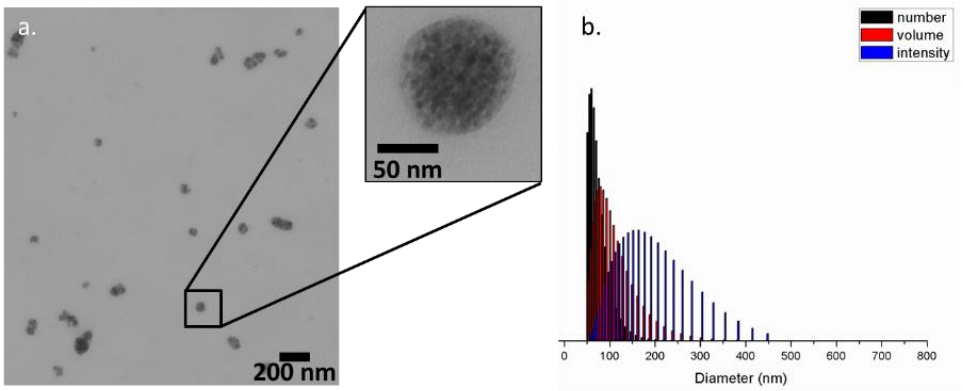

Figure 2.4. Characterization of magneto micelles. (a) TEM of micelles (not stained). (b) DLS histogram of magneto micelles.

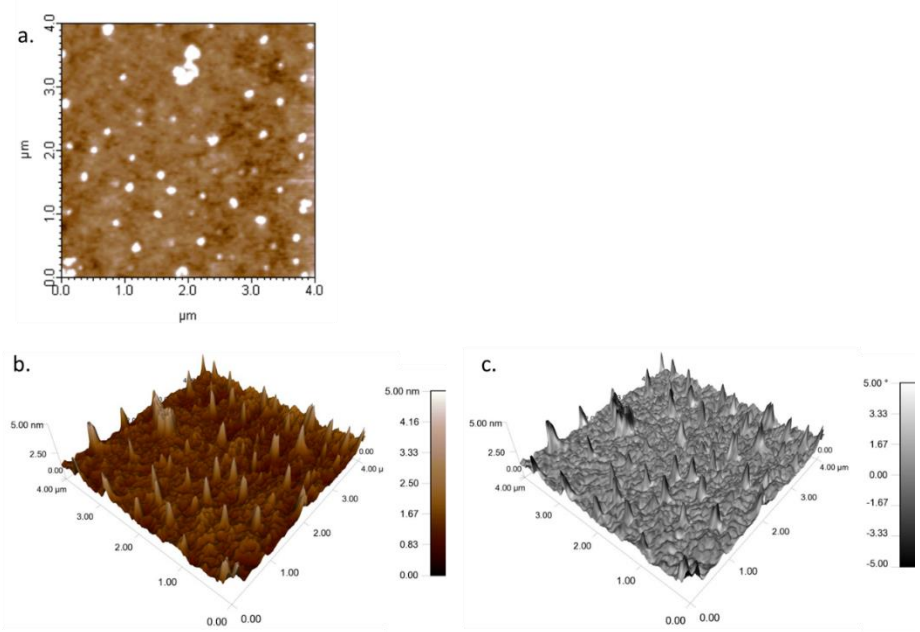

Figure 2.5. AFM characterization of MSCKs. (a) AFM of MSCKs drop-cast on glass.(b) 3D representation of AFM height image. (c) Phase image superimposed on 3D height profile.

Crosslinking of hybrid micelles *via* amidation. The MSCKs were obtained by crosslinking nominally 25% of the acrylic acid repeat units by amidation with the amine groups of the crosslinker (2,2'-ethylenedioxy)bis(ethylamine) in the presence of 1-(3-(dimethylamino)propyl)-3-ethyl-carbodiimide methiodide (EDCI). Extensive dialysis against nanopure water was performed to remove unreacted small molecules and reaction by-products. The MSCKs were characterized by TEM (Fig. 2.6a), atomic force

microscopy (AFM) (Fig. 2.7), DLS (Fig. 2.6), and IR spectroscopy. TEM imaging of the MSCKs demonstrated no morphological change after crosslinking.

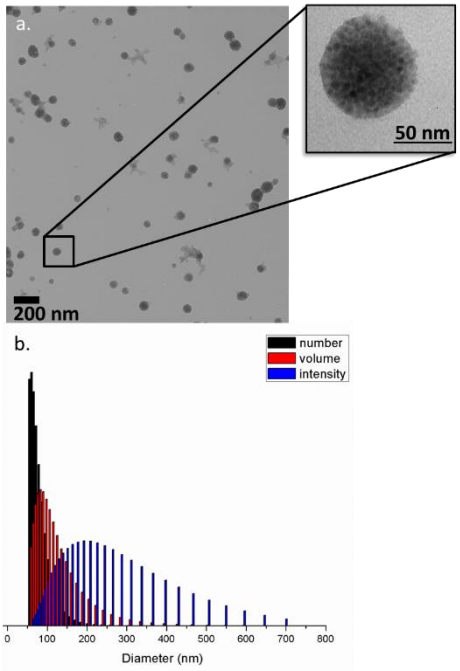

Figure 2.6. Characterization of magnetic iron oxide nanoparticles entrapped within PAA_{20}-*b*-PS_{280} MSCKs. (a) TEM of MSCKs drop deposited from water onto a formvar grid (not stained). (b) Number-, volume-, and intensity-averaged DLS histograms of MSCKs in water.

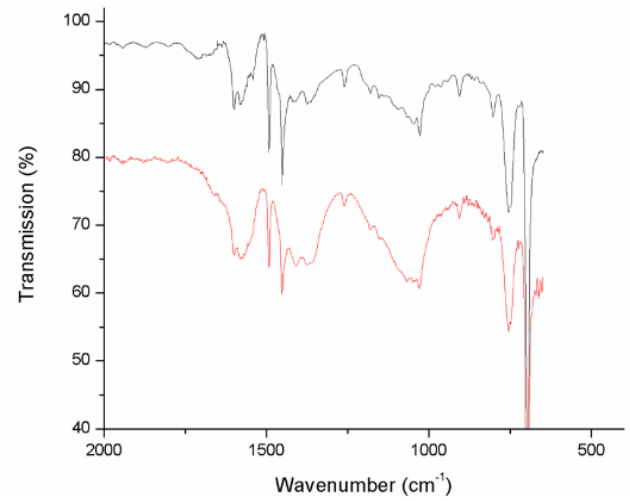

Figure 2.7. IR spectrum of magneto micelles (black) and IR spectrum of MSCKs (red).

DLS and TEM confirmed no significant size difference post modification. In contrast to the micelles, the MSCKs were structurally more robust, which allowed for sample preparation and AFM imaging to be conducted. Although deposition onto mica resulted in imaging difficulties, due to AFM tip disruptions of particle placements on the substrate and destruction of particle integrity, sample deposition onto glass provided adequate AFM images of the MSCKs, which showed nanoparticles having an average diameter of 109 ± 50 nm and an average height of 3 ± 1 nm (after counting over 30 nanoparticles).

This observation of a substantially greater diameter than height, together with the diameter being much larger when measured by AFM than by TEM or DLS, is characteristic of deformation of the particles when deposited onto the substrate used for AFM and/or during the AFM imaging procedure.[94, 100] Moreover, it was observed that the particles were distributed across the glass substrate within a layer of other, unknown soft material, which resulted in an inaccurately low value for the measured heights of the MSCKs. However, the combined TEM, DLS and AFM data provided determination of the particle size and shape, and the interesting extents of particle deformation on the substrates are being investigated further to probe the roles that the magnetic particles may be able to play on responsive morphology and shape changes for these types of MSCKs. The IR C=O stretch at 1720 cm^{-1} in the magneto-micelle sample shifted upon amidation, and stretching bands at 1650 and 1560 cm^{-1} were observed for the MSCKs, which indicated successful crosslinking (Fig. 2.8).[101]

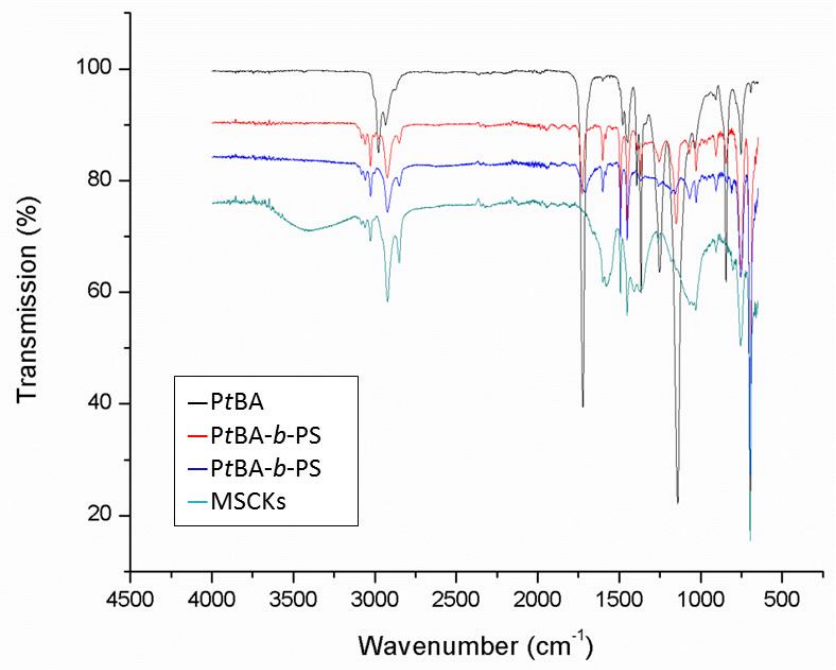

Figure 2.8. IR spectra of polymers: poly(*tert*-butyl acrylate) in black, poly(*tert*-butyl acrylate-*block*-polystyrene) in red, poly(acrylic acid-*block*-polystyrene) in blue, and MSCKs in cyan).

Oil sequestration by MSCKs. The ability of the MSCKs to serve as hybrid organic-magnetic sequestration vessels for oil spill recovery was assessed through a series of qualitative observations. The crude oil from the Texas-Oklahoma Enbridge pipeline was first weathered according to the method employed in experiments that investigated the Deepwater Horizon spill in the Gulf of Mexico.[102] The weathered oil was added to deionized (DI) water in order to mimic contaminated water samples (Fig. 2.9a) in 50 mL capped vials. The lyophilized powder samples of MSCKs were then added to the crude oil contaminated water at initial MSCK:oil weight ratios of 1:2, 1:5, 1:10, and 1:15. Visually, the oil sequestering capabilities of the well-defined MSCK nanoparticles were apparent (Fig. 2.9b). The floating MSCKs exhibited a noticeable change in color from light tan to black within seconds after addition into the contaminated environment. This color change was accompanied by aggregation of the MSCKs. The change in color and texture was thought to be an indicator of the sorbing of the hydrocarbon contaminants. The magnetic nanoparticles were then easily and quickly (in a matter of seconds) attracted to the external magnetic field of a neodymium magnet to allow for the decanting of the contaminated water (Fig. 2.9c). The remaining hydrocarbon contaminants were analyzed after being extracted from their aqueous environment through the use of chloroform (a favorable solvent for this type of light sweet crude oil).

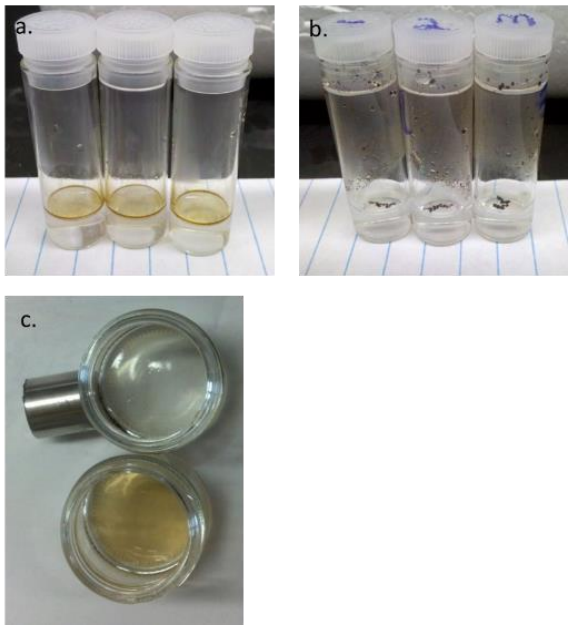

Figure 2.9. Images of oil sequestration experiment. (a) Vial containing crude oil-contaminated water. (b) Image showing vial after oil sorption by hybrid MSCK nanoparticles. (c) Top view comparison of crude oil-loaded nanoparticles captured against the vial wall by an external magnet (top) and crude oil-contaminated water (bottom).

Quantification of oil sequestration. The capacity for oil sequestration by MSCKs was further quantified by an analytical method. In order to quantify the oil sequestered by the MSCKs, the oil remaining in the aqueous phase after magnetic capture of the oil-sorbed MSCKs was extracted, analyzed and quantified using gel permeation chromatography (GPC). An internal standard of polystyrene (M_w= 70,000 Da) was used to spike each dilute oil sample prior to injection into the instrument. This

high molecular weight polymer was selected for its short retention time; the crude oil chromatogram is broad and has a relatively high retention time due to the inherently small to medium molecular weights of the crude oil components.

A refractive index (RI) detector was used as a concentration detector in a GPC system according to the RI detector theory.[103] Quantification of the oil recovery was made possible due to the proportionality between sample concentration and refractive indices. Several examples of this applied theory have been used to determine polymer concentration in both cyclic and linear systems.[104-106] Though this method is effective in more homogeneous systems, the heterogeneity of the crude oil sample led to complications during the development of this procedure. To compensate for this, a control group of "unrecovered" oil was used as a baseline for the oil quantification method. These control groups were used to derive an empirical coefficient relating the oil concentration in the sample to the integration region in the chromatogram for each set of experiments. This coefficient was later employed to determine the unknown oil concentration remaining after MSCK sequestration in the tested samples. Further details of this methodology can be found in the materials and methods.

The maximum sorption capacity of the MSCKs was determined by testing increasing initial nanoparticle:oil ratios through a series of experiments. For the initial ratio of 1:2.8, evaluation of the chromatographical data determined the total oil sorption to be 2.1 mg of oil per milligram of MSCKs used. For the remaining trials of 1:5.2, 1:11.5 and 1:16.8, the sorption limit was found to be 1:4.4, 1:9.6 and 1:10.2, respectively. The percentage oil recovery was also determined (Fig. 2.10). Following

the trend seen in the mass recovery data on the graph below, it can be speculated that the maximum sorption extent of the MSCKs is roughly ten times the initial dry weight of the material. Further attempts at increasing initial oil concentration resulted in inadequate recovery of the loaded nanoparticles; at higher oil concentrations, the viscosity of the thick oil layer prevented magnetic mobilization of the loaded nanoparticles.

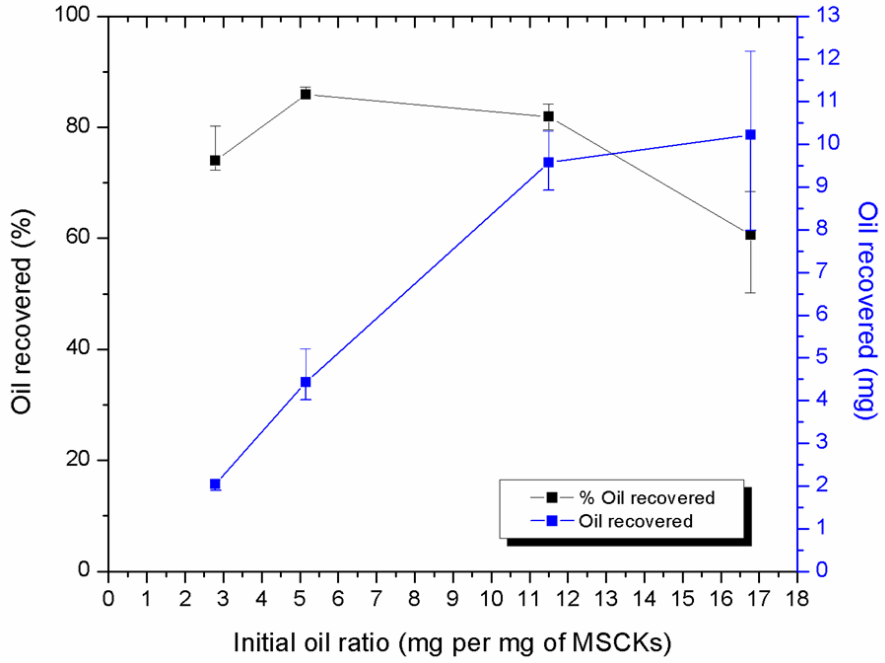

Figure 2.10. Oil recovery data. Percentage recovery in black. Mass recovered in blue.

Gas chromatography-mass spectrometry (GC-MS) was used to perform a qualitative comparison of the weathered crude oil and the oil extracted from the testing groups. The data from this test showed the successful sequestration of all oil components by MSCKs (Fig. 2.11), without any fractionation of the oil materials. This result suggests that fine-tuning of the organic component of the MSCK system could achieve selective recovery of a broad range of environmental pollutants, coincidentally, which may be useful for various applications.

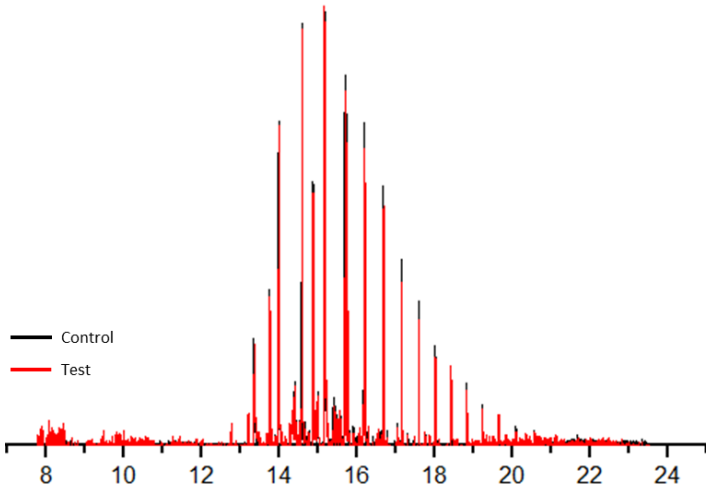

Figure 2.11. Gas chromatography-mass spectrometry (GC-MS) of oil extracted from control (black) and test (red) groups.

Recycling of MSCKs. The reuse of materials at oil spill sites decreases the waste produced during the clean-up efforts as well as enhances the overall effectiveness of the substance deployed. Other magnetic systems have been successfully recycled and re-deployed as recovery systems for environmental pollutants.[91] The magnetic permanently-confined micelle arrays used by Wang *et al*. were tested for their recyclability and were regenerated after thorough washings in methanol.[91] Solubility analysis of the crude oil determined that ethanol, rather than methanol, would be the better solvent suited for our particular crude oil system. Although chloroform could have also been used for the removal of the oil from the MSCK system, there were initial concerns regarding chloroform promoting morphological changes of the nanoparticles.

The oil sorbed in the nanoparticles was removed by extensive washings in ethanol with the help of sonication. The contaminated ethanol was decanted between each washing and the nanoparticles were retained in the vessel through magnetic force. Visually, the "clean" nanoparticles returned to their original light tan color. After *in vacuo* drying, IR spectroscopy was used to determine the state of the MSCKs (Fig. 2.12a).

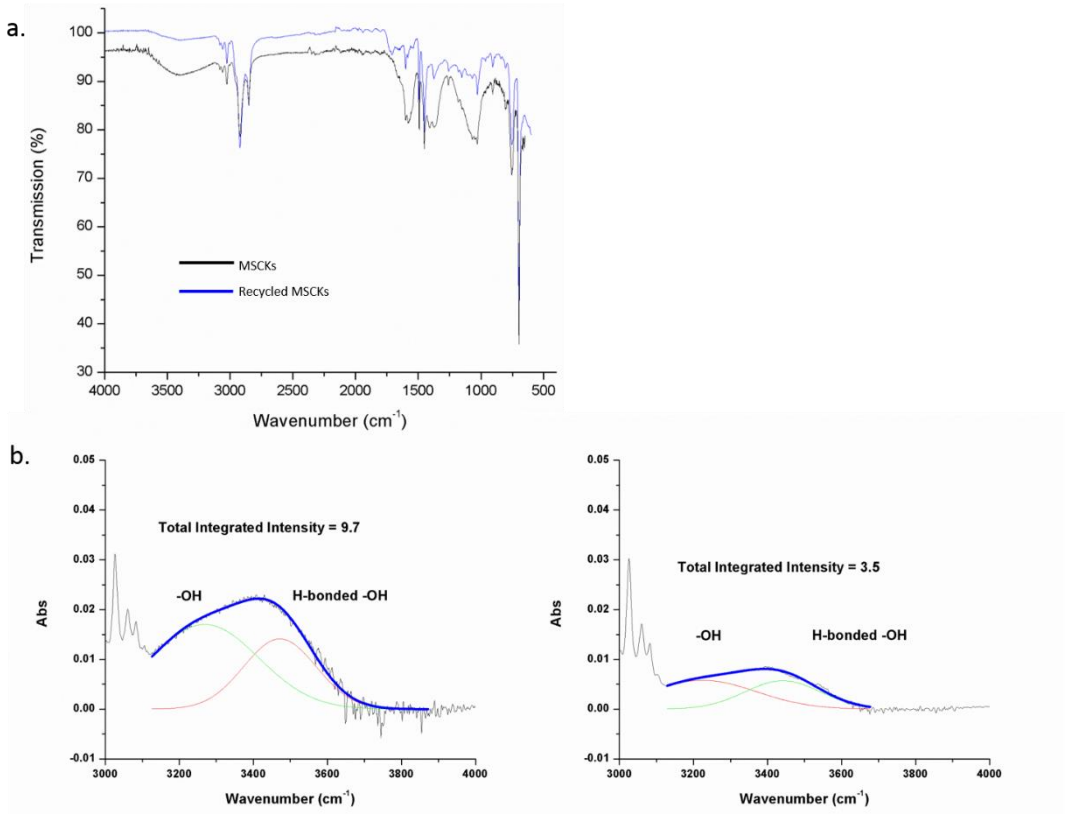

Figure 2.12. (a) IR spectra of pristine and recycled MSCKs. (b) Quantification of –OH functionality of pristine MSCKs. (c) Quantification of –OH functionality of recycled MSCKs.

As seen on the IR spectra of the pristine and recycled MSCKs, there were some observable changes after the washing procedure, in particular between 1700 and 800 cm^{-1}. We hypothesize these may be due to reorganization of the polymeric structures during the sonication washes; ongoing efforts include determining the molecular compositional origins of these changes. An additional aspect of the IR spectra that was

further investigated was the apparent loss of –OH functionality after the removal of the oil from the loaded MSCKs. Quantification of this loss was performed through the analysis of the IR absorption spectra by first normalizing the two data sets using a peak in which change did not occur, the C-H band of the polymer backbone at 1450 cm^{-1}. The data from this analysis as shown in Fig. 2.12b and c, demonstrate a 40% loss of the –OH functionality, presumably from dehydration and esterification of the acrylic acid groups in the polymer component of the MSCK system. Further detailed studies of the recycling method, with full mass analyses of the recovered hydrocarbon and MSCKs are underway to demonstrate that this loss was not artificially enhanced by the presence of remaining hydrocarbons. However, alcohol washing of pristine, lyophilized MSCK nanoparticles with sonication, also resulted in a reduction in the intensity of the –OH signal after analysis of the deconvoluted data, likely due to esterification of intermediate anhydrides. We believe that the anhydride moieties are formed during the freeze-drying process to obtain the powder MSCKs and/or during sonication. The presence of these anhydrides can be observed at 1000 cm^{-1} in Fig. 2.8.

Although further investigations into the changes experienced by the MSCKs after washing are ongoing, the recycled nanoparticles were redeployed into a polluted aqueous system with an initial MSCK:oil ratio of 1:15.7 to probe the reusability of these materials. After oil sequestration and analysis of remaining pollutants, the sorption ratio was calculated to be 1:10.9. These data were compared to those of the previous 1:15 initial ratio experiment where the oil sorption was calculated to be 1:10.2, demonstrating retention of their ultra-high oil sorption characteristics. This finding addresses a

challenge associated with the efficiency and effectiveness of this material in a real-world application.

2.3 Conclusions

MSCKs for removal of environmental pollutants have been prepared and their loading capabilities were determined. These well-defined nanoparticles showed efficient oil sorption capacity of ten-fold their initial dry weight when introduced into an aqueous environment polluted with a complex crude oil. Compared to materials that are typically employed in the field currently, which have capacities of *ca*. four-fold oil uptake to their dry mass, MSCKs offer distinct improvement.[20] Moreover, the recyclability of the robust MSCK material was also proven to be highly effective, despite some apparent chemical changes experienced during the recycling process. Furthermore, this type of material has high potential for additional applications in environmental remediation. The amphiphilic nature of the MSCK system expands the potential use of these materials to other applications such as the removal of submerged oil, groundwater remediation, and clean-up of contaminated soils. Modern advances in polymer science hold the promise of fine-tuning the complex composition of the polymer components, for a more targeted design to meet the demands of particular applications.

2.4 Materials and Methods

Materials. All chemicals were purchased from Aldrich Chemical Co. and used without further purification unless otherwise noted. *tert*-Butyl acrylate and styrene

monomers were purified through an alumina plug to remove stabilizer. Iron (III) acetylacetonate was purchased from Strem Chemicals, Inc. Nanopure water (18 MΩ•cm) was acquired by means of a Milli-Q water filtration system, Millipore Corp. (Bedford, MA). Neodymium magnet (90 lbs. pull) was purchased from magnets4less.com. Crude oil for this research was generously donated by Enbridge Energy Partners, L.P.

Characterization techniques. ^{1}H NMR and ^{13}C NMR spectra were recorded on an Inova 300 or Mercury 300 spectrometer interfaced to a UNIX computer using VnmrJ software. Samples were prepared as solutions in $CDCl_3$ or d_8-THF and solvent protons were used as internal standard. IR spectra were recorded on an IR Prestige 21 system (Shimadzu Corp., Japan). A small amount of sample was placed to cover the ATR crystal for IR measurements. Data were analyzed using IRsolution software. Differential scanning calorimetry studies were performed on a Mettler Toledo DSC822 (Mettler-Toledo, Inc., Columbus, OH) calibrated according to the standard procedures using indium. The heating rates were 10 °C min^{-1} and cooling rates were 10 °C min^{-1} with a temperature range of -100–150 °C. The T_g was taken as the midpoint of the inflection tangent, upon the third heating scan. Thermogravimetric analysis was performed under Ar atmosphere using a Mettler Toledo model TGA/DSC1 with a heating rate of 10 °C/min. Measurements were analyzed using Mettler Toledo *STAR*^{e} software v 10.00. THF gel permeation chromatography (GPC) was conducted on a system equipped with Waters chromatography, Inc. (Milford, MA) model 1515 isocratic pump and a model 2414 differential refractometer with a three-column set of Polymer

Laboratories, Inc. (Amherst, MA) Styragel columns (PL_{gel} 5 μm Mixed C, 500 Å, and 10^4 Å, 300 × 7.5 mm columns) and a guard column (PL_{gel} 5 μm, 50 × 7.5 mm). The system was equilibrated at 40 °C in THF, which served as the polymer solvent and eluent (flow rate set to 1.00 mL/min). The differential refractometer was calibrated with Polymer Laboratories, Inc., polystyrene standards (300 to 467 000 Da). Polymer solutions were prepared at a concentration of *ca.* 3 mg/mL with 0.05% vol toluene as flow rate marker and an injection volume of 200 μL was used. Data were analyzed using *Empower Pro* software from Waters Chromatography Inc. Chloroform GPC for oil analysis was conducted on a system equipped with a Tosoh Corporation (Tokyo, Japan) model HLC-8320 EcoSEC system with a two-column set of TOSOH Bioscience TSKgel columns (Super HM-M 6.0 mm ID x 15 cm columns) and a guard column (Super H-H 4 μm). The system was equilibrated at 40 °C in chloroform, which served as the polymer solvent and eluent (flow rate set to 0.600 mL/min). The differential refractometer was calibrated with Polymer Laboratories, Inc., polystyrene standards (580 to 370 000 Da). Polymer solutions were prepared at a concentration of *ca.* 3 mg/mL and an injection volume of 200 μL was used. Dynamic light scattering (DLS) measurements were conducted using Delsa Nano C from Beckman Coulter, Inc. (Fullerton, CA) equipped with a laser diode operating at 658 nm. Size measurements were made in water (n = 1.3329, η = 0.890 cP at 25 ± 1 °C; n = 1.3293, η = 0.547 cP at 50 ± 1 °C; n = 1.3255, η = 0.404 cP at 70 ± 1 °C). Scattered light was detected at 165° angle and analyzed using a log correlator over 70 accumulations for a 0.5 mL of sample in a glass sizing cell (0.9 mL capacity). The photomultiplier aperture and the attenuator were

automatically adjusted to obtain a photon counting rate of *ca*. 10 kcps. The calculations of the particle size distribution and distribution averages were performed using CONTIN particle size distribution analysis routines. Prior to analysis, the samples were filtered through a 0.45 μm Whatman nylon membrane filter (Whatman, Inc.). The samples in the glass sizing cell were equilibrated at the desired temperature for 5 min before measurements were made. The peak average of histograms from intensity, volume, or number distributions out of 70 accumulations was reported as the average diameter of the particles.

Synthesis of poly(*tert*-butyl acrylate) (P*t*BA$_{20}$) *via* ATRP. A flame-dried 100-mL Schlenk flask equipped with a magnetic stir bar was charged with PMDETA (1 eq., 451.0 mg, 2.6 mmol), *t*BA (30 eq., 9.6322 g, 75.1 mmol), ethyl α-bromoisobutyrate (1 eq., 489.5 mg, 2.5 mmol), and anisole (10 mL). The flask was sealed with a rubber septum and the reaction mixture was degassed by three freeze-pump-thaw cycles. Then, the CuBr (1 eq., 430.5 mg, 4.2 mmol) was added under a nitrogen flow to the frozen mixture. Following two additional freeze-pump-thaw cycles, the reaction mixture was allowed to return to room temperature and was allowed to stir for 10 min to ensure homogeneous mixing. The flask was then immersed into a pre-heated oil bath at 55 °C to start the polymerization. The polymerization was monitored by analyzing aliquots collected at pre-determined times by ^{1}H NMR spectroscopy. As the expected monomer conversion was reached, after *ca.* 1 h, the polymerization was quenched by quick immersion of the reaction flask into liquid N_2 and exposure to air. THF (20 mL) was added to the reaction flask and the polymer was purified by filtration through an alumina

plug followed by subsequent precipitation into 500 mL of a methanol/ice mixture (3×). The precipitants were collected and dried under vacuum overnight to afford 3.62 g of $PtBA_{20}$ as a white solid, giving 40% yield of the 95% conversion polymerization. $M_{n(NMR)}$ = 3.1 kDa, $M_{n(GPC)}$ = 2.8 kDa, PDI = 1.09. IR: 2975, 2720, 1725, 1465, 1440, 1390, 1360, 1250, 845, 750 cm^{-1}. ^{1}H NMR (300 MHz, $CDCl_3$) δ 4.12 (q, J = 7 Hz, 2H), 2.35 - 2.15 (br, 20H), 1.94 - 1.78 (br, 10H), 1.71 - 1.2 (m, 210H), 1.27 (t, J = 7 Hz, 3H), 1.12 (br, 6H) ppm. ^{13}C NMR (75 MHz, $CDCl_3$) δ 27.8 - 28.2, 35.0 - 37.6, 41.4 - 42.5, 80.2 - 80.7, 173.8 - 174.4 ppm. DSC: T_g = 28 °C. TGA: T_{onset} = 195 °C, $T_{decomposition}$: (195-204 °C) 43.5% mass loss; (207–455 °C) 46.5% mass loss; 10% mass remaining.

Synthesis of poly(*tert*-butyl acrylate)$_{20}$-*b*-polystyrene$_{280}$ (P*t*BA$_{20}$-*b*-PS$_{280}$) *via* ATRP. A flame-dried 25-mL Schlenk flask equipped with a magnetic stir bar was charged with PMDETA (1.6 eq., 18.1 mg, 0.1 mmol), styrene (500 eq., 3.1303 g, 30 mmol), P*t*BA$_{20}$ (1.3 eq., 257.6 mg, 0.1 mmol), and anisole (4 mL). The flask was sealed with a rubber septum and the reaction mixture was degassed by three freeze-pump-thaw cycles. Then, the CuBr (1 eq., 8.6 mg, 0.06 mmol) was added under a nitrogen flow to the frozen mixture. Following two more freeze-pump-thaw cycles, the reaction mixture was allowed to return to room temperature and was allowed to stir for 10 min to ensure homogeneous mixing. The flask was then immersed into a pre-heated oil bath at 95 °C to start the polymerization. The polymerization was monitored by analyzing aliquots collected at pre-determined times by ^{1}H NMR spectroscopy. As the expected monomer conversion was reached, after *ca.* 39 h, the polymerization was quenched by quick immersion of the reaction flask into liquid N_2 and exposure to air. THF (5 mL) was

added to the reaction flask and the polymer was purified through filtration by an alumina plug and precipitation into 200 mL of cold methanol (2×). The precipitants were collected and dried under vacuum overnight to afford $PtBA_{20}$-*b*-PS_{280} as an off-white solid, giving 64% yield of the 55% conversion polymerization. $M_{n(NMR)}$ = 31.7 kDa. $M_{n(GPC)}$ = 27.0 kDa. PDI = 1.18. IR: 3080, 3060, 3020, 2920, 2840, 1940, 1880, 1800, 1725, 1600, 1490, 1450, 1360, 1240, 1150, 1060, 1025, 910, 840, 750, 695 cm^{-1}. ^{1}H NMR (300 MHz, $CDCfl_3$) δ 7.43 – 6.8 (br, 840H), 6.8 - 6.13 (br, 560H), 4.12 (q, *J* = 7 Hz, 2H), 2.24 - 0.87 (br m, 1090H) ppm. ^{13}C NMR (75 MHz, $CDCl_3$) δ 27.8 - 28.2, 39.6 - 46.5, 80.2 - 80.7, 125.2 - 126.0, 127.0 - 128.4, 144.7 - 146.3, 173.8 - 174.4 ppm. DSC: T_g = 88 °C. TGA: T_{onset} = 237 °C, $T_{decomposition}$: (237 - 241 °C) 4% mass loss; (401– 435 °C) 73.6% mass loss; 22% mass remaining.

Synthesis of poly(acrylic acid)$_{20}$-*b*-polystyrene$_{280}$ (PAA_{20}-*b*-PS_{280}). P*t*BA_{20}-*b*-PS_{280} (1mol eq., 1.0666 g) was dissolved in dichloromethane (10 mL). Trifluoroacetic acid (TFA) (1000 mol eq., 3 mL) was added. The reaction mixture was left stirring vigorously for 16 h. After evaporation of the solvent and TFA, THF was added to re-dissolve the polymer which was then dialyzed for three days against nanopure water using dialysis tubing having MWCO 6 - 8 kDa, during which the product precipitated within the dialysis tubing. The precipitate was filtered and placed under high vacuum overnight. IR: 3080, 3060, 3025, 3000, 2920, 2850, 1925, 1860, 1800, 1700, 1600, 1490, 1450, 1370, 1260, 1170, 1150, 1065, 1025, 900 750, 700 cm^{-1}. ^{1}H NMR (300 MHz, THF) δ 10.88 (br, 10H), 7.3 – 6.8 (br, 840H), 6.8 - 6.59 (br, 560H), 4.07 (q, *J* = 7 Hz, 2H), 2.47 - 0.48 (br m, 930H). ^{13}C NMR (75 MHz, THF) δ 40.0 - 46.7, 125.2 -

126.0, 127.0 - 128.4, 144.7 - 146.3, 173.8 - 174.4 ppm. DSC: T_g = 99 °C. TGA: T_{onset} = 410 °C, $T_{decomposition}$: (410 - 441 °C) 89.5% mass loss; 10.5% mass remaining.

Synthesis of Fe_3O_4 nanoparticles. A flame-dried, 50 mL 3-neck flask equipped with a magnetic stir bar and condenser was charged with $Fe(acac)_3$ (1 mol eq., 719.5 mg, 2 mmol), oleic acid (3 mol eq., 2.3215 g, 6 mmol) and oleyl amine (3 mol eq., 2.0020 g, 6 mmol). After the addition of benzyl ether (20 mL) and 1,2- hexadecanediol (5 mol eq., 2.5808 g, 10 mmol), the reaction mixture was degassed by a three-cycle exposure to vacuum and nitrogen. The reaction temperature was taken to 140 °C and the pressure inside the reaction vessel was relieved by the insertion of a needle. After an hour, the needle was removed and the reaction temperature was taken to 200 °C for an additional hour, following an hour at 250 °C. Once the reaction mixture was cooled to RT, it was transferred into a centrifuge tube and the nanoparticles were precipitated by addition of EtOH (3×) and re-suspended in THF. Final nanoparticle size was determined *via* TEM and DLS as *ca.* 8 nm in diameter. IR: 2600, 2220, 1220, 500, 450, 420 cm^{-1}. TGA: T_{onset} = 210 °C, $T_{decomposition}$: (210 - 270 °C) 3.5% mass loss, (300 - 430 °C) 11.5% mass loss; 88.5% mass remaining.

Co-assembly of PAA_{20}-*b*-PS_{280} and Fe_3O_4 NPs. An organic solution containing 2 mL of a 10 mg/mL solution of PAA_{20}-*b*-PA_{280} in DMF was diluted with a mixture of 28.0 mL of DMF and 28.6 mL of THF. To this, 1.4 mL of a 14 mg/mL solution of iron oxide nanoparticles was added in a drop wise manner under stirring. The solution was allowed to stir vigorously for 30 min to ensure homogeneity. The 60 mL organic solution was added drop wise to an initial 20 mL of nanopure water at a rate

of 20 mL/h. Simultaneously, 60 mL of nanopure water were also added at the same rate. The resulting 70 nm micelles were crosslinked to nominally 25% based on acrylic acid units (1 mol eq., $1.51E^{-5}$ mol) with the aid of 2,2'-(Ethylenedioxy)bis(ethylamine) (0.125 mol eq., $1.89E^{-6}$ mol, 0.224 mg) and 1-[3-(Dimethylamino)propyl]-3-ethylcarbodiimide methiodide (EDCI) (0.275 mol eq., $4.15E^{-6}$ mol, 0.984 mg), assuming 80% polymer present after filtration through 5.0 μm filter. DLS, TEM, and AFM data were used to determine the size of the MSCKs to be 70 nm.

Representative procedure for oil sequestration. To a vial containing DI water, weathered crude oil originating from the Texas-Oklahoma pipeline (light sweet crude) was added, and the weight of the sample was recorded. To each testing vial, MSCKs in the form of powder were added (1 to 10 mg depending on scale of trial). After approximately 30 min with little to no agitation, the loaded MSCKs were attracted by an external magnetic field to allow for decantation of the oil contaminated water for oil extraction; the vial was washed three times with water to maximized removal of the oil/water mixture remaining. The oil was extracted using chloroform washings. The organic fraction containing the crude oil was spiked with a solution of polystyrene standard of 70,000 Da molecular weight to serve as an internal standard for comparative studies with the control group. The spiked samples were examined using a chloroform GPC. Oil recovery was determined by chromatogram comparison with data from the control group. Oil was also extracted from contaminated water in the control groups using chloroform. Experiments were conducted in triplicate.

Oil quantification through GPC analysis. To account for the behavior and RI response of the crude material through the column, the spiked samples from the control groups were analyzed through chloroform GPC. Using the known mass of oil present in the control samples, a relationship between the area under the chromatogram peak and oil mass was established (mathematically, this was accomplished through the use of coefficient k).

$$k \cdot \frac{\int_{soil}}{\int_{spike}} = \frac{M_{oil}}{M_{spike}}$$

The use of this coefficient was validated by the low percent variation of this number within a sample set (5 - 15%). This k value was subsequently used in the tested samples to determine the unknown oil mass in the samples (M_{oil}). A data sample can be observed in the table below where "T#" represents the testing groups, and "C#" the control groups.

Sample	Oil (mV·sec)	PS (mV·sec)	Oil Used (mg)	k
T1	235.679	270.429	15.9	-
T2	93.488	151.1	17.8	-
T3	48.255	71.898	16.6	-
C1	589.425	340.313	15.4	2.877
C2	718.811	339.255	18.8	2.872
C3	558.667	329.665	116.3	3.075

Table 2.1. Representative data of oil sequestration.

CHAPTER III

STRUCTURAL STUDY OF MAGNETIC SHELL CROSSLINKED KNEDEL-LIKE (MSCK) NANOPARTICLES AND THEIR USE IN MARINE ENVIRIONMENTS

3.1 Introduction

The seemingly frequent nature of oil spills in the past few years have triggered many environmental problems and continue to cause concern on a global scale. In the United States alone, over 20,000 spills were reported to the federal government in 2014 and already close to 8,000 have been reported this year.[15] Due to this rising concern, various materials have been developed to aid the efforts at oil spill sites. Sorbent materials have been of particular interest due to the effectiveness of this technique.

In recent years, modified foams and fabrics have been explored for oil recovery and oil-water separation.[22-24, 107-108] These materials have shown excellent separation of oily contaminants and unprecedented pick-up capabilities. Notably, Chen *et* al.'s ultralight magnetic foam removed over 100 times its weight in oil pollutants (*ca*. 90× of crude oil). Additionally, the incorporation of a magnetic component allowed for these foams to be magnetically driven over the surface of the water.[24] Other hybrid materials containing carbon nanotubes have also been explored for this environmental application.[35,36] Gui and co-workers developed a magnetic carbon nanotube sponge with a maximum loading capacity of over 50× when tested against different types of oils.[36] Additionally, Hu *et al*. developed a carbon nanotube-graphene hybrid aerogel for oil-water separation that was able to take-up over 100× its weight in pump oil, vegetable oil,

diesel, and gasoline.[35] However, these macroporous materials are intrinsically limited to their application onto larger, easily accessible areas, and *ex situ* and surface treatments. Additional issues arise with the incorporation of carbon nanotubes due to their status as an emerging contaminant by the United States Environmental Protection Agency (USEPA).[17]

Amphiphilic systems allow for a broader application of the material for recovery and loading. However, they suffer the drawback of lower loading capabilities when compared to larger materials such as the foams and fabrics previously mentioned. Materials based on mesoporous silica, such as Li *et al*.'s amphiphilic mesoporous silica nanospheres, have been tested for their enhanced adsorption of organic compounds from water. Li and co-workers developed a library of hybrid mesoporous materials and tested their loading capabilities against 4-heptylphenol; the material labeled 4C20@1Z10 demonstrated a maximum loading of 49 mg of the organic compound per g of material used (*ca*. 0.05× by weight).[37] Another notable example is that of Nayab *et al*.'s polyethyleneimine-coated mesoporous silica which was tested for its loading of anionic dyes; these particles were able to load Alizarin red S at 2× their weight. However, this loading is hypothesized to have been aided by the electrostatic interactions between the positively charged particle shell and the negatively charged dye.[38] Furthermore, magnetically active amphiphilic systems have also been investigated; Huang and co-workers developed magnetic permanently confined micelle arrays and tested them against various contaminants. Although the extent of loading was not fully explored, they were able to achieve a loading of 0.5 mg/mg (0.5× by weight) of atenolol as the

maximum loading reported.[39] Another magnetically active material, that of Palchoudhury and co-workers, was tested for oil-water separation and demonstrated a pick-up of over 2.5× its weight in oil.[109] Recently, our group reported the development and testing of MSCK nanoparticles for crude oil recovery from water systems. This novel material, comprised of the amphiphilic diblock copolymer PAA_{20}-*b*-PS_{280} and non-covalently incorporated iron oxide nanoparticles, showed a loading capacity of 10× by weight of crude oil and no loss in this uptake capacity after recycling and reuse.[110] More recently, these MSCKs have been studied for their application in groundwater remediation and have shown great promise for the treatment of contaminated groundwater. Due to the grand success of this system, herein we further explore the behavior and uptake capabilities of MSCKs in seawater environments with additional focus on their morphological behavior in different solvent systems and their field testing.

3.2 Results and Discussion

Design of MSCK nanoparticles. These hybrid magnetic core-shell nanoparticles (Scheme 3.1) were designed for oil extraction following the initial bulk recovery stage at oil spill sites. Current technologies for remediation of low oil concentrations, or sheen, are often ineffective and impractical due to time, cost and other constraints.[80,111] Amphiphilic poly(acrylic acid)-*block*-polystyrene (PAA-*b*-PS) was utilized as the organic component of this organic-inorganic hybrid system for the chemical stability of its backbone, reactivity of its side chain functionalities and its ability to assemble into the desired morphology. Additionally, the styrene groups in the

PS domain of the polymer are expected to aid in solubility of the aromatic fractions in the oil while the backbone of the polymer may aid in the solubility of the aliphatic fractions. Iron oxide nanoparticles were non-covalently incorporated in order to impart the system with a magnetic component for facile recovery and manipulation. The system was crosslinked in order to protect it from infinite dilution in aqueous environments and to allow for a greater loading potential through the formation of a stable vessel that can undergo reversible expansion.

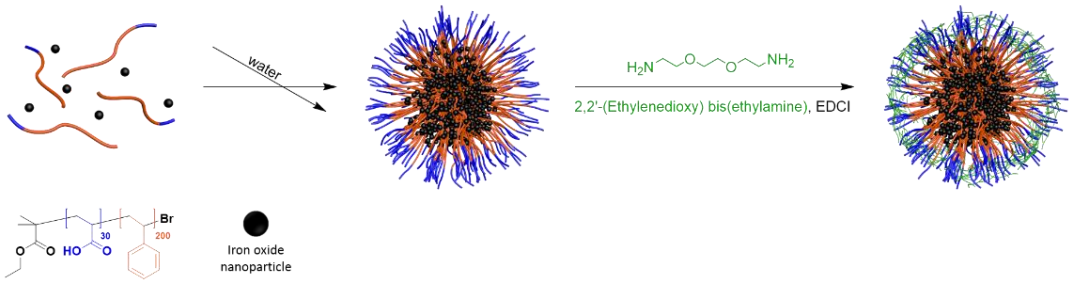

Scheme 3.1. Schematic representation of the co-assembly and crosslinking of MSCK nanoparticles.

Synthesis of PAA_{30}-*b*-PS_{200} amphiphilic diblock copolymer. The desired amphiphilic block copolymer was synthesized through a previously reported method. Briefly, the precursor poly(*tert*-butyl acrylate)$_{30}$-*block*-polystyrene$_{200}$ ($Pt BA_{30}$-*b*-PS_{200}) was obtained by the sequential atom transfer radical polymerizations (ATRP) of *tert*-butyl acrylate and styrene in anisole in the presence of CuBr and *N,N,N′,N′,N″*-pentamethyldiethylenetriamine (PMDETA) at 55 °C and 95 °C, respectively (Scheme 3.2). The polydispersity indices (PDI) of the $Pt BA_{30}$ homopolymer and the subsequent $Pt BA_{30}$-*b*-PS_{200} diblock, obtained through gel permeation chromatography (GPC), were 1.12 and 1.08, respectively. The final amphiphilic block copolymer was obtained following acidolysis with the aid of trifluoroacetic acid (TFA) in dichloromethane (DCM). Full characterization of the polymers can be found in the materials and methods section.

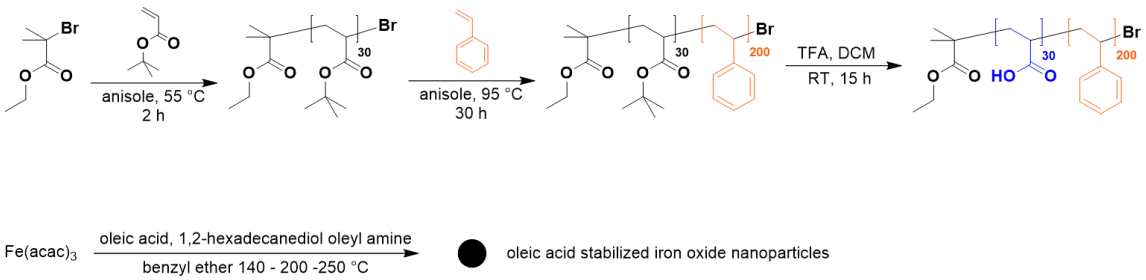

Scheme 3.2. Synthesis of PAA_{30}-*b*-PS_{200} polymeric component and oleic acid stabilized iron oxide nanoparticles.

Co-assembly of magneto micelles. Magneto micelles were produced from the co-assembly of the amphiphilic diblock copolymers and hydrophobic iron oxide nanoparticles, as previously reported. The PAA_{30}-*b*-PS_{200} polymers were dissolved at a 10 mg/mL concentration in *N*,*N*-dimethylformamide (DMF), followed by dilution with a 1:1 DMF and tetrahydrofuran (THF) mixture, and the addition of 2 mL of a 10 mg/mL solution of iron oxide nanoparticles in THF to afford a final concentration of 0.33 mg/mL for both inorganic and organic components. This organic solution was added in a dropwise manner, concurrently alongside an equal-volume of nanopure water, to a vessel containing 0.33× volume of nanopure water. The resulting hybrid micellar solution was filtered through a 5 µm filter in order to remove iron oxide precipitate formed during the co-assembly process. Finally, the excess organic solvent was removed through extensive dialysis (MWCO 12-14 kDa) against nanopure water for

24 h. The resulting nanoparticles were characterized through dynamic light scattering (DLS) and transmission electron microscopy (TEM). DLS analysis indicated an average number hydrodynamic radius of 79 ± 22 nm. TEM analysis showed nanoparticles of 70 ± 17 nm diameter (after counting over 50 micelles) (Fig. 3.1).

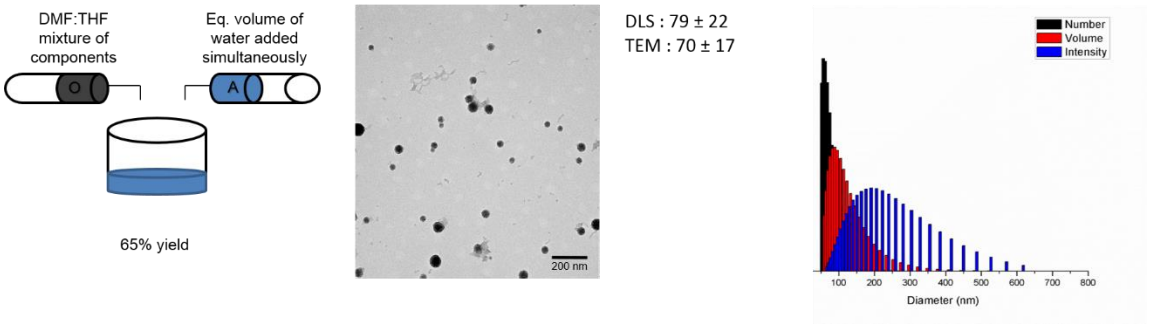

Figure 3.1. Co-assembly method, and TEM and DLS characterization of magneto micelles.

Crosslinking of magneto micelles. MSCKs were obtained by the nominal crosslinking of *ca*. 25% of the acrylic acid moieties utilizing the crosslinker (2,2'-

ethylenedioxy)bis(ethylamine) in the presence of 1-(3-(dimethylamino)propyl)-3-ethyl-carbodiimide methiodide (EDCI). Extensive dialysis against nanopure water was performed to remove unreacted small molecules and reaction by-products. The resulting MSCKs were characterized by DLS and TEM. DLS analysis indicated an average number hydrodynamic radius of 68 ± 18 nm. TEM analysis showed nanoparticles of 75 ± 30 nm diameter (after counting over 80 micelles) (Fig. 3.2).

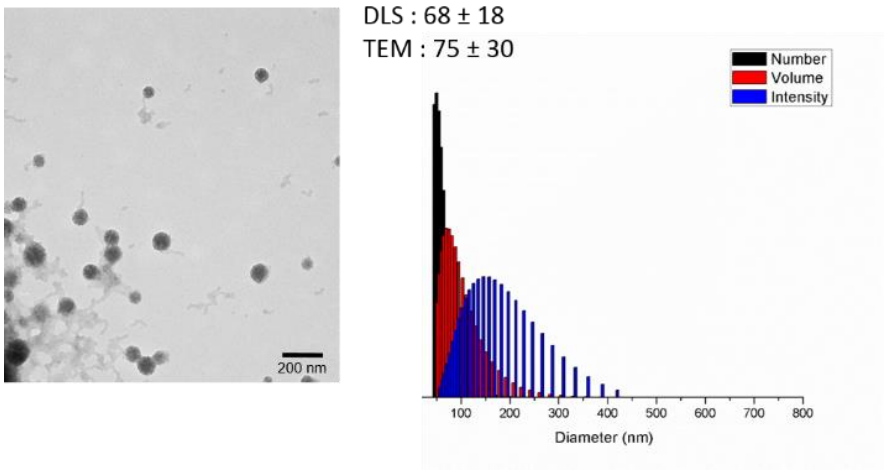

Figure 3.2. TEM and DLS characterization of MSCK nanoparticles produced through dual solvent co-assembly method.

Solvent effect studies. To assess morphological effects and behavior of these MSCK nanoparticles in different solvent systems, qualitative light scattering (Fig. 3.3), TEM (Fig. 3.4), and contact angle (Table 3.1) were employed. Aliquots of an MSCK solution in nanopure water were concentrated using Centricon centrifugal tubes (MWCO 100 kDa) and resuspended in deionized (DI) water, filtered seawater (obtained from Corpus Christi, Texas), artificial seawater,[112] ethanol, and chloroform. Resuspension in DI water was performed as a control study of the resuspension of the MSCKs; seawater and artificial seawater were chosen to assess the behavior of these hybrid nanoparticles in an ocean-water like environment. Ethanol has previously been utilized as a washing solvent during recyclability studies of the MSCKs,[110] and for this reason, ethanol was chosen as a solvent of interest. Chloroform is a favorable solvent for the type of light sweet crude oil used for the uptake experiments and was chosen to investigate its interaction with the MSCK system.

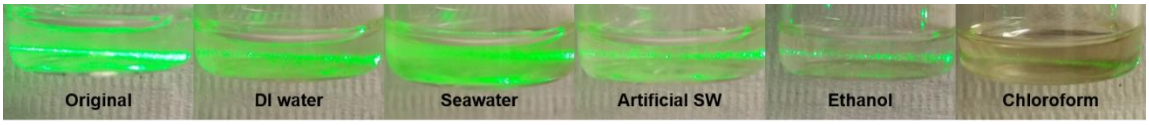

Figure 3.3. Images representing qualitative light scattering of MSCKs in various solvents.

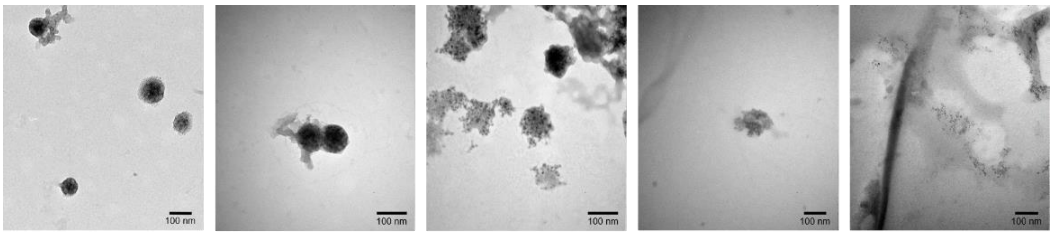

Figure 3.4. TEM characterization of MSCK nanoparticles in DI water, seawater (SW), artificial seawater (ASW), ethanol (EtOH), and chloroform ($CHCl_3$).

Solvent	Contact Angle of MSCK	Contact Angle of Glass Slide
DI Water	40° ± 4°	60° ± 1°
Seawater	45° ± 7°	61° ± 3°
Artificial Seawater	36° ± 6°	62° ± 6°
Ethanol	12° ± 1°	12° ± 2°
Chloroform	6° ± 1°	10° ± 1°

Table 3.1. Contact angle measurements of MSCK coated glass cover slides and corresponding controls.

Using a green handheld laser pointer, the light scattering of the resuspended solutions was determined qualitatively. From this experiment, it was observed that the MSCK nanoparticles resuspended well in DI and seawater due to the lack of precipitate observed and the similarity of the light scattering to the original MSCK solution. These results were corroborated by TEM results showing morphological stability and round

particles identical to those of the original MSCK system prior to resuspension. However, in the resuspension with artificial seawater some precipitate was observed, and there was poor light scattering of the laser through the sample. MSCK nanoparticles observed through TEM showed a circular-like morphology with ill-defined edges. A possible explanation could be due to excess salts as some issues were encountered during imaging due to salt deposits on the surface of the grid. A significant amount of precipitate was observed in the ethanol resuspension resulting in poor light scattering. The iron oxide nanoparticles precipitate in ethanol which could be the cause of the overall precipitation, and this hypothesis was supported by TEM characterization showing ill-defined MSCK nanoparticles with poorly demarked iron oxide nanoparticles. The chloroform sample was a noticeable brown with poor light penetration through the sample. It was hypothesized that a possible inversion or disassembly of the MSCKs could occur upon interaction with chloroform, which is visible in the TEM image showing free iron oxide nanoparticles throughout the grid with undistinguished polymer.

Glass cover slides were drop-casted with 3 mL of a MSCK solution in nanopure water and the solvent was allowed to evaporate over a period of 3 days. Contact angle measurements were taken using a 1 μL sessile drop of the desired solvent. Controls of the various solvent systems onto pristine glass cover slides were also performed under the same conditions. Due to the hydrophilic shell of the MSCK system, contact angles were hypothesized to be hydrophilic in all samples with the exception of chloroform. As expected, the contact angles for DI water, seawater, and artificial seawater showed

positive hydrophilic interactions between the solvents and the MSCK nanoparticles, supported by the light scattering similarity with the original solution, indicating stability in the resuspension. For the ethanol samples, comparable contact angles were observed for the MSCK and control slides. It is hypothesized that the MSCK contact angle observed is due to a lack of interaction between the MSCK system and solvent, and is a result of the precipitation of the iron oxide nanoparticles in ethanol as observed through the poor light scattering and the lack of well-defined MSCK nanoparticles through TEM characterization. From the qualitative light scattering experiment and TEM analysis of the chloroform samples, the MSCK system dissolves rather than resuspends in chloroform explaining the similarity in contact angles between the chloroform sample and the glass slide control. These results explain the physical changes, observed through infrared spectroscopy, experienced by the MSCK system following washings in ethanol prior to reuse.[110] Furthermore, the stability of this system in seawater broadens their potential impact in the field of nanoremediation.

Modified co-assembly and crosslinking of magneto micelles. Deployment of personnel and equipment is a vital response immediately following an oil spill. Although the longevity of an oil spill response is dependent on the size and environmental impact of the spill, transportation of chemicals and materials to and from the site incurs major expenses. In order to address the possibility of the use of MSCKs at oil spill sites and/or other environmental remediation sites, we have begun addressing the option of their on-site generation. The problems presented by the use of multiple organic solvents and the need of dual addition of organics and water for the co-assembly

of this system have been addressed through a modification of the original process. Magneto micelles were produced from the co-assembly of the amphiphilic diblock copolymers and hydrophobic iron oxide nanoparticles, as previously reported. The PAA_{30}-*b*-PS_{200} polymers were dissolved in THF and 2 mL of a 10 mg/mL solution of iron oxide nanoparticles in THF to afford a final concentration of 0.33 mg/mL for both inorganic and organic components. The modification into a purely THF systems bypasses the problem of needing to transport two organic solvents for the production of MSCKs. This organic solution was added in a dropwise manner, concurrently alongside an equal-volume of nanopure water, to a vessel containing 0.33× volume of nanopure water. The resulting hybrid micellar solution was filtered through a 5 μm filter in order to remove iron oxide precipitate formed during the co-assembly process. It should be noted, that the amount of precipitate generated through this modified method was visually greater than that generated through the dual solvent system. Finally, the excess organic solvent was removed through extensive dialysis (MWCO 12-14 kDa) against nanopure water for 24 h. The resulting nanoparticles were characterized through DLS and TEM. DLS analysis indicated an average number hydrodynamic radius of 75 ± 18 nm. TEM analysis showed nanoparticles of 70 ± 11 nm diameter (after counting over 50 micelles) (Fig. 3.5).

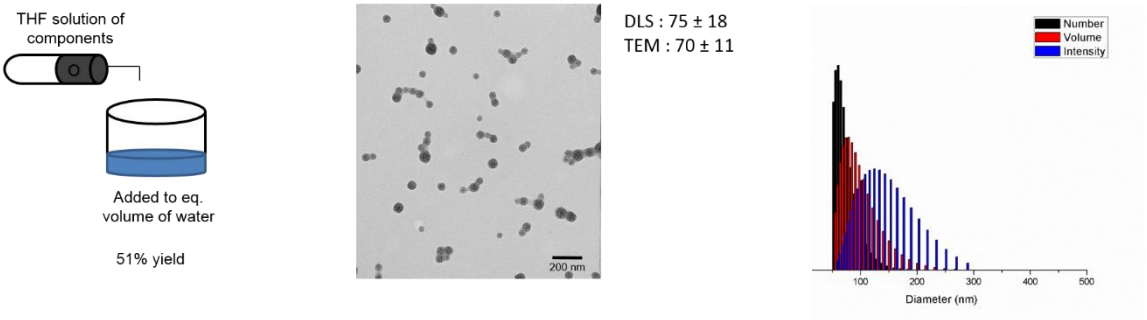

Figure 3.5. Co-assembly method, and TEM and DLS characterization of magneto micelles produced through mono solvent technique.

MSCKs were obtained by the nominal crosslinking of *ca*. 25% of the acrylic acid moieties utilizing the crosslinker (2,2'-ethylenedioxy)bis(ethylamine) in the presence of EDCI. Extensive dialysis against nanopure water was performed to remove unreacted small molecules and reaction by-products. The resulting MSCKs were characterized by DLS and TEM. DLS analysis indicated an average number hydrodynamic radius of 66 ± 16 nm. TEM analysis showed nanoparticles of 67 ± 14 nm diameter (after counting over 80 micelles) (Fig. 3.6). The yield of MSCK production was determined following lyophilization of the two MSCK solutions. A yield of 65% was obtained through the dual solvent co-assembly method, and although initial concerns were caused by the larger amounts of precipitate formed during co-assembly through the mono solvent system, a yield of 51% was achieved.

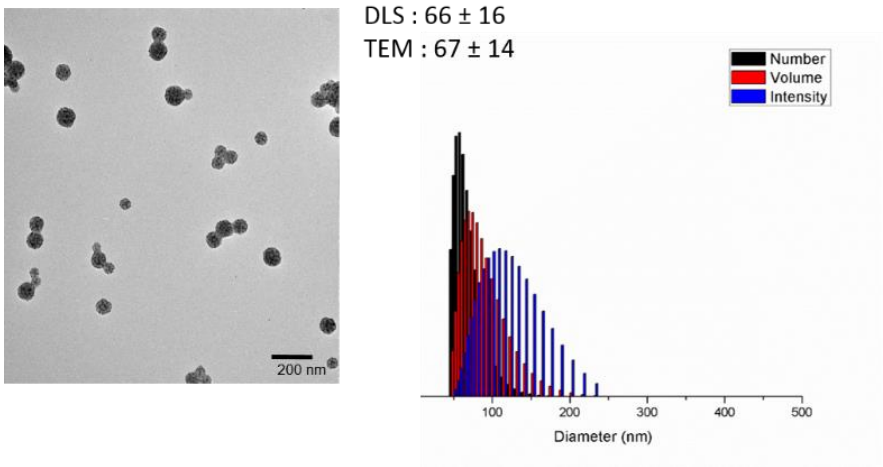

Figure 3.6. TEM and DLS characterization of MSCK nanoparticles produced through mono solvent co-assembly method.

Oil recovery in different aqueous environments. The ability of the MSCKs to serve as sequestration vessels for oil spill recovery in seawater environments was assessed by comparing to the MSCKs' innate capabilities in fresh water environments. Crude oil obtained from the Texas-Oklahoma Enbridge pipeline was first weathered in order to simulate the oil composition found in sheen.[102] The weathered oil was added to deionized (DI) water as a means of mimicking contaminated water in 5 mL vials. The lyophilized powdered nanoparticles were added to the oil contaminated water at initial MSCK:oil ratios of 1:5, 1:10 and 1:15 by weight. Oil sequestration was visually monitored through the change of the MSCK nanoparticles from a light tan to a thick,

dark solid (Fig. 3.7). Qualitatively complete MSCK loading was observed after *ca*. 30 - 45 min. The hybrid magnetic nanoparticles were quickly and efficiently (over 98% nanoparticle recovery) attracted to the external magnetic field of a neodymium magnet to allow for decanting of the polluted water. Extractions of the crude oil from the aqueous environment using chloroform were performed and the remaining hydrocarbon contaminates were analyzed and quantified using gel permeation chromatography (GPC). Using an internal standard of polystyrene (M_w = 70,000 Da) as a means of normalizing the data obtained, the integration of the crude oil peaks (observed in the chromatogram as a broad band with high retention time) was performed by developing a mathematical relationship between the area under the peak and the mass of oil present. This relationship was achieved with the use of control groups to derive an empirical coefficient relating oil concentration to the integration value in the chromatogram. This co-efficient was later utilized to determine the unknown oil concentration in the samples remediated by the MSCKs. Additional details of this methodology can be found in the supplemental information. This experimental procedure was repeated for filtered seawater and artificial seawater utilizing two sets of MSCK nanoparticles for a total of six experimental data sets displaying the two systems' ability to remove the crude oil contaminant (Fig. 3.8). As a control, oil sequestration in DI water was performed to determine the innate capabilities of the MSCK system. A sequestration ratio of 1:7.3 was found for MSCK nanoparticles produced through the di solvent system, with comparable remediation for seawater and artificial seawater at 1:9.5 and 1:8.5, respectively. For the nanoparticles produced through the mono solvent system,

sequestrations of 1:7.7, 1:7.6, and 1:8.2 were found for DI water, seawater, and artificial seawater, respectively. The remediation ratios for the MSCK nanoparticles produced through the two co-assembly systems are comparable, further suggesting that the alteration in the co-assembly technique does not affect the ability of the nanoparticles to sequester oil.

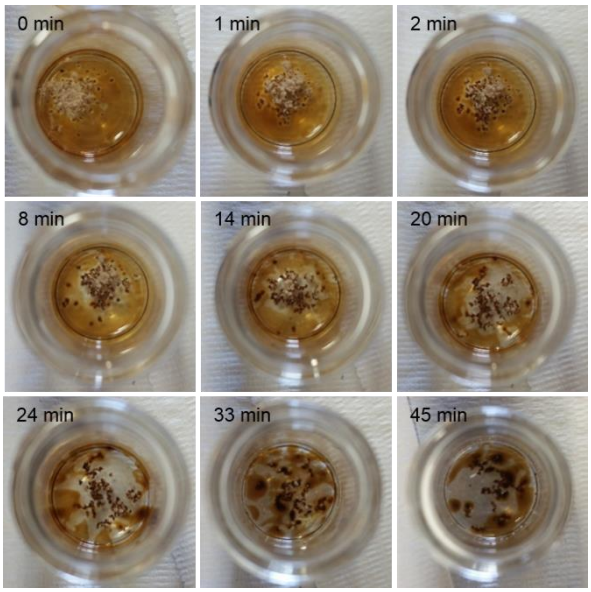

Figure 3.7. Time lapse of oil sequestration by MSCK nanoparticles in DI water over a 45 min time span. Slight agitation was needed to accomplish full visual loading.

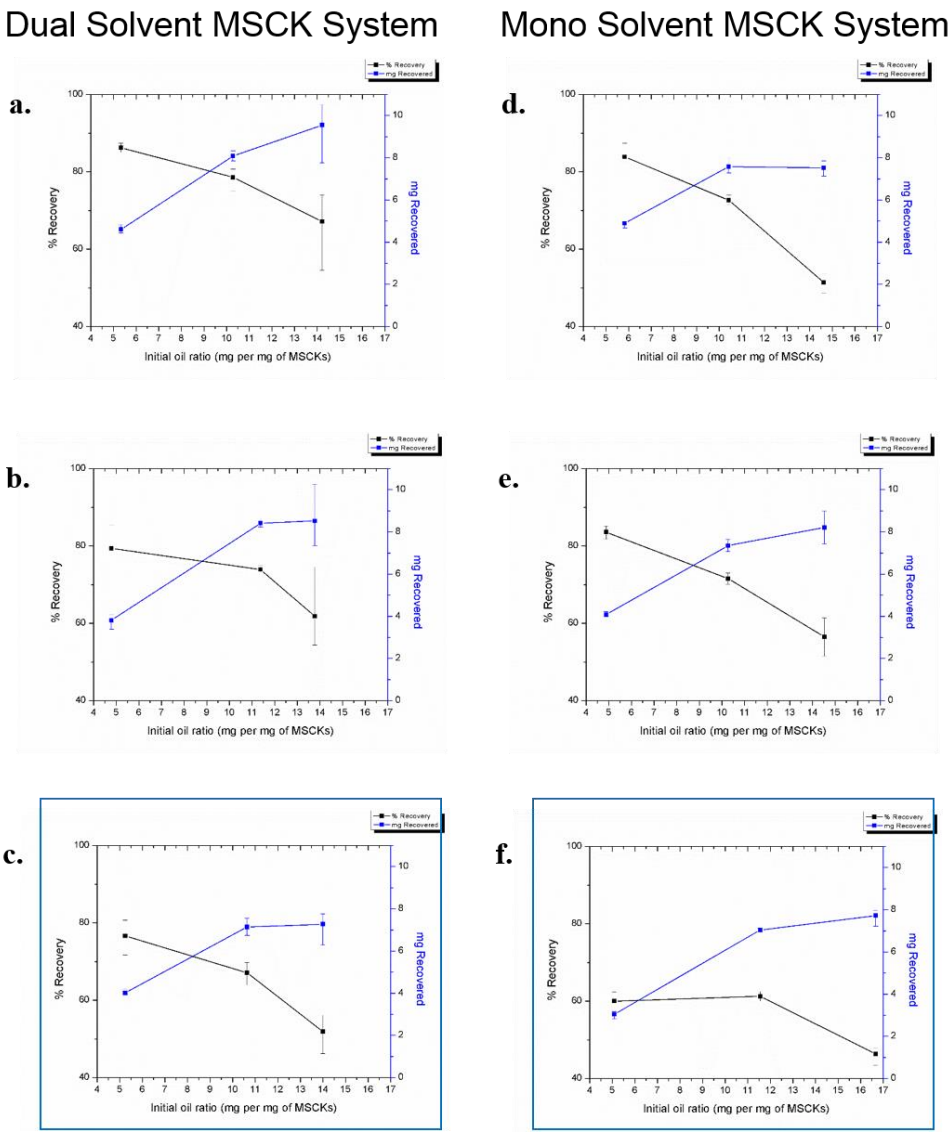

Figure 3.8. Oil recoveries of MSCK nanoparticles produced through dual solvent co-assembly method in seawater (a), artificial seawater (b), DI water (c), and mono solvent so-assembly methods using DI water (c and f), seawater and through mono solvent co-assembly method in seawater (d), artificial seawater (e), and DI water (f).

3.3 Conclusions

Well-defined hybrid nanoparticles tailored to aid in remediation at oil spill sites have been investigated for their crude oil uptake capabilities in seawater environments. It was found that the superb crude oil uptake capacity of these engineered nanoparticles translated into their new seawater environment. Solvent studies in seawater, artificial seawater, ethanol, and chloroform concluded that these MSCK nanoparticles hold their integrity in seawater and artificial seawater; however, some issues were encountered when they were resuspended in ethanol. Following resuspension in chloroform, it was found that MSCKs are dissolved by this organic solvent, potentially causing a breakdown of the morphological assembly. The first steps into the modification of the co-assembly process for on-site development of MSCKs have also been taken through the development of a mono solvent co-assembly method. The size regularity observed between the MSCKs produced by the two co-assembly methods and the 14% difference in the yield achieved hold promise for further advances in the technique to eventually develop a simpler and more efficient production of these engineered nanoremediation tools.

3.4 Materials and Methods

Polymerization of *t*BA *via* ATRP. A flame-dried 100-mL Schlenk flask equipped with a magnetic stir bar was charged with PMDETA (1 eq., 871.7 mg, 5.03 mmol), *t*BA (30 eq., 19.2567 g, 150.4 mmol), ethyl α-bromoisobutyrate (1 eq., 985.6 mg, 5.05 mmol), and anisole (10 mL). The flask was sealed with a rubber septum and

the reaction mixture was degassed by three freeze-pump-thaw cycles, after which the Cu(I)Br (1 eq., 717.9 mg, 5.00 mmol) was added under nitrogen to the frozen mixture. Following two more freeze-pump-thaw cycles, the reaction mixture was allowed to return to room temperature and was allowed to stir for 10 min to ensure homogeneous mixing. The flask was then immersed into a pre-heated oil bath at 55 °C to start the polymerization. The polymerization was monitored by analyzing aliquots collected at pre-determined times by ^{1}H NMR spectroscopy. As the expected monomer conversion was reached, after *ca*. 2 h, the polymerization was quenched by quick immersion of the reaction flask into liquid N_2 and opening to air. THF (20 mL) was added to the reaction flask and the polymer was purified by precipitation into a methanol:ice mixture (2×). The precipitants were collected and dried under vacuum overnight to afford P*t*BA$_{30}$ as a white solid, giving 42% yield of the 78% conversion polymerization. IR: 2978, 2932, 2870, 1720, 1471, 1450, 1388, 1365, 1250, 1142, 1033, 840, 756 cm^{-1}. ^{1}H NMR (300 MHz, $CDCl_3$) δ 4.132 – 4.03 (q, J = 7 Hz, 2H), 2.41 – 2.07 (br, m, 27H), 2.03 – 1.08 (br, m, 300H). ^{13}C NMR 23.5 – 31.7, 34.1 – 36.9, 36.9 – 38.8, 40.5 – 43.3, 80.3 – 81.1, 173.2 – 174.9 ppm. DSC: T_g = 20 °C. TGA: T_{onset} = 196 °C, $T_{decomposition}$ = (196 – 210 °C) 44% mass loss; (298 – 440 °C) 36% mass loss; 20% mass remaining.

Chain growth of styrene from P*t*BA$_{30}$. A flame-dried 25-mL Schlenk flask equipped with a magnetic stir bar was charged with P*t*BA$_{30}$ (1 eq., 994.9 mg, 0.2551 mmol), styrene (500 eq., 13.2868 g, 127.758 mmol), PMDETA (1.23 eq., 54.4 mg, 0.3139 mmol) and anisole (13 mL). The flask was sealed with a rubber septum and the reaction mixture was degassed by three freeze-pump-thaw cycles, after which the

Cu(I)Br (1 eq., 37.0 mg, 0.2579 mmol) was added under nitrogen to the frozen mixture. Following two more freeze-pump-thaw cycles, the reaction mixture was allowed to return to room temperature and was allowed to stir for 10 min to ensure homogeneous mixing. The flask was then immersed into a pre-heated oil bath at 95 °C to start the polymerization. As the expected monomer conversion was reached, after *ca*. 43 h, the polymerization was quenched by quick immersion of the reaction flask into liquid N_2 and opening to air. The polymer was purified by precipitation into a 1:1 methanol:ice water mixture (×3). After 40% conversion of the monomer, the polymer was retrieved with a 90% yield. GPC showed the M_n and PDI of 28,240 Da and 1.15, respectively, of the P*t*BA_{30}-*b*-PS_{200} polymer. IR: 3063, 3024, 2970, 2924, 2854, 1944, 1874, 1805, 1728, 1597, 1489, 1450, 1388, 1365, 1257, 1149, 1072, 1026, 902, 848, 756, 694 cm^{-1}. ^{1}H NMR (300 MHz, $CDCl_3$) δ 7.37 – 6.85 (br, m, 300H), 6.85 – 6.28 (br, m, 195H), 2.52 – 1.73 (br, m, 190H), 1.72 – 1.09 (br, m, 400H). ^{13}C NMR (75 MHz, $CDCl_3$) δ 27.8 – 30.9, 39.3 – 45.1, 123.1 – 132.3, 143.7 – 148.3 ppm. DSC: T_g = 100 °C. TGA: T_{onset} = 378 °C, $T_{decomposition}$ = (378 – 425 °C) 91% mass loss; 9% mass remaining.

Deprotection of P*t*BA_{30}-*b*-PS_{200}. P*t*BA_{30}-*b*-PS_{200} (1 eq., 5 g, 0.125 mmol) was dissolved in DCM (50 mL). TFA (4244 eq., 25 mL, 34,000 mol) was added to the stirring reaction mixture and allowed to react for 18 h. The amphiphilic product was dialyzed against nanopure water for 3 days to remove organic solvent and side products to afford a 95% yield. IR: 3680 – 2167, 3063, 3024, 2924, 2854, 1944, 1874, 1805, 1713, 1597, 1489, 1450, 1365, 1257, 1172, 1072, 1026, 902, 756, 694 cm^{-1}. ^{1}H NMR (300 MHz, THF) δ 7.33 – 6.82 (br, m, 300H), 6.82 – 6.28 (br, m, 200H), 2.52 – 1.72 (br,

m, 190H), 1.72 – 1.09 (br, m, 180H). ^{13}C NMR (75 MHz, $CDCl_3$) δ 27.8 – 30.9, 39.3 – 48.3, 124.0 – 131.9, 145.4 – 147.9, 176.4 – 177.0 ppm. DSC: T_g = 100 °C. TGA: T_{onset} = 383 °C, $T_{decomposition}$ = (383 – 430 °C) 92% mass loss; 8% mass remaining.

Thermolysis of iron oxide nanoparticles. A flame-dried, 100 mL 3-neck flask equipped with a magnetic stir bar and condenser and was charged with $Fe(acac)_3$ (1 eq., 1.2130 g, 3.6 mmol), oleic acid (3.6 eq., 3.4561 g, 12.2 mmol) and oleylamine (3.5 eq., 3.2098 g, 12.0 mmol). After addition of benzyl ether (20 mL) and 1,2-hexadecanediol (6.1 eq., 5.2355 g, 20.7 mmol), the reaction mixture was degassed by a four-cycle expose to vacuum and nitrogen. Reaction temperature was taken to 140 °C and pressure inside reaction vessel was controlled by the insertion of a needle. After an hour, the needle was removed and reaction temperature was taken to 200 °C for an additional hour, following an hour at 250 °C. Once reaction mixture was cooled to room temperature, it was transferred into a centrifuge tube and nanoparticles were precipitated by addition of ethanol (×3) and re-suspended in THF. Final nanoparticle size was determined *via* TEM and DLS as 8 ± 2 nm in diameter.

Co-assembly of original MSCK system. An organic solution containing 2 mL of a 10 mg/mL of PAA_{30}-*b*-PS_{200} in DMF was diluted with a mixture of 28 mL of DMF and 28 mL of THF. To this, 2 mL of a 10 mg/mL solution of iron oxide nanoparticles were added. The solution was allowed to stir vigorously for 20 minutes. The organic mixture (60 mL) and nanopure water (60 mL) were added at the same rate (20 mL/h) to an initial volume of 20 mL of nanopure water. Following filtering through a 5 μm filter, the resulting nanoparticles were dialyzed against nanopure water. Four batches were

produced in this manner and were combined for particle characterization. DLS analysis indicated an average number hydrodynamic radius of 79 ± 22 nm. TEM analysis showed nanoparticles of 70 ± 17 nm diameter (after counting over 50 micelles). MSCKs were obtained by crosslinking nominally 25% of the acrylic acid repeat units by amidation with the diamine crosslinker (2,2'-ethylenedioxy)bis(ethylamine) in the presence of 1-(3-(dimethylamino)propyl)-3-ethyl-carbodiimide methiodide (EDCI). Extensive dialysis against nanopure water was performed to remove unreacted small molecules and reaction by-products. The resulting MSCKs were characterized through DLS and TEM. DLS analysis indicated an average number hydrodynamic radius of 68 ± 18 nm. TEM analysis showed nanoparticles of 75 ± 30 nm diameter (after counting over 80 micelles). Yield for this process was calculated to be 65%.

Modified co-assembly and crosslinking of MSCK system. An organic solution containing 10 mg of PAA-*b*-PS in 29 mL of THF was made. To this, 1 mL of a 10 mg/mL solution of iron oxide nanoparticles were added. The solution was allowed to stir vigorously for 20 minutes. The organic mixture (30 mL) was added at a rate of 20 mL/h to an equal volume (30 mL) of nanopure water. Following filtering through a 5 μm filter, the resulting nanoparticles were dialyzed against nanopure water. Seven batches were produced in this manner and were combined for particle characterization. DLS analysis indicated an average number hydrodynamic radius of 75 ± 18 nm. TEM analysis showed nanoparticles of 70 ± 11 nm diameter (after counting over 50 micelles). MSCKs were obtained by crosslinking nominally 25% of the acrylic acid repeat units by amidation with the diamine crosslinker (2,2'-ethylenedioxy)bis(ethylamine) in the

presence of 1-(3-(dimethylamino)propyl)-3-ethyl-carbodiimide methiodide (EDCI). Extensive dialysis against nanopure water was performed to remove unreacted small molecules and reaction by-products. The resulting MSCKs were characterized through DLS and TEM. DLS analysis indicated an average number hydrodynamic radius of 66 ± 16 nm. TEM analysis showed nanoparticles of 67 ± 14 nm diameter (after counting over 80 micelles). Yield for this process was calculated to be 51%. It must be noted that visually, there was more precipitate formation during the co-assembly process using this modified method than with the original two solvent system.

Oil recovery experiments. Three different aqueous environments were tested for oil recovery by MSCKs: DI water, artificial seawater, and Corpus Christi seawater. Both of the seawater samples were filtered through a 5 μm filter prior to experimentation in order to remove any solid particulates (e.g. salts, sand, plant residue, etc.). Samples were performed in triplicate alongside controls groups, which were also performed in triplicate.

General procedure for oil recovery. Weathered crude oil was added drop-wise to 6 vials containing 3 mL of water. Half of the vials (labeled as controls), were set aside while the remaining three were treated with lyophilized MSCKs. Experiments at 1:5, 1:10, and 1:15 of MSCK to oil ratios were performed. Oil recovery by MSCKs was allowed to take place with minimal movement of the vials. After *ca*. 20-30 minutes, the MSCKs were magnetically separated. The remaining oil and water, in both the tested and control samples, were decanted and the original vials were rinsed (×3) to ensure maximum transfer of oil/water. The oil was extracted from the aqueous phase with

chloroform (2 mL ×3). The resulting brown/maroon organic solutions were dried over magnesium sulfate and filtered. Samples for quantification was prepared through the mixture of 1 mL of the oil solution and 0.5 mL of a 1 mg/mL solution of a 70,900 Da polystyrene standard in chloroform. These samples were injected into the $CHCl_3$ GPC for quantification. The control samples were used to derive an empirical coefficient, k, for a direct correlation between the areas under the peaks and the amount of oil corresponding to them. This experiment was performed for three types of aqueous systems (DI water, artificial seawater, and Corpus Christi seawater) and for two MSCK batches (co-assembled through a two-solvent system, and through a modified one-solvent system) for a grand total of 54 samples (triplicates for three different concentrations, for three types of water, and two batches of MSCKs).

The results of these studies indicate no difference in the uptake capabilities of the MSCKs, across the two different MSCK batches, as well as no uptake differences in the three different aqueous environments. The results of these studies suggest that the modification in the co-assembly of the MSCKs is a viable option for on-site particle development. Although there were was visually more precipitate observed in the modified co-assembly, the yield only varied slightly, 65% to 51%, between the original and modified method, respectively. These experiments also suggest that the aqueous environment does not affect the loading capabilities of the MSCKs, at least while the remediation occurs at the surface of the contaminated water. Currently ongoing are experiments regarding the morphological changes experienced by the MSCKs in different solvent environments.

CHAPTER IV

AN INNOVATIVE AND VERSATILE APPROACH FOR THE REMEDIAITON OF THE PERSISTENT AND UBIQUITOUS POLLUTANT PERFLUOROOCTANOIC ACID (PFOA) FROM AQUEOUS-BASED SYSTEMS

4.1 Introduction

Perfluorooctanoic acid (PFOA) is a man-made pollutant that has permeated our global environment through its release as a byproduct from fluorochemical facilities.[40] This contaminant's properties, notably its high water solubility (9.5 g/L) and moderate sorption to solids, present a particular threat to aqueous systems. Bioremediation of PFOA by natural fauna is virtually impossible and has resulted in its persistence in groundwater, wastewater, and drinking water throughout the Unites States.[48-50] In 2006, the United States Environmental Protection Agency (US EPA) began its PFOA Stewardship Program with the reduction of PFOA emissions as an immediate objective, and the phasing-out of this toxic chemical by the end of 2015.[51] In spite of this, this persistent organic pollutant continues to befoul the environment.[113,53] Due both to its low bio-degradability and moderate sorption to solids, PFOA has been found in human-desolate areas and has shown to have negative effects on animal species, including polar bears, sea otters, fish-eating birds, *etc.*[44-47] Additionally, PFOA is found in blood samples of the general population, and although its effects are still not fully understood, it has been linked to developmental defects and diseases,[41,42] and other health issues.[43] The unique properties of PFOA allow it to resist conventional remediation techniques

and has limited its treatment to *ex situ* methods,[40] with incineration as the primary method for complete removal.[53]

Recent advances for the removal or decomposition of PFOA include the use of activated carbon filters,[54,55] nanofiltration,[23] photochemical decomposition,[56-59] and adsorption.[60] As a notable example, Giri and coworkers demonstrated the full decomposition (*ca.* 1.78 E^{-3} mg) of PFOA using low-pressure UV lamps and potassium iodide in a 3 h period;[56] these experiments were one of the first examples of photoreductive degradation of this perfluorinated pollutant. However, despite this advance, the technique is restricted to surface and contained water due to the penetration limits of UV light, and additional issues may be encountered from the production of smaller-chained perfluorinated byproducts whose transport and other environmental effects are not well-known. More recently, the adsorption of perfluorinated pollutants, including PFOA, has been of particular interest due to the technique's efficiency.[61] For example, work by Nassi *et al*. testing different mesoporous silica materials showed significant PFOA adsorption. Of the materials tested, solvent extracted hexagonal mesoporous silica (HMSe) demonstrated the highest PFOA adsorption (almost 6.2 E^{-3} mg of PFOA per mg of HMSe) across a pH range of 5-9.[60]

Although mesoporous materials have shown promise for the removal of PFOA, tailored polymeric materials are expected to have better performance. Polymer brushes grafted onto cotton through surface modified atom transfer radical polymerization (ATRP) have shown a significant increase in PFOA sorption, notably that of 1.3 mg/mg for this engineered material.[114] However, the adsorption of PFOA onto non-modified

cotton was not performed, so it is unknown how effective the pristine material is for this particular application. Additionally, this technique is limited in its deployment due to feasibility constraints as this macromaterial would have to be constrained to mechanical manipulation and recovery, and furthermore, its application in groundwater systems is not feasible.

Another intricately designed polymeric system is that of Koda *et al.*'s fluorous microgel star polymers. This crosslinked system is comprised of a fluorinated core for enhanced solubility and stabilization of the perfluorinated pollutant and has shown to selectively separate perfluorinated pollutants from aqueous systems. However, this system is limited by its maximum uptake capabilities, which was determined to be *ca.* 4 E^{-3} mg/mg.[62] We anticipate that a nanoscopic amphiphilic polymeric system with a partially fluorinated core is necessary to obtain an enhanced loading of PFOA based on fluorous interactions in the core, while also allowing the system to be stable, well-suspended in an aqueous environment, and allow for its future application in porous groundwater environments. Moreover, the non-covalent incorporation of magnetic iron oxide nanoparticles is expected to facilitate the manipulation and recovery of the material.[110]

4.2 Results and Discussion

Design of MSCK-F_9 nanoparticles for PFOA removal. These MSCK-F_9 nanoparticles are part of a library of inorganic-organic structures for pollutant remediation,[110,115] and were tailored with the removal of PFOA and other perfluorinated

pollutants in mind. Four polymeric systems were co-assembled and crosslinked in order to afford the four desired MSCK-F_9 nanoparticles (Scheme 4.1). The magnetic component of these structures was incorporated as a means of facile recovery and manipulation. Iron oxide nanoparticles were chosen as the inorganic magnetic component due to their potential for low toxicity.[92, 116-117]. In order to increase the interaction, and therefore the solubility of the perfluorinated pollutant with the nanoparticle core, a partially fluorinated polymeric component containing P(S-*co*-TFS-F_9) as the hydrophobic domain on the amphiphilic block copolymer was chosen. Polymeric components differing in the composition of their hydrophilic domain were produced in order to study the effect that electrostatic interactions between the perfluorinated pollutant and nanoparticle shell have on the material's inherent pollutant recovery capabilities. These hybrid polymeric systems were shell crosslinked to protect this amphiphilic system from infinite dilution in aqueous environments and to create a more stable and robust system. The non-covalent incorporation of multiple iron oxide nanoparticles allows for reversible expansion and contraction during pollutant loading.

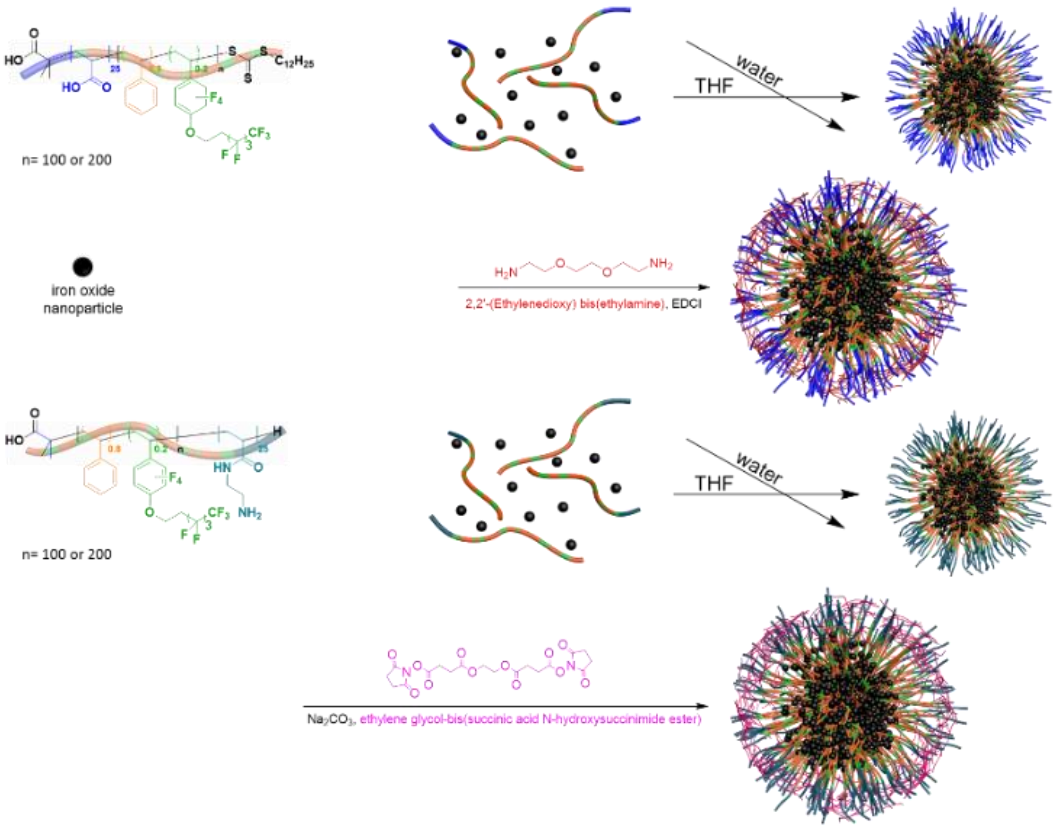

Scheme 4.1. Pictographic representation of co-assembly and crosslinking of MSCK-F_9 nanoparticles. Four polymeric components were co-assembled with iron oxide nanoparticles and shell crosslinked to provide four separate types of MSCK-F_9 nanoparticles.

Fluorinated monomer synthesis. The fluorinated monomer TFS-F_9 was synthesized through a modified process of a previously established method.[118] First, the alcohol, 1H,1H,2H,2H-perfluoro-1-hexan-1-ol, was deprotonated with the use of sodium

hydride in a dry THF reaction mixture, followed by the subsequent addition of 2,3,4,5,6-pentafluorostyrene (PFS) to the cold (0 °C) solution. The reaction was heated to 65 °C and was quenched by the addition of hexanes after full consumption of the PFS starting material. The precipitate was then filtered and the supernatant was washed with a saturated solution of sodium bicarbonate and further extracted with hexanes. The product was purified through column chromatography with hexanes.

Synthesis of fluorinated amphiphilic polymers of PAA-*b*-P(S-*co*-TFS-F_9) and P(S-*co*-TFS-F_9)-*b*-PAEA compositions. The amphiphilic block polymers were produced through sequential reversible addition-fragmentation chain-transfer (RAFT) polymerizations. Polymers with PAA-*b*-P(S-*co*-TFS-F_9) composition were synthesized by the sequential RAFT polymerization of *tert*-butyl acrylate and the copolymerization of styrene and TFS-F_9 monomer in the presence of 2,2′-azobis(2-methylpropionitrile) (AIBN) at 65 °C to afford the hydrophobic precursor of the desired polymer (Scheme 4.2). The polydispersity indices (PDI) of the three polymers produced, the initial poly(*tert*-butyl acrylate)$_{25}$ (P*t*BA_{25}) homopolymer and the subsequent P*t*BA_{25}-*b*-P(S-*co*-TFS-F_9)$_n$ (where n is either 100 or 200), were below 1.2, indicating a monodisperse material (Fig. 4.1). The final amphiphilic block copolymers were obtained by the removal of the *tert*-butyl groups through acidolysis with the aid of trifluoroacetic acid (TFA) in dichloromethane (DCM).

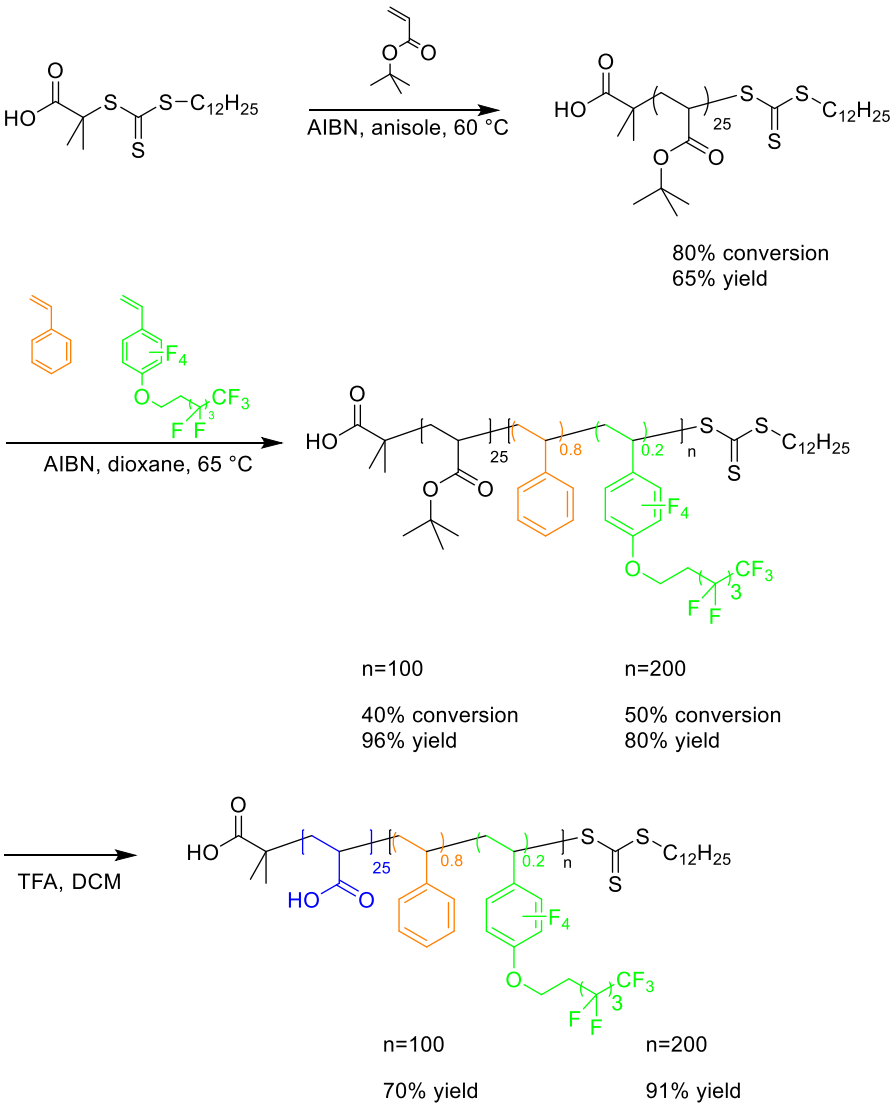

Scheme 4.2. Synthesis of block copolymers of PAA-*b*-P(S-*co*-TFS-F_9) composition.

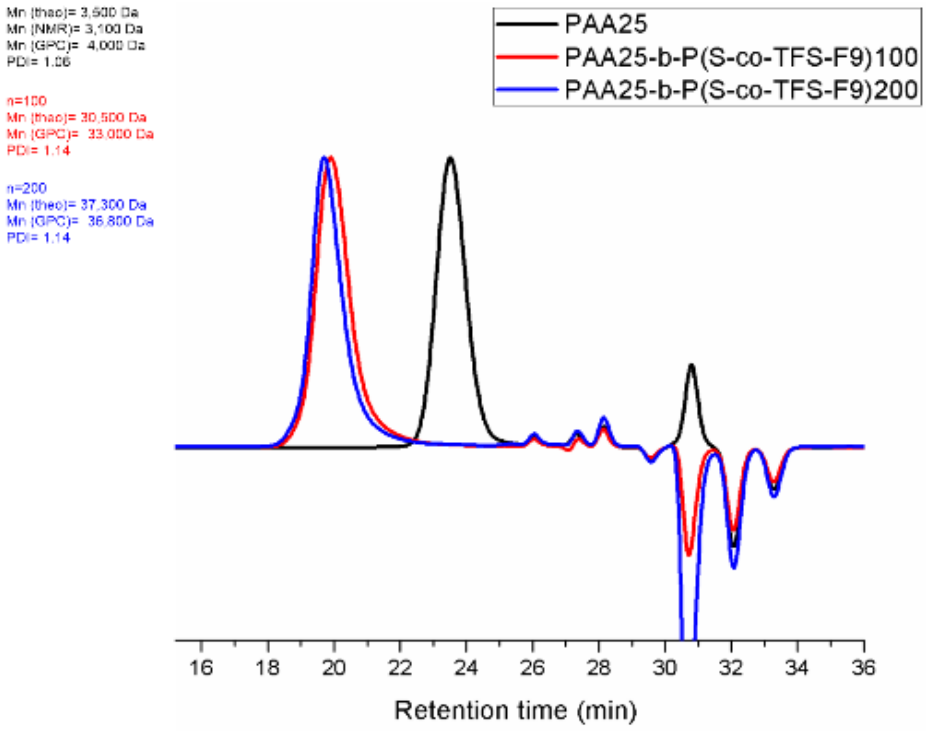

Figure 4.1. GPC traces of PAA homopolymer and PAA-*b*-P(S-*co*-TFS-F_9) block copolymers.

The copolymerization of styrene and PFS-F_9 from poly(*tert*-butyl (2-acrylamidoethyl)carbamate) (PAEA*boc*) resulted in polymers with a PDI of over 1.3, therefore, the order of polymerization was reversed and the polymers with P(S-*co*-TFS-F_9)-*b*-PAEA composition were synthesized by the sequential RAFT copolymerization of styrene and PFS-F_9 monomer and polymerization of *tert*-butyl (2-acrylamidoethyl)carbamate in the presence of AIBN at 65 °C (Scheme 4.3). The polydispersity indices of the four polymers, the initial P(S-*co*-TFS-F_9)$_n$ and the subsequent P(S-*co*-TFS-F_9)$_n$-*b*-PAEA*boc*$_{30}$ (where n is either 100 or 200), were below 1.2 (Fig. 4.2). Difficulties during the co-assembly of these polymers were encountered due to the 12-carbon chain on the ω chain-end of the polymers. This long hydrophobic chain is located at the end of the hydrophilic domain of the polymer and is hypothesized to cause solubility issues during the assemblies (Fig. 4.3). In order to remedy this co-assembly issue, a radical-induced reduction utilizing azobis(cyclohexanenitrile) (ACHN) in the presence of N-ethylpiperidine hypophosphite (EPHP) was performed to substitute the ω chain-end with a hydrogen.[119,120]

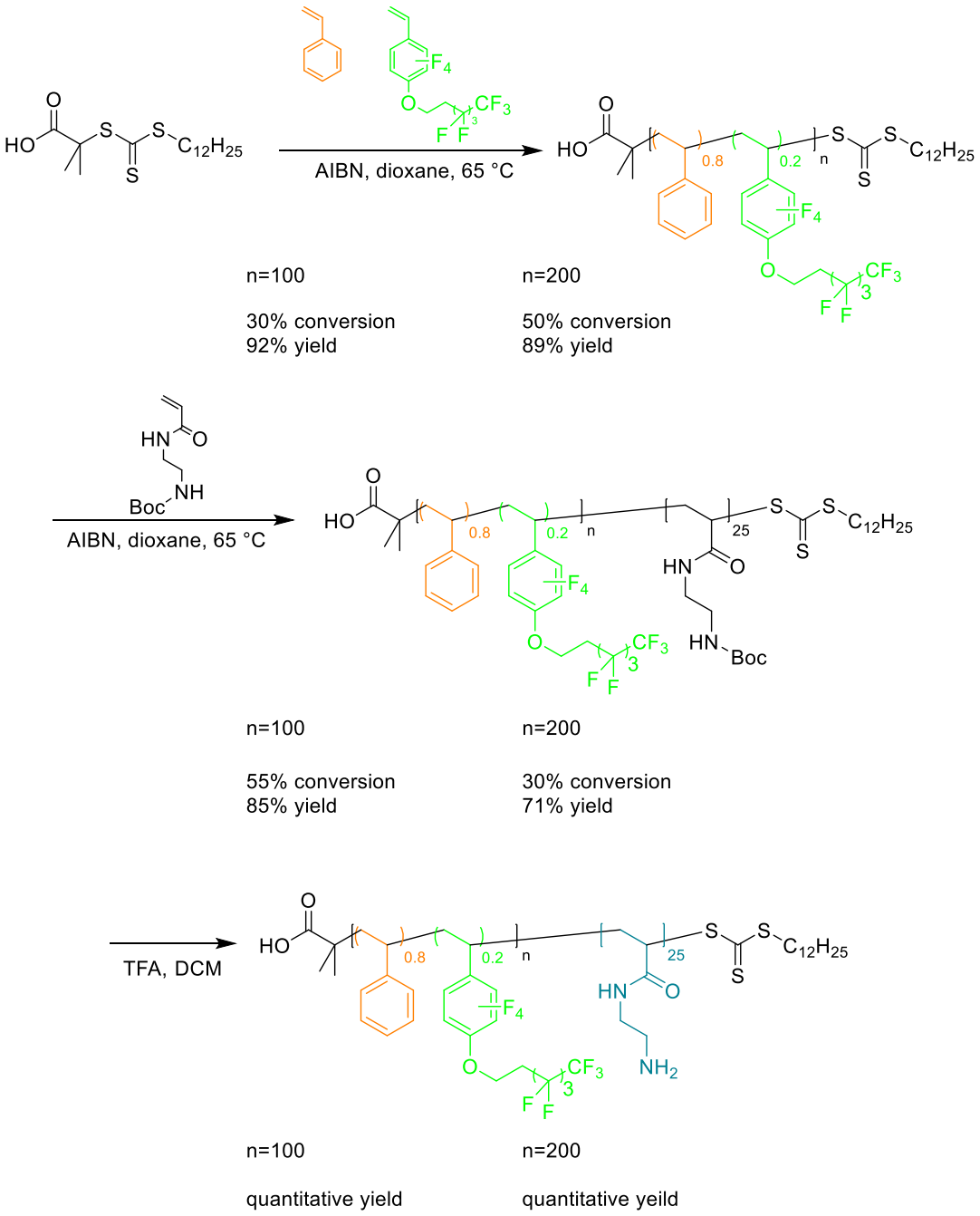

Scheme 4.3. Synthesis of block copolymers of P(S-*co*-TFS-F_9)-*b*-PAEA composition.

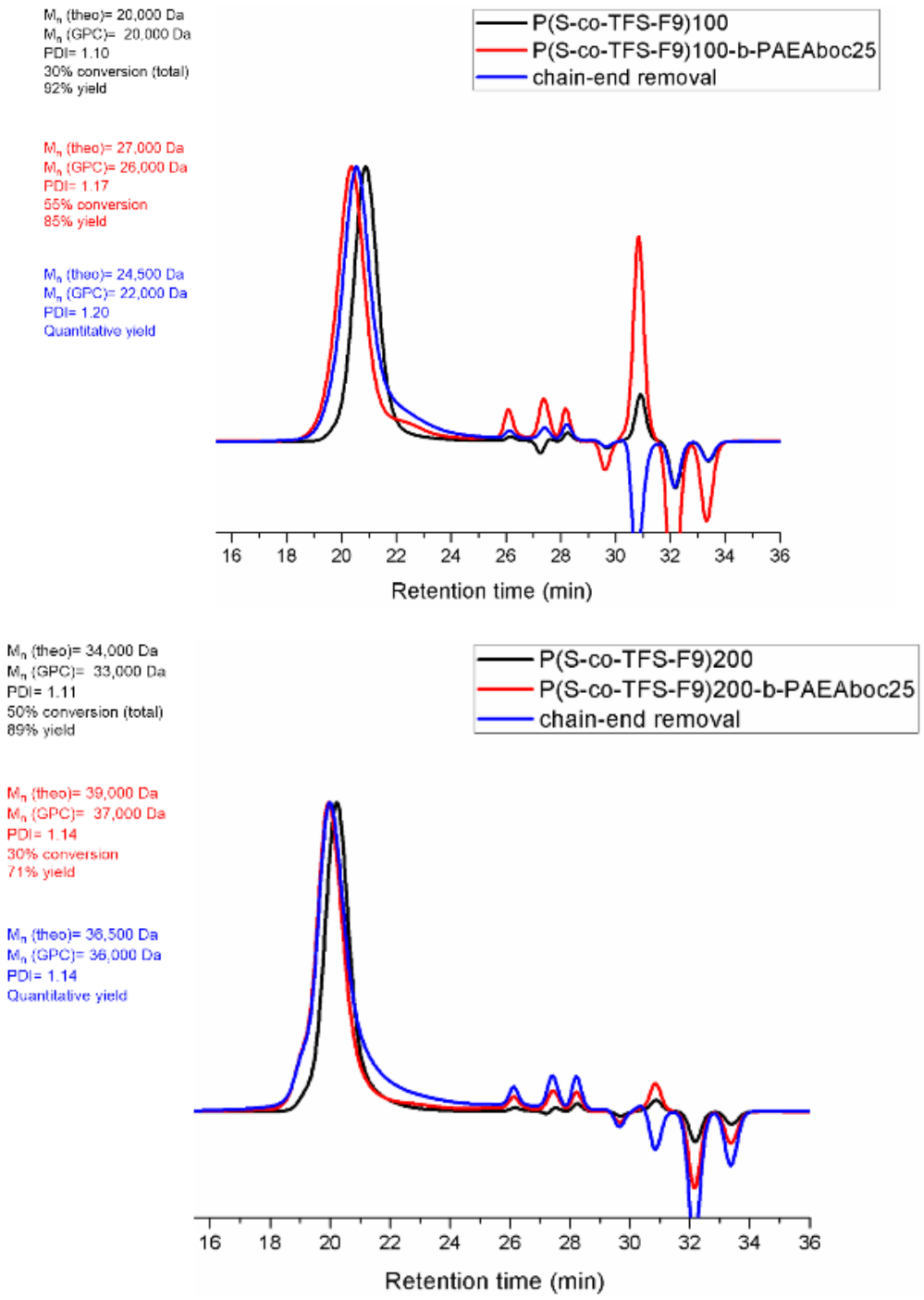

Figure 4.2. GPC traces of P(S-*co*-TFS-F_9)$_{100}$ and P(S-*co*-TFS-F_9)$_{100}$-*b*-PAEA*boc*$_{25}$ block copolymers (top), and P(S-*co*-TFS-F_9)$_{200}$ and P(S-*co*-TFS-F_9)$_{200}$-*b*-PAEA*boc*$_{25}$ block copolymers (bottom).

Confirmation of this removal was observed in the UV-vis spectra of the starting materials and products which showed the removal of the trithiocarbonate functional group at *ca*. 310 nm (Fig. 4.4). Similarly to the other polymers synthesized, the amphiphilic nature of the block copolymers was obtained by a deprotection reaction using TFA in dichloromethane. It should be mentioned here that a total of four amphiphilic polymers were synthesized with two varying lengths of the hydrophobic section of the polymer, that of 100 and 200, all with *ca.* 20% incorporation of the fluorinated monomer, in order to observe the possible difference that an increased concentration of the perfluorinated material would have in the uptake capabilities of the MSCK-F_9 nanoparticles. Due to the highly fluorinated nature of these polymers, an increase in the feed ratio of the fluorinated monomer during the copolymerization of styrene and TFS-F_9 resulted in highly fluorinated polymers with little to no solubility in THF, 1,2-dioxane, or *N*,*N*-dimethylformamide (DMF), and therefore in materials that could not be co-assembled to form hybrid micellar structures.

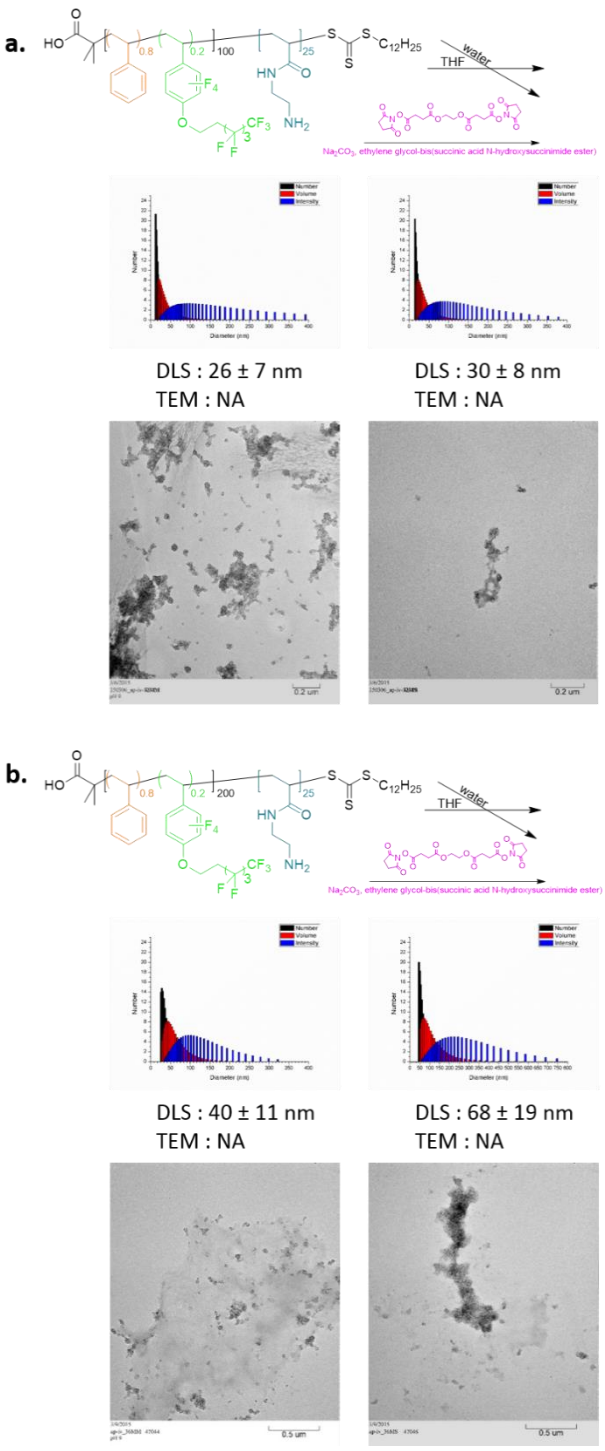

Figure 4.3. DLS and TEM characterization of nanoparticles comprised of P(S-*co*-TFS-F_9)-*b*-PAEA polymeric systems.

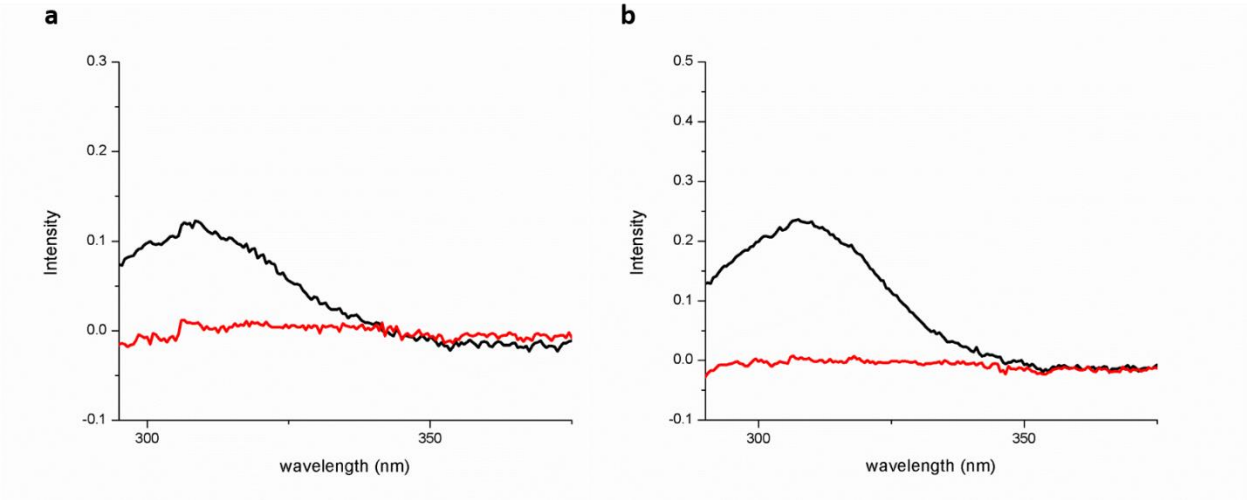

Figure 4.4. UV-vis characterization of the removal of trithiocarbonate functionally from P(S-*co*-TFS-F9)$_{100}$-*b*-PAEA$_{30}$ (a) and P(S-*co*-TFS-F$_9$)$_{200}$-*b*-PAEA$_{25}$ (b). Black lines represent the starting material and the red lines indicate the reaction product. Solutions were prepared in THF at a concentration of 0.6 mg/mL.

General co-assembly of hybrid fluorinated micelles. The co-assembly of the fluorinated magneto micelles was accomplished through a modified method of a previously reported technique.[110] Briefly, 20 mg of the polymeric component were dissolved in THF to achieve a concentration of 0.34 mg/mL. To the stirring solution, 2 mL of a 10 mg/mL iron oxide nanoparticles solution in THF were added and thoroughly mixed. This organic solution was added in a drop wise manner at a rate of 20 mL/h to an equal volume (60 mL) of nanopure water.

Micellar and MSCK-F_9 nanoparticles of PAA-*b*-P(S-*co*-TFS-F_9) composition. During the co-assembly process, it was noted that some dark precipitate had been generated. This precipitate is hypothesized to be iron oxide nanoparticles and is not unusual for the assembly of MSCK systems.[110] Following co-assembly, the resulting nanoparticles were filtered through a 5 μm nylon filter to remove the un-assembled iron oxide nanoparticles. The excess organic solvent was removed through extensive dialysis (tubing having MWCO 12-14 kDa) against nanopure water for over 24 h. The micellar structures were characterized by transmission electron microscopy (TEM) and dynamic light scattering (DLS) (Fig. 4.5). It was observed that the nanoparticles comprised of polymers with a longer hydrophobic segment had slightly larger hydrodynamic radii than those of their shorter-segment counterparts. DLS analysis of hybrid micellar assemblies formed using PAA_{25}-*b*-P(S-*co*-TFS-F_9)$_{100}$ indicated an average number hydrodynamic radius of 54 ± 13 nm and TEM analysis showed nanoparticles of 52 ± 6 nm (after counting over 50 micelles). DLS analysis of hybrid micellar assemblies formed using PAA_{25}-*b*-P(S-*co*-TFS-F_9)$_{200}$ indicated an average number hydrodynamic radius of 63 ± 16 nm and TEM analysis showed nanoparticles of 61 ± 10 nm (after counting over 50 micelles). The magneto micelles were nominally crosslinked using 25% of the pendant acrylic acid groups using (2,2'-ethylenedioxy)bis(ethylamine) in the presence of 1-(3-(dimethylamino)propyl)-3-ethyl-carbodiimide methiodide (EDCI). Extensive dialysis against nanopure water was performed to remove unreacted small molecules and reaction byproducts. TEM and DLS characterization was once again performed in order to confirm that no size or

morphological changes were experienced during the crosslinking process (Fig. 4.5). DLS analysis of MSCKs formed using PAA_{25}-*b*-P(S-*co*-TFS-F_9)$_{100}$ indicated an average number hydrodynamic radius of 60 ± 15 nm and TEM analysis showed nanoparticles of 54 ± 10 nm (after counting over 50 nanoparticles.). DLS analysis of MSCKs formed using PAA_{25}-*b*-P(S-*co*-TFS-F_9)$_{200}$ indicated an average number hydrodynamic radius of 77 ± 22 nm and TEM analysis showed nanoparticles of 68 ± 11 nm (after counting over 50 nanoparticles.).

Micellar and MSCK-F_9 nanoparticles of P(S-*co*-TFS-F_9)-*b*-PAEA composition. Unlike in the co-assemblies using polymers of composition PAA-*b*-P(S-*co*-TFS-F_9), no precipitate was observed during the co-assemblies with polymers of composition P(S-*co*-TFS-F_9)-*b*-PAEA. However, the micellar solutions were filtered through a 5 µm nylon filter for consistency. The excess organic solvent was removed through extensive dialysis (tubing having MWCO 12-14 kDa) against nanopure water for over 24 h. The micellar structures were characterized by TEM and DLS (Fig. 4.6). Similarly, the nanoparticles comprised of polymers with a longer hydrophobic segment had slightly larger hydrodynamic radii than those of their shorter-segment counterparts.

DLS analysis of hybrid micellar assemblies formed using P(S-*co*-TFS-F_9)$_{100}$-*b*-$PAEA_{25}$ indicated an average number hydrodynamic radius of 27 ± 8 nm and TEM analysis showed nanoparticles of 31 ± 10 nm (after counting over 40 micelles). DLS analysis of hybrid micellar assemblies formed using P(S-*co*-TFS-F_9)$_{200}$-*b*-$PAEA_{25}$ indicated an average number hydrodynamic radius of 31 ± 10 nm and TEM analysis showed nanoparticles of 43 ± 12 nm (after counting over 50 micelles). The magneto micelles were nominally crosslinked using 25% of the amine functionalities and ethylene glycol-bis(succinic acid N-hydroxysuccinimide ester) at a pH of 9. Extensive dialysis against nanopure water was performed to remove unreacted small molecules and reaction byproducts. DLS analysis of MSCKs formed using P(S-*co*-TFS-F_9)$_{100}$-*b*-$PAEA_{25}$ indicated an average number hydrodynamic radius of 59 ± 19 nm and TEM analysis showed nanoparticles of 38 ± 8 nm (after counting over 50 micelles). DLS analysis of MSCKs formed using P(S-*co*-TFS-F_9)$_{200}$-*b*-$PAEA_{25}$ indicated an average number hydrodynamic radius of 60 ± 17 nm and TEM analysis showed nanoparticles of 42 ± 5 nm (after counting over 50 micelles) (Fig. 4.6).

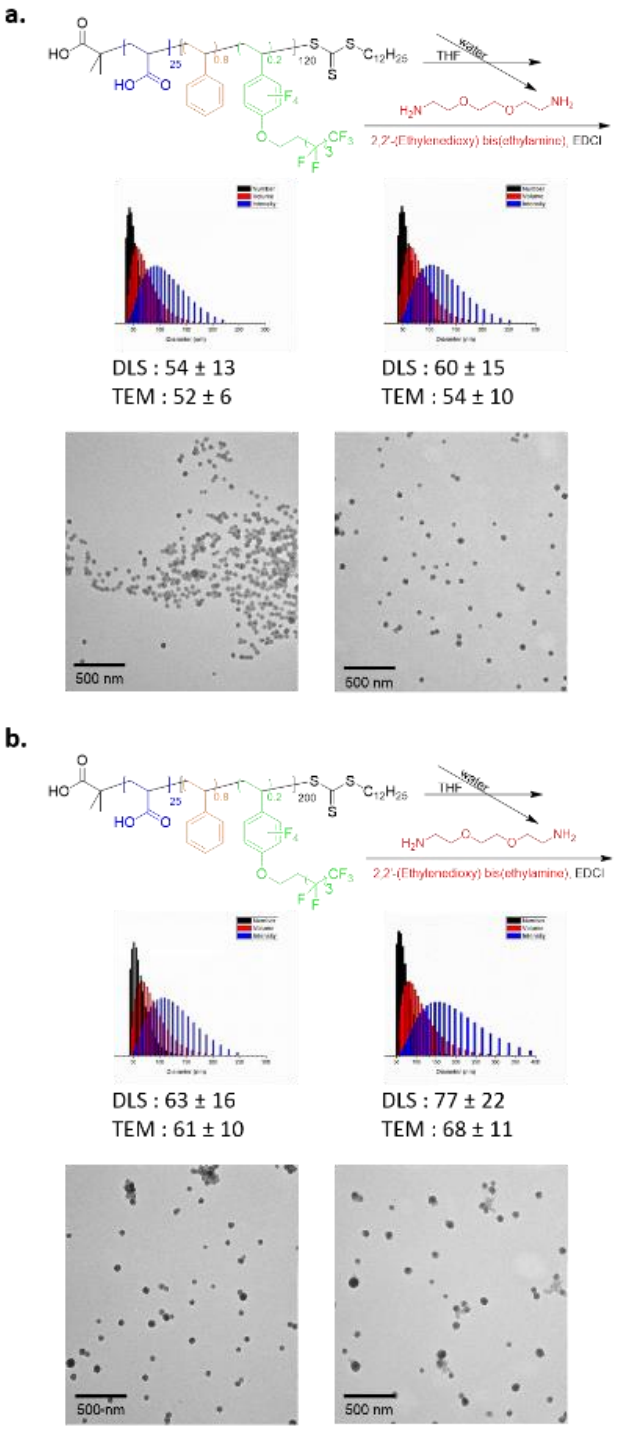

Figure 4.5. DLS and TEM characterization of micellar and MSCK systems comprised of PAA_{25}-b-$P(S\text{-}co\text{-}TFS\text{-}F_9)_{100}$ (a) and PAA_{25}-b-$P(S\text{-}co\text{-}TFS\text{-}F_9)_{200}$ (b).

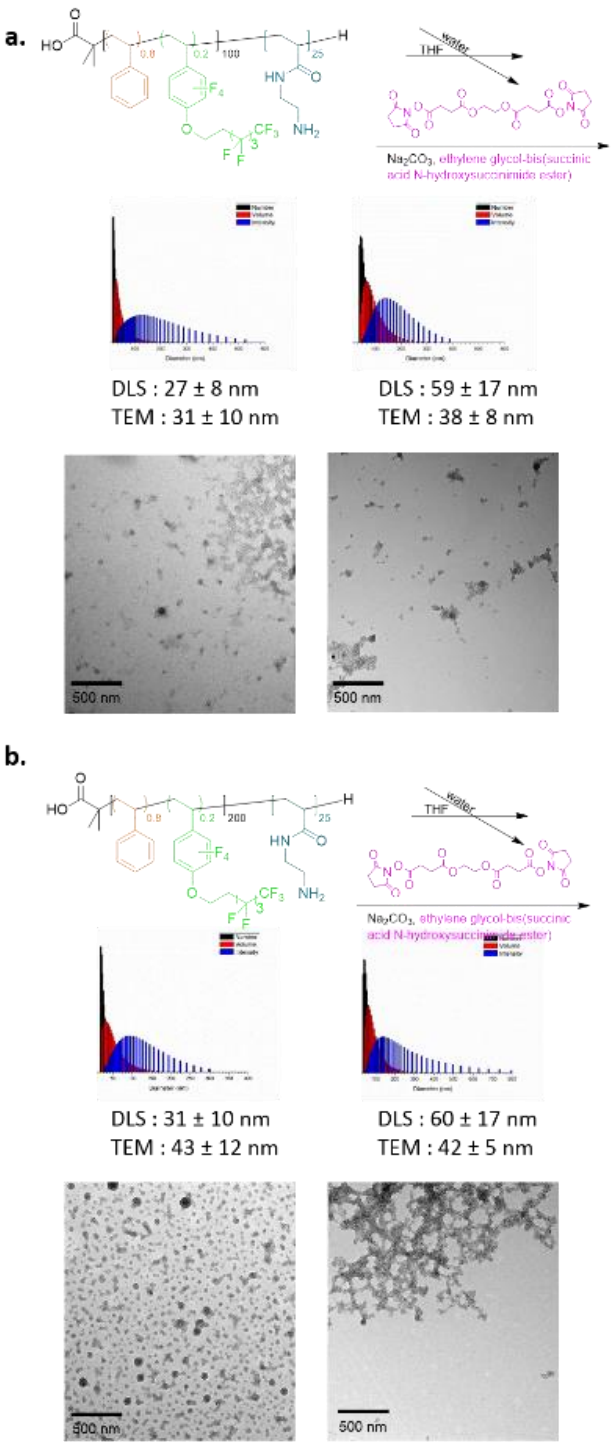

Figure 4.6. DLS and TEM characterization of micellar and MSCK systems comprised of P(S-*co*-TFS-F_9)$_{100}$-*b*-PAEA$_{25}$ (a) and P(S-*co*-TFS-F_9)$_{200}$-*b*-PAEA$_{25}$ (b).

PFOA removal experiments. A 1.5 mg/mL solution of PFOA in deuterated water (D_2O) was prepared as a stock solution of contaminated aqueous media. Experiments were performed for the four MSCK-F_9 nanoparticle systems and eight time points were chosen for these kinetic experiments: 20 min, 45 min, 1.5 h, 3 h, 10 h, 30 h, 100 h, and 200 h, in triplicate. The initial MSCK-F_9 to PFOA ratio used for these experiments was 1:1. A standard loading experiment began by the addition of the lyophilized MSCK-F_9 nanoparticles to the PFOA-polluted solutions. Upon addition, the powdered particles appeared to re-suspend well and throughout the aqueous solution. Following the predetermined amount of time, the MSCK-F_9 nanoparticles were separated using a magnet to allow for aliquots of the solution to be taken; these aliquots were spiked with a solution of TFA-d to aid in quantification. Quantification of PFOA removal was performed through ^{19}F NMR by comparing the integration values of the –CF_3 groups in both PFOA and TFA-d (Fig. 4.7). Briefly, the integrations for the –CF_3 fluorine peak of PFOA in the control samples were set to 100%. The integrations obtained for the –CF_3 fluorine peaks of the TFA-d in the control samples were averaged and utilized in the tested samples, giving an integration value lower than 100 which is directly related to the percent of PFOA remaining in the aqueous systems. Overall, it was observed that PFOA was quickly removed by the MSCK-F_9 nanoparticles and sequestration declined after *ca*. 3 h. Although PFOA sequestration slowed significantly after 30 h, time points at 100 h and 200 h showed continued removal.

It was hypothesized that the MSCK-F_9 nanoparticles composed of P(S-*co*-TFS-F_9)-*b*-PAEA block copolymers would have great PFOA removal due to the favorable

interactions between the positively charged nanoparticle shell and the negatively charge PFAO in solution, but PFOA kinetics showed that 10-20% more PFOA remained in solution after recovery with these PAEA-shelled nanoparticles. However, this discrepancy is thought to be influenced by the size of the particle; the mathematical volumes of a spherical particles with diameters similar to those of these fluorinated nanoparticles are almost an order of magnitude larger for the PAA-shelled MSCK-F_9 nanoparticles than those of the PAEA-shelled nanoparticles. Additionally, it can be assumed that the PAEA-shelled particles also contain a higher amount of iron oxide nanoparticles due to the lack of precipitate formed during the co-assembly process.

The PFOA recoveries of the MSCK-F_9 systems with the four different polymeric systems tested, PAA_{25}-*b*-P(S-*co*-TFS-F_9)$_{100}$, PAA_{25}-*b*-P(S-*co*-TFS-F_9)$_{200}$, P(S-*co*-TFS-F_9)$_{100}$-*b*-$PAEA_{25}$, and P(S-*co*-TFS-F_9)$_{200}$-*b*-$PAEA_{25}$ after 30 h showed removal yield of 20%, 24%, 11%, and 10%, respectively, with slow but continued removal after 30 h achieving a maximum observed removal of 25%, 35%, 13%, and 10%, respectively (Fig. 4.8). These nanoparticles were designed for their eventual use for *in situ* injection treatment and are expected to serve well for this application based on their short term pick up performance. However, their continued recovery after prolonged periods of time opens their application for longer-term groundwater management solutions such as their use in permeable reactive barriers.[121,122]

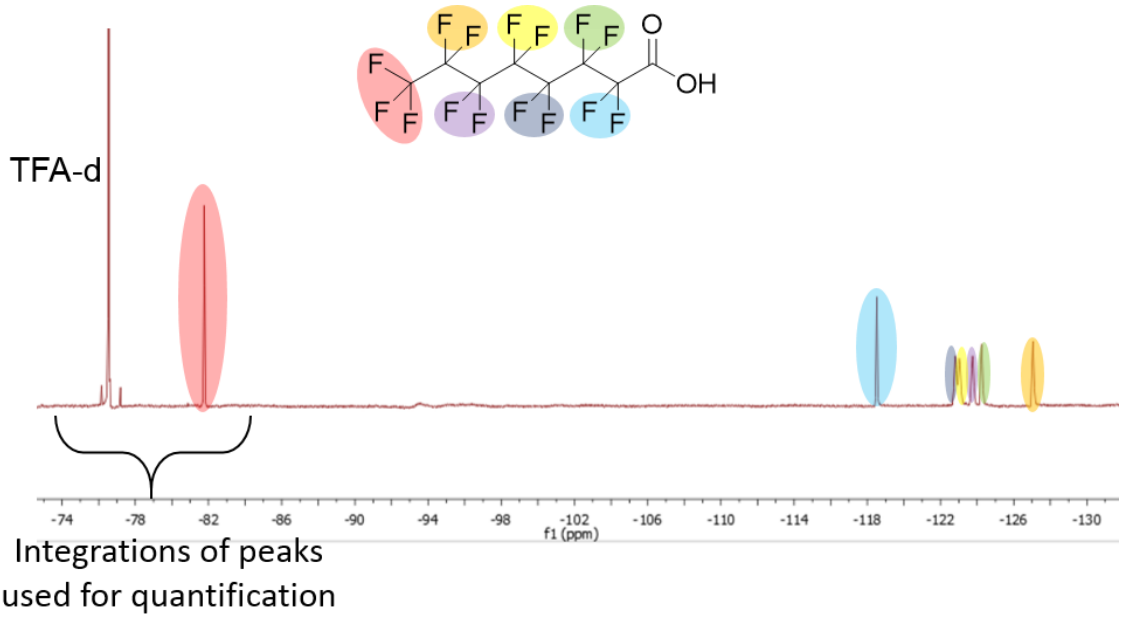

Figure 4.7. Assignments for PFOA in D_2O with TFA-d spike. TFA-d was used as an internal standard; left-most peaks were used for quantifying the decrease of PFOA in the samples.[103]

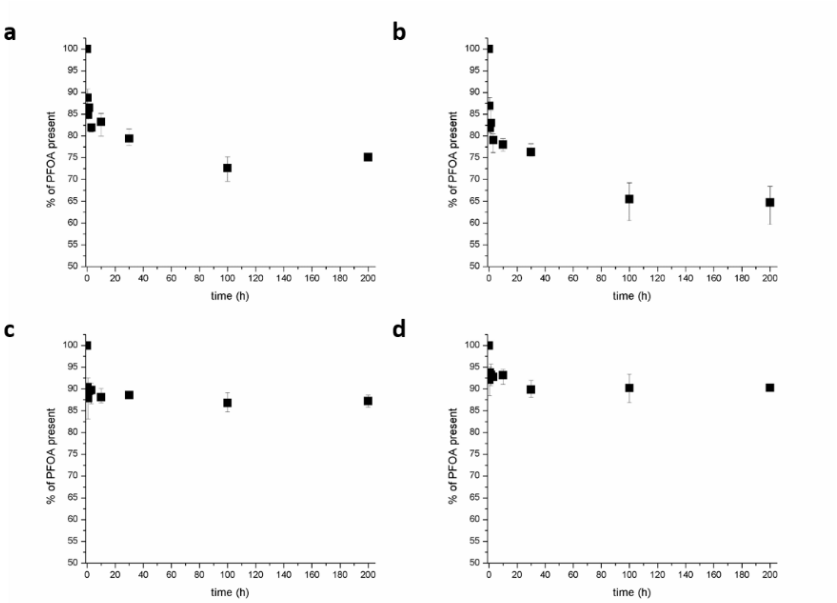

Figure 4.8. Sequestration of PFAO by MSCK-F_9 nanoparticles comprised of PAA_{25}-*b*-P(S-*co*-TFS-F_9)$_{100}$ (a), PAA_{25}-*b*-P(S-*co*-TFS-F_9)$_{200}$ (b), P(S-*co*-TFS-F_9)$_{100}$-*b*-$PAEA_{25}$ (c), and P(S-*co*-TFS-F_9)$_{200}$-*b*-$PAEA_{25}$ (d) block copolymers.

PFOA removal from blood serum. PFOA is a toxic and potentially lethal contaminate that has widespread exposure and is found in measurable blood concentrations in the vast majority of the US population.[123] Based on the success of PFOA removal from an aqueous system, preliminary testing of the efficiency of PFOA removal in blood serum by MSCK-F_9 nanoparticles was performed. Bovine serum was studied due to PFOA's demonstrated interactions with serum proteins. In particular, PFOA has shown interactions with drug-binding sites on albumin,[124] potentially making extraction from the blood more challenging than other aqueous systems. 0.1 micron-filtered bovine calf serum, iron fortified (ATCC) was evaporated and resuspended in a 1.5 mg/mL PFOA solution in D_2O. It was observed that white precipitate was formed but quickly disappeared following the resuspension. A kinetic study with time points at 45 min, 1.5 h, and 10 h was performed deploying MSCK-F_9 nanoparticles comprised of PAA_{25}-*b*-P(S-*co*-TFS-F_9)$_{200}$, in triplicate. The same procedure as previously detailed was employed for the quantification of PFOA removal. The ^{19}F NMR PFOA peaks in serum were very broad compared to those observed only in D_2O (Fig. 4.9); this broadening is thought to be due to strong interactions between this toxic chemical and the serum.[124]

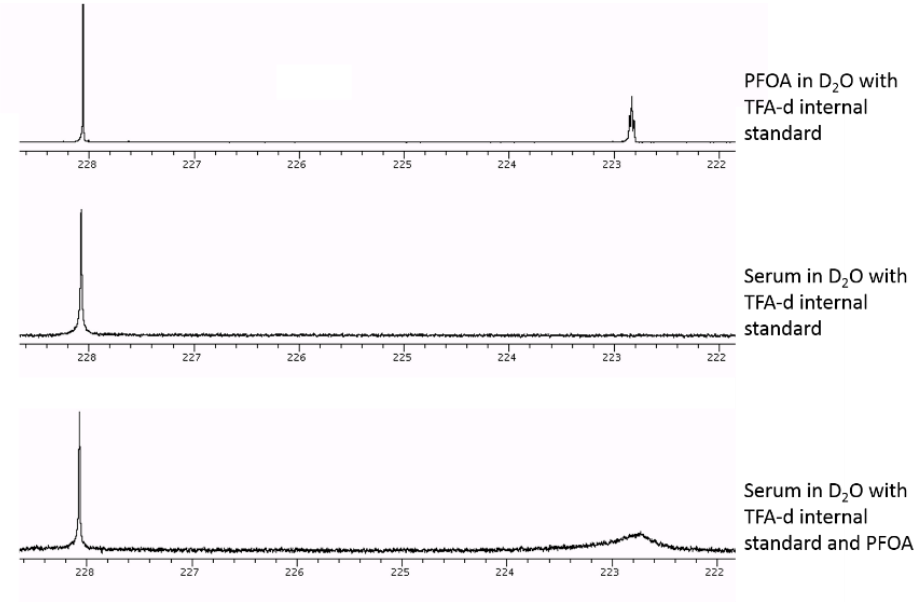

Figure 4.9. ^{19}F NMR of PFOA in D_2O, bovine calf serum in D_2O, and bovine calf serum with PFOA in D_2O.

The PFOA recovery by the MSCK-F_9 system tested in serum at 10 h, 7% (Fig. 4.10), was a fraction of the recovery observed by the same nanoparticle system at 10 h in D_2O, 22%. This difference is most likely due to the strong interactions between the PFOA and its serum environment. Removal by the MSCK-F_9 system would, by the nature of the loading, require the interruption of these interactions and their replacement with a less favorable interaction between the PFOA and the nanoparticle system.

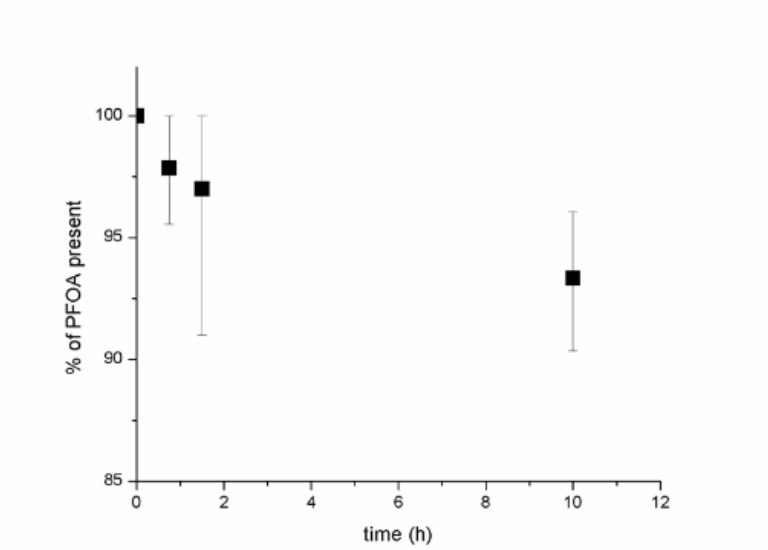

Figure 4.10. Sequestration of PFOA by MSCK-F_9 nanoparticle system comprised of PAA_{25}-*b*-P(S-*co*-TFS-$F_9)_{200}$ polymeric component.

4.3 Conclusions

MSCK-F_9 nanoparticles tailored for the removal of toxicant and carcinogenic PFOA have been prepared and investigated for their environmental deployment and preliminary biomedical use. An array of this new family of hybrid magnetic polymeric nanoparticles was prepared and tested in a PFOA polluted aqueous environment. Although it was initially hypothesized that the nanoparticles comprised of P(S-*co*-TFS-$F_9)_{100}$-*b*-$PAEA_{25}$ and P(S-*co*-TFS-$F_9)_{200}$-*b*-$PAEA_{25}$ block copolymers would have greater PFOA removal capabilities due to the favorable interactions between the positively charged shell of the PAEA nanoparticles and the negatively charged PFOA, it was found

that the nanoparticle systems comprised of PAA_{25}-*b*-P(S-*co*-TFS-F_9)$_{100}$ and PAA_{25}-*b*-P(S-*co*-TFS-F_9)$_{200}$ performed better in this application. However, this increased performance is thought to be due to the size difference between the nanoparticles systems of *ca*.30 nm in diameter. Nevertheless, all four of these systems were capable of removing PFOA at two orders of magnitude above previously reported nanotechnology, with the highest of this system removing 0.25 mg/mg of MSCK-F_9 deployed. Moreover, preliminary testing of PFOA removal in bovine calf serum suggests that this generation of MSCK nanoparticles could have applications in biomedicine.

4.4 Materials and Methods

Materials. All chemicals were purchased from Aldrich Chemical Co. and used without further purification unless otherwise noted. Styrene and other monomers were purified through an alumina plug to remove stabilizer. Iron (III) acetylacetonate was purchased from Strem Chemicals, Inc. 1H,1H,2H,2H-perfluoro-1-hexan-1-ol was purchased from Matrix Scientific. *tert*-Butyl (2-acrylamidoethyl)carbamate monomer were synthesized as reported.[125] Nanopure water (18 MΩ•cm) was acquired by means of a Milli-Q water filtration system, Millipore Corp. (Bedford, MA).

Characterization techniques. ^{1}H NMR and ^{13}C NMR spectra were recorded on an Inova 300 or Mercury 300 spectrometer interfaced to a UNIX computer using VnmrJ software. Samples were prepared as solutions in $CDCl_3$ or d_8-THF and solvent protons were used as internal standard. IR spectra were recorded on an IR Prestige 21 system

(Shimadzu Corp., Japan). A small amount of sample was placed to cover the ATR crystal for IR measurements. Data were analyzed using IRsolution software. Differential scanning calorimetry studies were performed on a Mettler Toledo DSC822 (Mettler-Toledo, Inc., Columbus, OH) calibrated according to the standard procedures using indium. The heating rates were 10 °C min–1 and cooling rates were 10 °C min–1 with a temperature range of -100–150 °C. The T_g was taken as the midpoint of the inflection tangent, upon the third heating scan. Thermogravimetric analysis was performed under argon atmosphere using a Mettler Toledo model TGA/DSC1 with a heating rate of 10 °C/min. Measurements were analyzed using Mettler Toledo STARe software v 10.00. THF gel permeation chromatography (GPC) was conducted on a system equipped with Waters chromatography, Inc. (Milford, MA) model 1515 isocratic pump and a model 2414 differential refractometer with a three-column set of Polymer Laboratories, Inc. (Amherst, MA) Styragel columns (PLgel 5 μm Mixed C, 500 Å, and 104 Å, 300 × 7.5 mm columns) and a guard column (PLgel 5 μm, 50 × 7.5 mm). The system was equilibrated at 40 °C in THF, which served as the polymer solvent and eluent (flow rate set to 1.00 mL/min). The differential refractometer was calibrated with Polymer Laboratories, Inc., polystyrene standards (300 to 467 000 Da). Polymer solutions were prepared at a concentration of *ca*. 3 mg/mL with 0.05% vol toluene as flow rate marker and an injection volume of 200 μL was used. Data were analyzed using Empower Pro software from Waters Chromatography Inc. Dynamic light scattering (DLS) measurements were conducted using Delsa Nano C from Beckman Coulter, Inc. (Fullerton, CA) equipped with a laser diode operating at 658 nm. Size

measurements were made in water (n = 1.3329, η = 0.890 cP at 25 ± 1 °C; n = 1.3293, η = 0.547 cP at 50 ± 1 °C; n = 1.3255, η = 0.404 cP at 70 ± 1 °C). Scattered light was detected at 165° angle and analyzed using a log correlator over 70 accumulations for a 0.5 mL of sample in a glass sizing cell (0.9 mL capacity). The photomultiplier aperture and the attenuator were automatically adjusted to obtain a photon counting rate of *ca*. 10 kcps. The calculations of the particle size distribution and distribution averages were performed using CONTIN particle size distribution analysis routines. Prior to analysis, the samples were filtered through a 5.0 μm 30 mm Nylon syringe filters (Thermo Scientific). The samples in the glass sizing cell were equilibrated at the desired temperature for 5 min before measurements were made. The peak average of histograms from intensity, volume, or number distributions out of 70 accumulations was reported as the average diameter of the particles.

Synthesis of tetrafluorostyrene-3-perfluorohexanol (TFS-F_9). NaH (2.06 eq., 1.2557 g, 52.3 mmol) was added to a flame-dried 50 mL 2-neck flask equipped with a stir bar and a condenser under a nitrogen atmosphere followed by the drop wise addition of 1H,1H,2H,2H-perfluoro-1-hexan-1-ol (1.2 eq., 8.0514 g, 30.5 mmol) and dry THF (4 mL). Following 2 h, PFS (1 eq., 4.9239 g, 25.4 mmol) was added drop wise to the reaction mixture. The reaction was monitored through thin layer chromatography (TLC) and was quenched at 1 h. Hexanes (30 mL) were added to the reaction mixture, and the precipitate was filtered. The yellow reaction mixture was washed with a concentrated solution of sodium bicarbonate (×3) and extracted with hexanes (×3). The product was dried over sodium sulfate and concentrated. The product was purified through column

chromatography at 100% hexanes with a yield of 48%. IR: 3117, 3035, 2976, 2912, 2358, 2162, 1977, 1869, 1745, 1710, 1647, 1500, 1487, 1431, 1406, 1355, 1296, 1219, 1132, 1084, 991, 966, 931, 877, 856, 748, 736, 717, 653 cm^{-1}. ^{1}H NMR (300 MHz, CDCl3) δ 6.63 (dd, *J* = 18.0, 11.9 Hz, 1H), 6.05 (dd, *J* = 18.0, 0.4 Hz, 1H), 5.66 (dd, *J* = 18.0, 0.4 Hz, 1H), 4.50 (t, *J* = 6.7 Hz, 2H), 2.80-2.47 (m, 2H) ppm. ^{13}C NMR (75 MHz, $CDCl_3$) δ 31.2 – 25.4, 66.0 – 68.0, 111.5 – 112.0, 113.8 – 114.0, 115.0 – 115.8, 116.5 – 117.5, 119.0- 119.8, 120.0, 121.7 – 123.5, 135.0 – 136.0, 139.2 – 139.8, 142.5 – 144.0, 146.2 – 147.2 ^{19}F NMR (376 MHz, D_2O) δ -81 (tt, *J* = 9.6, 3.1 Hz, 1F), -110.69 - -114.72 (m, 1F), -122.22 - -125.19 (m, 1F), -125.19 - -127.71 (m, 1F), -144.40 (dd, *J* = 20.4, 8.5 Hz, 1F), -158.13 (dd, *J* = 20.7, 88 Hz, 1F).

Synthesis of Fe_3O_4 nanoparticles. A flame-dried, 50 mL 3-neck flask equipped with a magnetic stir bar and condenser and was charged with $Fe(acac)_3$ (1 eq., 1.4023 g, 4 mmol), oleic acid (3 eq., 3.4291g, 12 mmol) and oleyl amine (3 eq., 3.2130 g, 12 mmol). After addition of benzyl ether (40 mL) and 1,2- hexadecanediol (5 eq., 5.1287 g, 20 mmol), the reaction mixture was degassed by a four-cycle expose to vacuum and nitrogen. Reaction temperature was taken to 140 °C and pressure inside reaction vessel was controlled by the insertion of a needle. After an hour, the needle was removed and reaction temperature was taken to 200 °C for an additional hour, following an hour at 250 °C. Once reaction mixture was cooled to room temperature, it was transferred into a centrifuge tubes and nanoparticles were precipitated by the addition of ethanol (×2), re-suspended and filtration in THF, followed by one final precipitation in ethanol. Final

nanoparticle size was determined *via* TEM as 7 ± 2 nm (after analysis of over 50 particles).

RAFT polymerization of *t*BA using 2-(dodecylthiocarbonothioylthio) propionic acid. A flame-dried 50-mL Schlenk flask equipped with a magnetic stir bar was charged with 2-(dodecylthiocarbonothioylthio) propionic acid (1 eq., 475.0 mg, 1.3 mmol), *t*BA (30 eq., 5.0048 g, 39.0 mmol), AIBN (0.01 eq., 2.3 mg, 0.014 mmol), and anisole (15 mL). The reaction mixture was exposed to four cycles of freeze-pump-thaw (FPT) and allowed to homogenize at room temperature before being introduced into an oil bath at 65 °C. As the expected monomer conversion was reached, after *ca.* 4 h, the polymerization was quenched by immersion of the reaction flask into liquid N_2 and exposure to air. The polymer was precipitated in a methanol/ice mixture (×3) to obtain a sticky yellow solid. Following *in vacuo* drying, the polymer was redissolved in THF, for transferring purposes, and dried. The yellow product was produced with a yield of 2.8403 g or 63.4%. $M_{w(theo)}$ = 3,500, $M_{w(NMR)}$ = 3,100, $M_{w(GPC)}$ = 4,000; PDI = 1.06. IR: 3458-2517, 2974, 2928, 2856, 2633, 2278, 2038, 1977, 1722, 1477, 1450, 1392, 1365, 1334, 1252, 1140, 1074, 1035, 844, 750 cm^{-1}. ^{1}H NMR (300 MHz, $CDCl_3$) δ 3.32 (t, *J* = 7.3 Hz, 2H), 2.25 (br, 27 H), 1.84 (br, m, 15 H), 1.75 - 0.96 (br, m, 346H, 0.87 (t, *J* = *6*.7 Hz, 4H) ppm. ^{13}C NMR (75 MHz, $CDCl_3$) δ l4.0 – 14.6, 22.7 – 22.9, 23.9 – 24.9, 24.5 – 25.4, 25.5 – 26.2, 26.2 – 27.1, 27.1 – 27.7, 27.8 – 28.7, 28.8 – 29.3, 29.3 – 30.2, 30.3 – 30.8, 30.8- 31.6, 31.6 – 32.7, 34.2 – 37.0, 37.0 – 38.0, 40.6 – 43.3, 80.3 – 80.9, 173.5 – 174.5, 175.0 – 175.5 ppm. TGA: T_{onset} = 237 °C, $T_{decomposition}$ = (237 – 450 °C) 87% mass loss; 13% mass remaining. DSC: T_g = 26 °C.

RAFT polymerization of styrene and tetrafluorostyrene-3-perfluorohexanol (TFS-F_9) from P*t*BA (P*t*BA_{25}-*b*-P(S-*co*-TFS-F_9)$_{200}$). A flame-dried 10 mL Schlenk flask equipped with a magnetic stir bar was charged with P*t*BA (1 eq., 102.1 mg, 0.0300 mmol), AIBN (0.3 eq., 1.6 mg, 0.0098 mmol), TFS-F_9 (39.8 eq., 523.0 mg, 1.1941 mmol), styrene (353.9 eq., 1.1042 g, 10.6173 mmol) and 1,2-dioxane (1.5 mL). The reaction mixture was exposed to four cycles of FPT and allowed to homogenize at room temperature before being inserted into an oil bath at 65 °C. The reaction was quenched after 50% monomer conversion or 40 h. The resulting polymer was precipitated in cold methanol and ice (×3) to afford a white solid. The product was produced with a yield of 800.1 mg or 80%. $M_{w(theo)}$ = 37,300, $M_{w(GPC)}$ = 36,800; PDI = 1.14. IR: 3084, 3060, 3027, 3003, 2978, 2922, 2852, 2628, 2355, 2337, 2322, 2285, 1980, 1942, 1876, 1807, 1726, 1650, 1600, 1490, 1452, 1394, 1367, 1234, 1220, 1132, 1084, 1022, 968, 880, 850, 754, 698 cm^{-1}. ^{1}H NMR (300 MHz, $CDCl_3$) δ 7.25 – 6.82 (br, m, 610H), 6.82 - 6.30 (br, m, 415 H), 4.45 – 4.15 (br, m, 80H), 2.82 – 2.48 (br, 75H), 2.48 – 2.08 (br, 37H), 2.07 – 1.69 (br, m, 152H), 1.69 – 1.05 (br, m, 932H) ppm. ^{13}C NMR (75 MHz, $CDCl_3$) δ 27.8 – 28.5, 29.5 – 30.0, 31.0 – 32.5, 39.9 – 43.0, 43.0 – 45.0, 80.4 – 80.8, 125.2 – 129.0, 133.7 – 134.8, 138.2 – 138.6, 141.8 – 147.4, 173.5 – 174.7 ppm. TGA: T_{onset} = 237 °C, $T_{decomposition}$ = (237 – 250 °C) 3% mass loss; (396 – 450 °C) 80% mass loss; 17% mass remaining. DSC: T_g = 78 °C.

Deprotection of PAA_{25}-*b*-P(S-*co*-TFS-F_9)$_{200}$. The copolymer (1 eq., 501.6 mg) was dissolved in DCM (3 mL), followed by addition of TFA (100 eq. per AA group, 2.6 mL). The deprotection reaction was allowed to take place overnight. The solvent and

excess TFA were evaporated off and the redissolved polymer (in THF) was dialyzed against nanopure water for three days. The product was produced with a yield of 446 m g or 91%. IR: 3650 – 2160, 3082, 3060, 3026, 2922, 2852, 2636, 2357, 2324, 2052, 1990, 1942, 1872, 1805, 1708, 1649, 1600, 1490, 1452, 1404, 1355, 1300, 1220, 1132, 1084, 1004, 958, 877, 752, 698 cm^{-1}. ^{1}H NMR (300 MHz, $CDCl_3$) δ 7.33 – 6.79 (br, m, 610H), 6.80 – 6.25 (br, m, 415H), 4.49 – 4.16 (br, m, 80H), 2.89 – 2.52 (br, 91H), 2.52-2.02 (br, m, 43H), 2.01 – 0.98 (br, m, 1060H) ppm. ^{13}C NMR (75 MHz, THF) δ 30.1 – 31.1, 31.5 – 34.5, 41.0 – 45.5, 125.7 – 127.4, 127.4 – 129.8, 134.0 – 136.0, 138.5 – 141.8, 142.0 – 149.0 ppm. TGA: T_{onset} = 395 °C, $T_{decomposition}$ = (395 – 450 °C) 77% mass loss; 23% mass remaining. DSC: T_g = 82 °C.

Co-assembly and crosslinking of PAA_{25}-*b*-P(S-*co*-TFS-F_9)$_{200}$. An organic solution containing 20 mg of the polymer in 58 mL of THF was made. To this, 2 mL of a 10 mg/mL solution of iron oxide nanoparticles were added. The solution was homogenized. The organic mixture (60 mL) was added at a rate of 20 mL/hr to an equal volume (60 mL) of nanopure water under vigorous stirring. Following full addition, the solution was allowed to continue mixing for an additional hour. Following filtering through a 5 μm filter, the resulting nanoparticles were dialyzed against nanopure water. Two batches of magneto micelle solutions were produced. The batches were combined for particle characterization prior to crosslinking. Nanoparticles sizes were determined to be 63 ± 16 and 61 ± 10 for DLS and TEM, respectively. MSCKs were obtained by crosslinking nominally 25% of the acrylic acid repeat units by amidation with the diamine crosslinker (2,2'-ethylenedioxy)bis(ethylamine) in the presence of 1-(3-

(dimethylamino)propyl)-3-ethyl-carbodiimide methiodide (EDCI). Extensive dialysis against nanopure water was performed to remove unreacted small molecules and reaction by-products. Nanoparticles sizes were determined to be 77 ± 22 and 68 ± 11 for DLS and TEM, respectively.

RAFT polymerization of styrene and tetrafluorostyrene-3-perfluorohexanol (TFS-F_9) from P*t*BA (P*t*BA_{25}-*b*-P(S-*co*-TFS-F_9)$_{100}$). A flame-dried 10 mL Schlenk flask equipped with a magnetic stir bar was charged with P*t*BA (1 eq., 101.8 mg, 0.0299 mmol), AIBN (0.3 eq., 1.5 mg, 0.0091 mmol), TFS-F_9 (39.5 eq., 516.8 mg, 1.1799 mmol), styrene (356.8 eq., 1.1095 g, 10.6683 mmol) and 1,2-dioxane (3 mL). The reaction mixture was exposed to four cycles of FPT and allowed to homogenize at room temperature before being inserted into an oil bath at 65 °C. The reaction was quenched after 35% monomer conversion or 44 h. The resulting polymer was precipitated in cold methanol and ice (×3) to afford an off-white solid. The product was produced with a yield of 771.2 mg or 96%. $M_{w(theo)}$ = 30,500, $M_{w(GPC)}$ = 33,000; PDI = 1.14. IR: 3082, 3059, 3026, 2978, 2924, 2853, 2625, 2359, 2054, 1956, 1880, 1803, 1730, 1651, 1600, 1491, 1452, 1392, 1365, 1232, 1220, 1132, 1078, 1020, 1003, 962, 904, 875, 847, 750, 698 cm^{-1}. ^{1}H NMR (300 MHz, $CDCl_3$) δ 7.22 – 6.80 (br, m, 306H), 6.80 – 6.25 (br, m, 224H), 4.45 – 4.15 (br, m, 40H), 2.77 – 2.42 (br, 44H), 2.42 – 2.01 (br, m, 33H), 2.01-0.89 (br, m, 585H) ppm. ^{13}C NMR (75 MHz, $CDCl_3$) δ 27.8 – 28.5, 29.5 – 30.0, 31.0 – 32.5, 39.9 – 43.0, 43.0 – 45.0, 80.4 – 80.8, 125.2 – 129.0, 133.7 – 134.8, 138.2 – 138.6, 141.8 – 147.4, 173.5 – 174.7 ppm. TGA: T_{onset} = 239 °C, $T_{decomposition}$ = (239 – 250 °C) 4% mass loss; (391 – 450 °C) 81% mass loss; 15% mass remaining. DSC: T_g = 72 °C.

Deprotection of PAA_{25}-*b*-$P(S\text{-}co\text{-}TFS\text{-}F_9)_{100}$. The copolymer (1 eq., 500.8 mg) was dissolved in DCM (3 mL), followed by addition of TFA (100 eq. per AA group, 4.0 mL). The deprotection reaction was allowed to take place overnight. The solvent and excess TFA were evaporated off and the redissolved polymer (in THF) was dialyzed against nanopure water for three days. The product was produced with a yield of 303.8 m g or 70%. IR: 3728 – 2156, 3082, 3060, 3026, 2922, 2854, 2621, 2347, 2083, 1948, 1872, 1807, 1708, 1651, 1600, 1490, 1450, 1404, 1360, 1232, 1220, 1132, 1083, 1020, 1004, 966, 904, 877, 856, 754, 698 cm^{-1}. ^1H NMR (300 MHz, $CDCl_3$) δ 7.25 – 6.78 (br, m, 306H), 6.78 – 6.28 (br, m, 224H), 4.50 – 4.20 (br, m, 40H), 2.89 – 2.25 (br, m, 30H), 2.20 – 0.81 (br, m, 478H) ppm. ^{13}C NMR (75 MHz, THF) δ 30.1 – 31.1, 31.5 – 34.5, 41.0 – 45.5, 125.7 – 127.4, 127.4 – 129.8, 134.0 – 136.0, 138.5 – 141.8, 142.0 – 149.0 ppm. TGA: T_{onset} = 392 °C, $T_{decomposition}$ = (392 – 450 °C) 82% mass loss; 18% mass remaining. DSC: T_g = 82 °C.

Co-assembly and crosslinking of PAA_{25}-*b*-$P(S\text{-}co\text{-}TFS\text{-}F_9)_{100}$. An organic solution containing 20 mg of the polymer in 58 mL of THF was made. To this, 2 mL of a 10 mg/mL solution of iron oxide nanoparticles were added. The solution was homogenized. The organic mixture (60 mL) was added at a rate of 20 mL/hr to an equal volume (60 mL) of nanopure water under vigorous stirring. Following full addition, the solution was allowed to continue mixing for an additional hour. Following filtering through a 5 μm filter, the resulting nanoparticles were dialyzed against nanopure water. Two batches of magneto micelle solutions were produced. The batches were combined for particle characterization prior to crosslinking. Nanoparticles sizes were determined

to be 54 ± 13 and 52 ± 6 for DLS and TEM, respectively. MSCKs were obtained by crosslinking nominally 25% of the acrylic acid repeat units by amidation with the diamine crosslinker (2,2'-ethylenedioxy)bis(ethylamine) in the presence of EDCI. Extensive dialysis against nanopure water was performed to remove unreacted small molecules and reaction by-products. Nanoparticles sizes were determined to be 60 ± 15 and 54 ± 10 for DLS and TEM, respectively.

RAFT polymerization of styrene and tetrafluorostyrene-3-perfluorohexanol (TFS-F_9) (P(S-*co*-TFS-F_9)$_{200}$). A flame-dried 25 mL Schlenk flask equipped with a magnetic stir bar was charged with 2-(dodecylthiocarbonothioylthio) propionic acid (1 eq., 29.9 mg, 0.0821 mmol), AIBN (0.3 eq., 4.2 mg, 0.0256 mmol), TFS-F_9 (34 eq., 1.2190 g, 2.7831 mmol), styrene (351 eq., 3.0002 g, 28.8481 mmol), and 1,2-dioxane (5 mL). The reaction mixture was exposed to four cycles of FPT and allowed to homogenize at room temperature before being inserted into an oil bath at 65 °C. The reaction was quenched after 56 h or 50% monomer conversion. The resulting polymer was precipitated in cold methanol and ice (×3) to afford a white solid. The product was produced with a yield of 1.9624 g or 89%. $M_{w(theo)}$ = 34,000, $M_{w(GPC)}$ = 33,000; PDI = 1.11. IR: 3060, 3024, 2920, 2858, 2634, 2326, 1944, 1870, 1800, 1740, 1647, 1600, 1490, 1450, 1400, 1354, 1230, 1130, 1080, 1002, 964, 875, 752, 698 cm^{-1}. ^1H NMR (300 MHz, $CDCl_3$) δ 7.54 – 6.80 (br, m, 480H), 6.80 – 6.25 (br, m, 328H), 4.46 – 4.14 (br, m, 45H), 2.80 – 2.44 (br, 50H), 2.20 – 1.01 (br, m, 602H), 0.89 (br, m, 9H) ppm. ^{13}C NMR (75 MHz, $CDCl_3$) δ 28.9 – 33.5, 38.2 – 46.3, 65.2 – 67.5, 116.6 – 117.6, 125.1

– 129.8, 133.6 – 134.9, 141.8- -147.7 ppm. TGA: T_{onset} = 370 °C, $T_{decomposition}$ = (370 – 430°C) 92% mass loss; 8% mass remaining. DSC: T_g = 82 °C.

RAFT polymerization of *tert*-butyl (2-acrylamidoethyl)carbamate monomer from P(S-*co*-TFS-F$_9$)$_{200}$. A flame-dried 10 mL Schlenk flask equipped with a magnetic stir bar was charged with P(S-*co*-TFS-F$_9$) (1 eq., 399.7 mg, 0.0125 mmol), AIBN (0.3 eq., 0.7 mg, 0.0043 mmol), *tert*-butyl (2-acrylamidoethyl)carbamate (40 eq., 106.9 mg, 0.4995 mmol), and 1,2-dioxane (5 mL). The reaction mixture was exposed to four cycles of FPT and allowed to homogenize at room temperature before being inserted into an oil bath at 65 °C. The reaction was quenched after 60% monomer conversion or 24 h. The resulting polymer was precipitated in cold methanol and ice (×3) to afford a white solid. The product was produced with a yield of 202.6 mg or 43%. $M_{w(theo)}$ = 39,000, $M_{w(GPC)}$ = 37,000; PDI = 1.14. IR: 3668 – 3120, 3059, 3028, 2924, 2854, 2638, 2322, 2283, 2070, 1982, 1944, 1870, 1800, 1693, 1650, 1600, 1530, 1492, 1450, 1392, 1365, 1226, 1165, 1130, 1002, 964, 906, 875, 852, 752, 698 cm^{-1}. ^{1}H NMR (300 MHz, $CDCl_3$) δ 7.22 – 6.75 (br, m, 480H), 6.75 – 6.25 (br, m, 326H), 4.46 – 4.15 (br, m, 40H), 3.40 – 3.0 (br, 41H), 2.75 – 2.41 (br, 42H), 2.22 – 0.95 (br, m, 978H), 0.95 – 0.75 (br, m, 20H). ^{13}C NMR (75 MHz, $CDCl_3$) δ 28.9 – 33.5, 38.2 – 46.3, 65.2 – 67.5, 75.4 – 78.2, 116.6 – 117.6, 125.1 – 129.8, 133.6 – 134.9, 141.8- -147.7, 189.0 – 189.5 ppm. TGA: T_{onset} = 400 °C, $T_{decomposition}$ = (400 – 450°C) 70% mass loss; 30% mass remaining. DSC: T_g = 80 °C.

Removal of ω chain-end of P(S-*co*-TFS-F$_9$)$_{200}$-*b*-PAEA*boc*$_{25}$. A flame-dried 10 mL Schlenk flask equipped with a magnetic stir bar was charged with EPHP (95 eq.,

67.4 mg, 0.3765 mmol), ACHN (0.3 eq., 0.3 mg, 0.0012 mmol), P(S-*co*-TFS-F_9)$_{200}$-*b*-PAEA*boc*$_{25}$ (1 eq., 150.2 mg, 0.0039 mmol), and toluene (2 mL). The reaction mixture was exposed to three cycles of FPT and immersed into a heating bath at 100 °C. The reaction was quenched following 2 h by immersion into liquid nitrogen and exposure to air. The product mixture was dissolved in THF and dialyzed against nanopure water for 3 days in order to remove the trithiocarbonate side product and solvent. The solid product was the filtered and dried *in vacuo* to obtain 114.6 mg or 76% yield. UV-vis characterization was performed in THF at a concentration of 0.6 mg/mL. A peak was observed in the starting product at *ca*. 310 nm corresponding to the trithiocarbonate functional group; this peak was no longer present in the product.[120] $M_{w(theo)}$ = 36,500, $M_{w(GPC)}$ = 36,000; PDI = 1.14. IR: 3666 – 3125, 3082, 3060, 3026, 2922, 2852, 2640, 2324, 1979, 1946, 1876, 1798, 1689, 1654, 1600, 1535, 1490, 1452, 1394, 1363, 1435, 1220, 1199, 1132, 1084, 1020, 1002, 960, 908, 875, 850, 754, 696 cm^{-1}. ^{1}H NMR (300 MHz, $CDCl_3$) δ 7.37 – 6.84 (br, m, 480H), 6.84 – 6.27 (br, m, 306H), 4.52 – 4.11 (br, m, 42H), 3.59 – 2.87 (br, 40H), 2.80 – 2.42 (br, 38H), 2.16 – 1.04 (br, m, 678H), 1.03 – 0.76 (br, m, 6H) ppm. ^{13}C NMR (75 MHz, $CDCl_3$) δ 1.1 – 1.3, 28.3 – 29.0, 30.4 – 30.6, 31.2 – 32.6, 39.3 – 46.2, 66.2 – 61.1, 78.9 – 80.7, 115.6 – 118.2, 125.1 – 129.8, 133.6 – 134.9, 138.4 – 139.8, 141.8 – 147.7, 156.4 – 157.2, 175.0 – 176.5 ppm. UV-vis characterization available in the supporting information.

Deprotection of P(S-*co*-TFS-F_9)$_{200}$-*b*-PAEA$_{25}$. The copolymer (1 eq., 80.2 mg) was dissolved in DCM (1.5 mL), followed by addition of TFA (100 eq. per AA group, 400 µL). The deprotection reaction was allowed to take place overnight. The solvent

and excess TFA were evaporated off and the redissolved polymer (in THF) was dialyzed against nanopure water for three days. The product was produced with a quantitative yield. IR: 3650 – 2376, 3082, 3060, 3026, 2922, 2850, 2640, 2314, 2075, 1978, 1938, 1874, 1799, 1649, 1600, 1490, 1452, 1394, 1355, 1232, 1220, 1199, 1180, 1132, 1080, 1016, 960, 904, 877, 800, 754, 717, 698 cm^{-1}. ^{1}H NMR (300 MHz, $CDCl_3$) δ 7.25 – 6.84 (br, m, 480H), 6.82 – 6.30 (br, m, 280H), 4.60 – 4.20 (br, m, 40H), (3.19 – 2.38 (br, 40H), 2.11 – 1.13 (br, m, 659H), 0.95 – 0.83 (br, m, 12H) ppm. ^{13}C NMR (75 MHz, THF) δ 30.0 – 31.2, 39.8 – 46.2, 125.1 – 129.8, 133.6 – 134.9, 138.4 – 139.8, 141.8 – 147.7 ppm. TGA: T_{onset} = 342 °C, $T_{decomposition}$ = (342 – 400 °C) 53% mass loss; 47% mass remaining. DSC: T_g = 81 °C

RAFT polymerization of styrene and tetrafluorostyrene-3-perfluorohexanol (TFS-F_9) (P(S-*co*-TFS-F_9)$_{100}$). A flame-dried 25 mL Schlenk flask equipped with a magnetic stir bar was charged with 2-(dodecylthiocarbonothioylthio) propionic acid (1 eq., 30.2 mg, 0.0830 mmol), AIBN (0.3 eq., 4.0 mg, 0.0244 mmol), TFS-F_9 (39 eq., 1.4062 g, 3.2105 mmol), styrene (348 eq., 3.0021 g, 28.8663 mmol), and 1,2-dioxane (5 mL). The reaction mixture was exposed to four cycles of FPT and allowed to homogenize at room temperature before being inserted into an oil bath at 65 °C. The reaction was quenched after 21 h or 25% monomer conversion. The resulting polymer was precipitated in cold methanol and ice (×3) to afford a white solid. The product was produced with a yield of 1.2728 g or 80%. $M_{w(theo)}$ = 20,000, $M_{w(GPC)}$ = 20,000; PDI = 1.10. IR: 3063, 3028, 2924, 2854, 2630, 2326, 2175, 2021, 1798, 1747, 1701, 1647, 1600, 1489, 1450, 1404, 1358, 1296, 1222, 1130, 1080, 1006, 964, 875, 752, 698 cm^{-1}.

^{1}H NMR (300 MHz, $CDCl_3$) δ 7.23 – 6.79 (br, m, 240H), 6.78 – 6.25 (br, m, 156H), 4.44 – 4.16 (br, m, 31H), 2.82 – 2.50 (br, 42H), 2.12 – 1.05 (br, m, 300H), 1.05 – 0.79 (br, m, 12H). ^{13}C NMR (75 MHz, $CDCl_3$) δ 28.9 – 33.5, 38.2 – 46.3, 65.2 – 67.5, 116.6 – 117.6, 125.1 – 129.8, 133.6 – 134.9, 141.8- -147.7 ppm. TGA: T_{onset} = 373 °C, $T_{decomposition}$ = (373 – 430°C) 92% mass loss; 8% mass remaining. DSC: T_g = 67 °C.

RAFT polymerization of *tert*-butyl (2-acrylamidoethyl)carbamate monomer from P(S-*co*-TFS-F$_9$)$_{100}$. A flame-dried 10 mL Schlenk flask equipped with a magnetic stir bar was charged with P(S-*co*-TFS-F_9)$_{100}$ (1 eq., 400.6 mg, 0.0200 mmol), AIBN (0.3 eq., 1.0 mg, 0.0061 mmol), *tert*-butyl (2-acrylamidoethyl)carbamate (33 eq., 171.4 mg, 0.6607 mmol), and 1,2-dionxane (5 mL). The reaction mixture was exposed to four cycles of FPT and allowed to homogenize at room temperature before being inserted into an oil bath at 65 °C. The reaction was quenched after 80% monomer conversion or 19 h. The resulting polymer was precipitated in cold methanol and ice (×3) to afford a white solid. The product was produced with a yield of 337.0 mg or 62%. $M_{w(theo)}$ = 27,000, $M_{w(GPC)}$ = 26,000; PDI = 1.17. IR: 3700 – 3120, 3063, 3028, 2974, 2927, 2627, 2314, 2048, 1867, 1689, 1654, 1527, 1492, 1450, 1392, 1365, 1230, 1165, 1134, 1002, 968, 875, 852, 752, 698 cm^{-1}. ^{1}H NMR (300 MHz, $CDCl_3$) δ 7.23 – 6.79 (br, m, 240H), 6.78 – 6.25 (br, m, 156H), 4.44 – 4.16 (br, m, 32H), 3.51 – 3.01 (br, 81H), 2.82 – 2.45 (br, 40H), 2.0- 1.16 (br, m, 940H), 1.05 – 0.79 (br, m, 12H). ^{13}C NMR (75 MHz, $CDCl_3$) δ 28.9 – 33.5, 38.2 – 46.3, 65.2 – 67.5, 75.4 – 78.2, 116.6 – 117.6, 125.1 – 129.8, 133.6 – 134.9, 141.8- -147.7, 189.0 – 189.5 ppm. TGA: T_{onset} = 390 °C, $T_{decomposition}$ = (390 – 430°C) 50% mass loss; 50% mass remaining. DSC: T_g = 79 °C.

Removal of ω chain-end of P(S-*co*-TFS-F$_9$)$_{100}$-*b*-PAEA*boc*$_{30}$. A flame-dried 10 mL Schlenk flask equipped with a magnetic stir bar was charged with EPHP (79 eq., 79.8 mg, 0.4402 mmol), ACHN (0.36 eq., 0.5 mg, 0.0020 mmol), P(S-*co*-TFS-F$_9$)$_{100}$-*b*-PAEA*boc*$_{30}$ (1 eq., 150.3 mg, 0.0056 mmol), and toluene (2 mL). The reaction mixture was exposed to three cycles of FPT and immersed into a heating bath at 100 °C. The reaction was quenched following 2 h by immersion into liquid nitrogen and exposure to air. The product mixture was dissolved in THF and dialyzed against nanopure water for 3 days in order to remove the trithiocarbonate side product and solvent. The solid product was the filtered and dried *in vacuo* to obtain 99.8 mg or 67% yield. UV-vis characterization was performed in THF at a concentration of 0.6 mg/mL. A peak was observed in the starting product at *ca*. 310 nm corresponding to the trithiocarbonate functional group; this peak was no longer present in the product.[120] $M_{w(theo)}$ = 24,500, $M_{w(GPC)}$ = 22,000; PDI = 1.20. IR: 3711 – 3132, 3086, 3061, 3026, 2978, 2924, 2852, 2619, 2063, 1946, 1876, 1809, 1691, 1651, 1600, 1530, 1490, 1452, 1394, 1365, 1338, 123, 1220, 1166, 1132, 1076, 1016, 1001, 962, 908, 877, 854, 752, 698 cm^{-1}. ^{1}H NMR (300 MHz, $CDCl_3$) δ 7.23 – 6.84 (br, m, 240H), 8.84 – 6.28 (br, m, 188H), 4.55 – 4.10 (br, 32 H), 3.61- -2.91 (br, 72H), 2.78 – 2.42 (br, 42H), 2.38 – 1.02 (br, m, 700H), 1.01 – 0.79 (br, m, 12H) ppm. ^{13}C NMR (75 MHz, $CDCl_3$) δ 1.1 – 1.3, 28.3 – 29.0, 30.4 – 30.6, 31.2 – 32.6, 39.3 – 46.2, 66.2 – 61.1, 78.9 – 80.7, 115.6 – 118.2, 125.1 – 129.8, 133.6 – 134.9, 138.4 – 139.8, 141.8 – 147.7, 156.4 – 157.2, 175.0 – 176.5 ppm. TGA: T_{onset} = 397 °C, $T_{decomposition}$ = .(397 - 440 °C) 79% mass loss; 21% mass remaining. UV-vis characterization available in the supporting information.

Deprotection of P(S-*co*-TFS-F$_9$)$_{100}$-*b*-PAEA$_{30}$. The copolymer (1 eq., 80.7 mg) was dissolved in DCM (1.5 mL), followed by addition of TFA (100 eq. per *boc* group, 700 µL). The deprotection reaction was allowed to take place overnight. The solvent and excess TFA were evaporated off and the redissolved polymer (in THF) was dialyzed against nanopure water for three days. The product was produced with a quantitative yield. IR: 3700 – 2382, 3082, 3061, 3026, 2960, 2922, 2852, 2642, 2333, 1944, 1880, 1805, 1676, 1650, 1600, 1544, 1490, 1452, 1400, 1358, 1303, 1259, 1234, 1219, 1201, 1132, 1080, 1020, 958, 880, 837, 800, 754, 720, 698 cm^{-1}. ^{1}H NMR (300 MHz, THF) δ 7.23 – 6.84 (br, m, 240H), 8.84 – 6.28 (br, m, 180H), 4.55 – 4.10 (br, 34 H), 3.61- -2.91 (br, 72H), 2.78 – 2.42 (br, i42H), 2.38 – 1.02 (br, m, 400H), 1.01 – 0.79 (br, m, 12H) ppm. ^{13}C NMR (75 MHz, THF) δ 30.0 – 31.2, 39.8 – 46.2, 125.1 – 129.8, 133.6 – 134.9, 138.4 – 139.8, 141.8 – 147.7 ppm. TGA: T_{onset} = 352 °C, $T_{decomposition}$ = (352 – 400 °C) 60% mass loss; 40% mass remaining. DSC: T_g = 78 °C

CHAPTER V

CONCLUSIONS

This dissertation has focused on the design, development, and deployment of novel hybrid magnetic polymeric nanoparticles for nanoremediation of toxic and hazardous materials. Alterations of the polymeric components of these hybrid structures allowed for the tailoring of engineered nanoparticles (ENPs) with specific pollutants in mind. Hybrid well-defined magnetic shell crosslinked knedel-like (MSCK) nanoparticles comprised of iron oxide nanoparticles encapsulated in amphiphilic block copolymer micellar assemblies and selectively crosslinked throughout the hydrophilic shell domain of the assembly were investigated for their crude oil uptake capabilities. This simple poly(acrylic acid)-*block*-polystyrene (PAA-*b*-PS) system demonstrated an unanticipated 10× loading of a complex crude oil pollutant from aqueous systems. Moreover, it was found that all fractions of the crude oil were equally removed by this nanoparticle system. Additionally, MSCK were able to be recycled and reused with no loss of their superb crude oil remediation.

Chapter III explored the stability of these MSCK nanoparticles in seawater environments and organic solvents. It was found that the fabulous oil uptake capabilities of MSCKs translated well into seawater environments. The chemical and morphological stability of these nanoparticles in ethanol and chloroform were limited and could account for the structural changes observed during the previously studied recycling of the system. Additionally, the first step into the development of a more facile technique for

the co-assembly of MSCKs was taken through the modification into a mono solvent co-assembly procedure. The MSCK nanoparticles obtained through this method were nearly identical in both their physical characterization and their crude oil uptake capabilities.

Fluorinated MSCK (MSCK-F_9) nanoparticles were also investigated for the remediation of perfluorooctanoic acid (PFAO) from water. A library of four fluorinated systems was developed in order to probe the effect size/fluorine content and shell charge would have on the recovery efficiency of PFOA by these intricately designed materials. Initial hypotheses of the potential uptake of these four nanoparticle systems were countered by the size difference of the nanoparticles obtained. Nevertheless, the removal of this toxic and ubiquitous pollutant from aqueous systems, although significantly lower than that of the original MSCK system against crude oil, was found to be two orders of magnitude greater than any other reported engineered nanotechnology against tested PFOA. Due to the fact that PFOA is found in the blood of most Americans, preliminary testing of MSCK-F_9 nanoparticles in blood serum suggests that this nanotechnology could be utilized in the field of nanomedicine to aid in the removal of PFOA from our bodies.

Overall, the experiments and results obtained from this work suggest that these novel ENPs have the potential to be fine-tuned for specific nanoremediation needs. The greater MSCK family has shown great promise for both environmental and medical applications. Future work should focus heavily in the development of tailored particles

for other toxic pollutants in both aqueous and groundwater systems, and the development for partially degradable MSCK nanoparticles for biomedical applications.

REFERENCES

1. Feyman, R. P., There's Plentoy of Room at the Bottom. *Eng. Sci.* **1960,** *23*, 22-36.

2. Kroto, H. W.; Heath, J. R.; O'Brien, S. C.; Curl, R. F.; Smalley, R. E., C_{60}: Buckminsterfullerene. *Nature* **1985,** *318*, 162-163.

3. Drexler, E., *Engines of Creation: The Coming Era of Nanotechnology*. Anchor: 1987.

4. Qiu, X.; Fang, Z.; Yan, X.; Gu, F.; Jiang, F., Emergency Remediation of Simulated Chromium (VI)-polluted River by Nanoscale Zero-valent Iron: Laboratory study and numerical simulation. *Chem. Eng. J.* **2012,** *193–194*, 358-365.

5. McPherson, A. W.; Goltz, M. N.; Agrawal, A., Pollutant Degradation by Nanoscale Zero Valent Iron (nZVI): Role of Polyelectrolyte Stabilization and Catalytic Modification on nZVI Performance. In *Interactions of Nanomaterials with Emerging Environmental Contaminants*, American Chemical Society: 2013; Vol. 1150, pp 159-191.

6. Crane, R. A.; Scott, T. B., Nanoscale Zero-valent Iron: Future prospects for an emerging water treatment technology. *J. Hazard. Mater.* **2012,** *211-212*, 112-125.

7. Virender, K. S.; Karolina, M. S.; Radek, Z., Magnetic Bimetallic Fe/Ag Nanoparticles: Decontamination and Antimicrobial Agents. In *Interactions of Nanomaterials with Emerging Environmental Contaminants*, American Chemical Society: 2013; Vol. 1150, pp 193-209.

8. He, F.; Zhao, D.; Liu, J.; Roberts, C. B., Stabilization of Fe−Pd Nanoparticles with Sodium Carboxymethyl Cellulose for Enhanced Transport and Dechlorination of Trichloroethylene in Soil and Groundwater. *Ind. Eng. Chem. Res.* **2007,** *46*, 29-34.

9. Georgi, A.; Schierz, A.; Mackenzie, K.; Kopinke, F.-D., Colloidal Activated Carbon for I*n-situ* Groundwater Remediation — Transport characteristics and adsorption of organic compounds in water-saturated sediment columns. *J. Contam. Hydrol.* **2015,** *179*, 76-88.

10. Chen, B.; Ma, Q.; Tan, C.; Lim, T.-T.; Huang, L.; Zhang, H., Carbon-based Sorbents with Three-dimensional Architectures for Water Remediation. *Small* **2015,** *11*, 3319-3336.

11. Mauter, M. S.; Elimelech, M., Environmental Applications of Carbon-Based Nanomaterials. *Environ. Sci. Technol.* **2008,** *42*, 5843-5859.

12. Chen, B., *et al.*, One-pot, Solid-phase Synthesis of Magnetic Multiwalled Carbon Nanotube/iron Oxide Composites and Their Application in Arsenic Removal. *J. Colloid Interface Sci.* **2014,** *434*, 9-17.

13. Sun, H., *et al.*, Hydrophobic Carbon Nanotubes for Removal of Oils and Organics from Water. *J. Mater. Sci.* **2014,** *49*, 6855-6861.

14. Yu, F.; Ma, J.; Wu, Y., Adsorption of toluene, ethylbenzene and xylene isomers on multi-walled carbon nanotubes oxidized by different concentration of NaOCl. *Front. Environ. Sci. Eng. China* **2012,** *6*, 320-329.

15. Krol, M. M.; Oleniuk, A. J.; Kocur, C. M.; Sleep, B. E.; Bennett, P.; Xiong, Z.; O'Carroll, D. M., A Field-Validated Model for *In Situ* Transport of Polymer-stabilized nZVI and Implications for Subsurface Injection. *Environ. Sci. Technol.* **2013,** *47*, 7332-7340.

16. Schrick, B.; Hydutsky, B. W.; Blough, J. L.; Mallouk, T. E., Delivery Vehicles for Zerovalent Metal Nanoparticles in Soil and Groundwater. *Chem. Mater.* **2004,** *16* (11), 2187-2193.

17. R., K. S.; Choi, H., Transport Characteristics of Surface-modified Nanoscale Zero-valent Iron in Porous Media. *Water Sci. Technol.* **2007,** *55*, 157-162.

18. Luo, G.; Yao, H.; Xu, M.; Cui, X.; Chen, W.; Gupta, R.; Xu, Z., Carbon Nanotube-silver Composite for Mercury Capture and Analysis. *Energy Fuels* **2010,** *24*, 419-426.

19. Adebajo, M. O.; Frost, R. L.; Kloprogge, J. T.; Carmody, O.; Kokot, S., Porous Materials for Oil Spill Cleanup: A review of synthesis and absorbing properties. *J. Porous Mater.* **2003,** *10*, 159-170.

20. Teas, C.; Kalligeros, S.; Zanikos, F.; Stournas, S.; Lois, E.; Anastopoulos, G., Investigation of the Effectiveness of Absorbent Materials in Oil Spills Clean Up. *Desalination* **2001,** *140*, 259-264.

21. Use of Sorbent Materials in Oil Spill Response. Limited, T. I. T. O. P. F., Ed. 2012.

22. Zheng, X.; Guo, Z.; Tian, D.; Zhang, X.; Li, W.; Jiang, L., Underwater Self-cleaning Scaly Fabric Membrane for Oily Water Separation. *ACS Appl. Mater. Inter.* **2015,** *7*, 4336-4343.

23. Kong, L.-H.; Chen, X.-H.; Yu, L.-G.; Wu, Z.-S.; Zhang, P.-Y., Superhydrophobic Cuprous Oxide Nanostructures on Phosphor-Copper Meshes and

Their Oil–Water Separation and Oil Spill Cleanup. *ACS Appl. Mater. Inter.* **2015,** *7*, 2616-2625.

24. Chen, N.; Pan, Q., Versatile Fabrication of Ultralight Magnetic Foams and Application for Oil–Water Separation. *ACS Nano* **2013,** *7*, 6875-6883.

25. Gui, X., *et al.*, Soft, Highly Conductive Nanotube Sponges and Composites with Controlled Compressibility. *ACS Nano* **2010,** *4*, 2320-2326.

26. Zhang, Z.; Sèbe, G.; Rentsch, D.; Zimmermann, T.; Tingaut, P., Ultralightweight and Flexible Silylated Nanocellulose Sponges for the Selective Removal of Oil from Water. *Chem. Mater.* **2014,** *26*, 2659-2668.

27. Lin, J.; Shang, Y.; Ding, B.; Yang, J.; Yu, J.; Al-Deyab, S. S., Nanoporous Polystyrene Fibers for Oil Spill Cleanup. *Marine Pollution Bulletin* **2012,** *64*, 347-352.

28. Hu, H.; Zhao, Z.; Gogotsi, Y.; Qiu, J., Compressible Carbon Nanotube–Graphene Hybrid Aerogels with Superhydrophobicity and Superoleophilicity for Oil Sorption. *Environ. Sci. Technol. Lett.* **2014,** *1*, 214-220.

29. Li, X.; Guo, Y.; Zhang, J.; Zhang, L., Preparation of Polysulfone Microspheres with a Hollow Core/porous Shell Structure and their Application for Oil Spill Cleanup. *J. Appl. Polym. Sci.* **2013,** *128*, 2994-2999.

30. Cho, Y. K.; Park, E. J.; Kim, Y. D., Removal of Oil by Gelation using Hydrophobic Silica Nanoparticles. *J. Ind. Eng. Chem.* **2014,** *20*, 1231-1235.

31. Zhu, Q.; Tao, F.; Pan, Q., Fast and Selective Removal of Oils from Water Surface *via* Highly Hydrophobic Core-shell Fe2O3@C Nanoparticles Under Magnetic Field. *ACS Appl. Mater. Interfaces* **2010,** *2*, 3141-3146.

32. Zhu, L., *et al.*, A Simple Method to Synthesize Modified Fe3O4 for the Removal of Organic Pollutants on Water Surface. *Appl. Surf. Sci.* **2012,** *258*, 6326-6330.

33. Yuan, J.; Liu, X.; Akbulut, O.; Hu, J.; Suib, S. L.; Kong, J.; Stellacci, F., Superwetting Nanowire Membranes for Selective Absorption. *Nature Nanotechnology* **2008,** *3*, 332-336.

34. Chu, Y.; Pan, Q., Three-Dimensionally Macroporous Fe/C Nanocomposites as Highly Selective Oil-Absorption Materials. *ACS Appl. Mater. Interfaces* **2012,** *4*, 2420-2425.

35. Hu, H.; Zhao, Z.; Gogotsi, Y.; Qiu, J., Compressible Carbon Nanotube–Graphene Hybrid Aerogels with Superhydrophobicity and Superoleophilicity for Oil Sorption. *Environmental Science & Technology Letters* **2014,** *1* (3), 214-220.

36. Gui, X., *et al.*, Magnetic and Highly Recyclable Macroporous Carbon Nanotubes for Spilled Oil Sorption and Separation. *ACS Appl. Mater. Inter.* **2013,** *5*, 5845-5850.

37. Li, S.; Jiao, X.; Yang, H., Hydrophobic Core/Hydrophilic Shell Structured Mesoporous Silica Nanospheres: Enhanced Adsorption of Organic Compounds from Water. *Langmuir* **2013,** *29*, 1228-1237.

38. Nayab, S., *et al.*, Design and Fabrication of Branched Polyamine Functionalized Mesoporous Silica: An Efficient Absorbent for Water Remediation. *ACS Appl. Mater. Interfaces* **2014,** *6*, 4408-4417.

39. Huang, Y.; Keller, A. A., Magnetic Nanoparticle Adsorbents for Emerging Organic Contaminants. *ACS Sustain. Chem. Eng.* **2013,** *1*, 731-736.

40. Cooke, M., Emerging Contaminants- Perfluorooctane Sulfonate (PFOS) and perfluorooctanoic acid (PFOA). Unites States Environmental Protection Agency: 2014.

41. Perfluorooctanoic Acid (PFOA) and Fluorinated Telomers. http://www.epa.gov/oppt/pfoa/ (accessed May 7, 2015).

42. Zhao, G., *et al.*, Mutagenicity of PFOA in Mammalian Cells: Role of mitochondria-dependent reactive oxygen species. *Environ. Sci. Technol.* **2011,** *45*, 1638-1644.

43. Lu, Y.; Luo, B.; Li, J.; Dai, J., Perfluorooctanoic Acid Disrupts the Blood–testis Barrier and Activates the TNFα/p38 MAPK Signaling Pathway I*n Vivo* and *In Vitro*. *Arch. Toxicol.* **2015**, 1-13.

44. Houde, M.; De Silva, A. O.; Muir, D. C.; Letcher, R. J., Monitoring of Perfluorinated Compounds in Aquatic Biota: An updated review. *Environ. Sci. Technol.* **2011,** *45*, 7962-7973.

45. Giesy, J. P.; Kannan, K., Perfluorochemical Surfactants in the Environment. *Environ. Sci. Technol.* **2002,** *36*, 147A-152A.

46. Bytingsvik, J., *et al.*, Transthyretin-binding Activity of Contaminants in Blood from Polar Bear (Ursus Maritimus) Cubs. *Environ. Sci. Technol.* **2013,** *47* (9), 4778-4786.

47. Roos, A.; Berger, U.; Jarnberg, U.; van Dijk, J.; Bignert, A., Increasing Concentrations of Perfluoroalkyl Acids in Scandinavian Otters (Lutra lutra) Between 1972 and 2011: A new threat to the otter population? *Environ. Sci. Technol.* **2013,** *47*, 11757-11765.

48. Post, G. B.; Louis, J. B.; Cooper, K. R.; Boros-Russo, B. J.; Lippincott, R. L., Occurrence and Potentioal Significance of Perfluorooctanoic Acid (PFOA) Detected in New Jersey Public Drinking Water Systems. *Environ. Sci. Technol.* **2009,** *43*, 4547-4554.

49. Appleman, T. D.; Higgins, C. P.; Quiñones, O.; Vanderford, B. J.; Kolstand, C.; Zeigler-Holady, J. C.; Dickenson, E. R. V., Treatment of Poly- and Perfluoroalkyl Substances in U.S. Full-scale Water Treatment Systems. *Water Res.* **2014,** *51*, 246-255.

50. Quiñones, O.; Snyder, S., Occurrence of Perfluoroalkyl Carboxylates and Sulfonates in Drinking Water Utilities and Related Waters from the United States. *Environ. Sci. Technol.* **2009,** *43*, 9089-9095.

51. 2010/2015 PFOA Stewardship Program. http://www.epa.gov/opptintr/pfoa/pubs/stewardship/ (accessed May 7).

52. Navy Case Study: Occurrence of two emerging contaminants (PFOA & PFOS) at former NAS South Weymouth, MA. Command, N. F. E., Ed. 2013.

53. Vecitis, C. D.; Park, H.; Cheng, J.; Mader, B. T.; Hoffmann, M. R., Treatment Technologies for Aqueous Perfluorooctanesulfonate (PFOS) and Perfluorooctanoate (PFOA). *Front. Environ. Sci. Eng. China* **2009,** *3*, 129-151.

54. Lampert, D. J.; Frisch, M. A.; Speitel Jr., G. E., Removal of Perfluorooctanoic Acid and Perfluorooctave Sulfonate from Wastewater by Ion Exchange. *Pract. Period. Hazard. Toxic Radioact. Waste Manage.* **2007,** *11*, 60-68.

55. Du, Z.; Deng, S.; Chen, Y.; Wang, B.; Huang, J.; Wang, Y.; Yu, G., Removal of Perfluorinated Carboxylates from Washing Wastewater of Perfluorooctanesulfonyl Fluoride Using Activated Carbons and Resins. *J. Hazard. Mater.* **2015,** *286*, 136-143.

56. Giri, R. R.; Ozaki, H.; Guo, X.; Takanami, R.; Taniguchi, S., Oxidative–reductive Photodecomposition of Perfluorooctanoic Acid in Water. *Int. J. Environ. Sci. Te.* **2013,** *11* (5), 1277-1284.

57. Hori, H., *et al.*, Decomposition of Environmentally Persistent Perfluorooctanoic Acid in Water by Photochemical Approaches. *Environ. Sci. Technol.* **2004,** *38*, 6118-6124.

58. Li, X.; Chen, S.; Quan, X.; Zhang, Y., Enhanced Adsorption of PFOA and PFOS on Multiwalled Carbon Nanotubes Under Electrochemical Assistance. *Environ. Sci. Technol.* **2011,** *45*, 8498-8505.

59. Wang, Y.; Zhang, P. Y.; Pan, G.; Chen, H., Photochemical Degradation of Environmentally Persistent Perfluorooctanoic Acid (PFOA) in the Presence of Fe(III). *Chin. Chem. Lett.* **2008,** *19*, 371-374.

60. Nassi, M., *et al.*, Removal of Perfluorooctanoic Acid from Water by Adsorption on Sigh surface Area Mesoporous Materials. *J. Porous Mater.* **2014,** *21*, 423-432.

61. Yao, Y.; Volchek, K.; Brown, C. E.; Robinson, A., Comparative Study on Adsorption of Perfluorooctane Sulfonate (PFOS) and Perfluorooctanoate (PFOA) by Different Adsorbents in Water. *Water Sci. Technol.* **2014,** *7*, 1983-1991.

62. Koda, Y.; Taerashima, T.; Sawamoto, M., Fluorous Microgel Star Polymers: Selective recognition and separation of polyfluorinated surfactants and compounds in water. *J. Am. Chem. Soc.* **2014,** *136*, 15742-15748.

63. Kato, M.; Kamigaito, M.; Sawamoto, M.; Higashimura, T., Polymerization of Methyl Methacylate with the Carbon Tetrechloride/dichlorotris-(triphenylphosphine)ruthenium(II)/Methylaluminum Bis (2,6-di-tert-butylphenoxide) Initiating System: Possibility of living radical polymerization. *Macromolecules* **1995,** *28*, 1721-1723.

64. Wang, J. S.; Matyjaszewski, K., Controlled/"living" Radical Polymerization: Atom transfer radical polymerization in the presence of transition-metal complexes. *J. Am. Chem. Soc.* **1995,** *117*, 5614-5615.

65. Matyjaszewski, K.; Xia, J., Atom Transfer Radical Polymerization. *Chem. Rev.* **2001,** *101*, 2921-2990.

66. Chmielarz, P.; Park, S.; Simakova, A.; Matyjaszewski, K., Electrocemically Mediated ATRP of Acrylamides in Water. *Polymer* **2015,** *60*, 302-307.

67. Pan, X.; Lamson, M.; Yan, J.; Matyjaszewski, K., Photoinduced Metal-free Atom Transfer Radical Polymerization of Acrylonitrile. *ACS Macro. Lett.* **2015,** *4*, 192-196.

68. Okada, S.; Park, S.; Matyjaszewski, K., Initiators for Continuous Activator Regeneration Atom Transfer Radical Polymerization of Methyl Methacrylate and Styrene with N-heterocyclic Carbene as Ligands for Fe-based Catalysts. *ACS Macro Letters* **2014,** *3*, 944-947.

69. Mendonça, P. V., *et al.*, Straightforward ARGET ATRP for the Synthesis of Primary Amine Polymethacrylate with Improved Chain-end Functionality under Mild Reaction Conditions. *Macromolecules* **2014,** *47*, 4615-4621.

70. Mackenzie, M. C.; Shrivats, A. R.; Konkolewicz, D.; Averick, S. E.; McDermott, M. C.; Hollinger, J. O.; Matyjaszewski, K., Synthesis of Poly(meth)acrylates with Thioether and Tertiary Sulfonium Groups by ARGET ATRP and Their Use as siRNA Delivery Agents. *Biomacromolecules* **2015,** *16*, 236-245.

71. Lewis, S. N.; Miller, J. J.; Winstein, S., 1,2-Migrations in alkyl radicals. *J. Org. Chem* **1972,** *37*, 1478-1485.

72. Barton, D. H. R.; McCombie, S. W., A New Method for the Deoxygenation of Secondary Alcohols. *J. Chem. Soc., Perkin Trans. 1* **1975,** (16), 1574-1585.

73. Meijs, G. F.; Rizzardo, E., Chain Transfer by an Addition-fragmentation Mechanism. The use of α-benzyloxystyrene for the preparation of low-molecular-weight poly(methyl methacrylate) and polystyrene. *Macromol. Rapid Commun.* **1988,** *9*, 547-551.

74. Moad, G.; Rizzardo, E.; Thang, S. H., Radical Addition-fragmentation Chamistry in Polymer Synthesis. *Polymer* **2008,** *49*, 1079-1131.

75. Hickey, R. J.; Haynes, A. S.; Kikkawa, J. M.; Park, S. J., Controlling the Self-Assembly Structure of Magnetic Nanoparticles and Amphiphilic Block-Copolymers: From Micelles to Vesicles. *J. Am. Chem. Soc.* **2011,** *133*, 1517-1525.

76. Testimony of Lisa P. Jackson Administrator. U.S. Environmental Protection Agency: 2010.

77. White, H. K., *et al.*, Impact of the Deepwater Horizon Oil Spill on a Deep-Water Coral Community in the Gulf of Mexico. *Proc. Natl. Acad. Sci. U.S.A* **2012,** *109*, 20303-20308.

78. Barron, M. G., Ecological Impacts of the Deepwater Horizon Oil Spill: Implications for Immunotoxicity. *Toxicologic pathology* **2012,** *40*, 315-320.

79. Identification of Oil on Water: Aerial Observation and Identification Guide. Authority, A. M. S., Ed. 2009.

80. Understanding Oil Spills and Oil Spill Response. In *Office of Emergency and Remedial Response*, U.S. Environmental Protection Agency: 1999.

81. Cong, H.; Ren, X.; Wang, P.; Yu, S., Macroscopic Multifunctional Graphene-based Hydrogels and Aerogels by a Metal Ion Induced Self-assembly Process. *ACS Nano* **2012,** *6*, 2693-2703.

82. Korhonen, J. T.; Kettunen, M.; Ras, R. H.; Ikkala, O., Hydrophobic Nanocellulose Aerogels as Floating, Sustainable, Reusable, and Recyclable Oil Absorbents. *ACS Appl. Mater. Interfaces* **2011,** *3*, 1813-1816.

83. Basak, S.; Nanda, J.; Banerjee, A., A New Aromatic Amino Acid Based Organogel for Oil Spill Recovery. *J. Mater. Chem.* **2012,** *22*, 11658-11664.

84. Zhu, Q.; Pan, Q.; Liu, F., Facile Removal and Collection of Oils from Water Surfaces through Superhydrophobic and Superoleophilic Sponges. *J. Phys. Chem. C* **2011,** *115*, 17464-17470.

85. Calcagnile, P., *et al.*, Magnetically Driven Floating Foams for the Removal of Oil Contaminants from Water. *ACS Nano* **2012,** *6*, 5413-5419.

86. More Efficient Cleanup of Oil Spills. *Tribol Lubr. Technol.* **2008,** *64*, 12-13.

87. Pyun, J., Nanocomposite Materials from Functional Polymers and Magnetic Colloids. *Polym. Rev.* **2007,** *47*, 231-263.

88. Wang, S.; Li, M.; Lu, Q., Filter Paper with Selective Absorption and Separation of Liquids that Differ in Surface Tension. *ACS Appl. Mater. Interfaces* **2010,** *2*, 677-683.

89. Feng, X. J.; Jiang, L., Design and Creation of Superwetting/antiwetting Surfaces. *Adv. Mater.* **2006,** *18*, 3063-3078.

90. Dollhopf, R., Proposed Order for Recovery of Submerged Oil. Agency, U. S. E. P., Ed. 2012.

91. Wang, P.; Shi, Q.; Shi, Y.; Clark, K. K.; Stucky, G. D.; Keller, A. A., Magnetic Permanently Confined Micelle Arrays for Treating Hydrophobic Organic Compound Contamination. *J. Am. Chem. Soc.* **2009,** *131*, 182-188.

92. Wu, A.; Ou, P.; Zeng, L., Biomedical Applications of Magnetic Nanoparticles. *Nano Brief Reports Rev.* **2010,** *05*, 245-270.

93. Zeisberger, M.; Dutz, S.; Müller, R.; Hergt, R.; Matoussevitch, N.; Bönnemann, H., Metallic Cobalt Nanoparticles for Heating Applications. *J. Magn. Magn. Mater.* **2007,** *311*, 224-227.

94. O'Reilly, R. K.; Joralemon, M. J.; Hawker, C. J.; Wooley, K. L., Facile Syntheses of Surface-Functionalized Micelles and Shell Cross-Linked Nanoparticles. *J. Polym. Sci., Part A: Polym. Chem.* **2006,** *44*, 5203-5217.

95. Lin, L. Y.; Lee, N. S.; Zhu, J.; Nystrom, A. M.; Pochan, D. J.; Dorshow, R. B.; Wooley, K. L., Tuning Core *vs*. Shell Dimensions to Adjust the Performance of Nanoscopic Containers for the Loading and Release of Doxorubicin. *J. Controlled Release* **2011,** *152*, 37-48.

96. Sun, S.; Zeng, H.; Robinson, D. B.; Raoux, S.; Rice, P. M.; Wang, S. X.; Li, G., Monodisperse MFe2O4 (M= Fe, Co, Mn) Nanoparticles. *J. Am. Chem. Soc.* **2004,** *126*, 273-279.

97. Bao, N.; Shen, L.; Wang, Y.; Padhan, O.; Gupta, A., A Facile Thermolysis Route to Monodisperse Ferrite Nanocrystals. *J. Am. Chem. Soc.* **2007,** *129*, 12374-12375.

98. Davis, K. A.; Charleux, B.; Matyjaszewski, K., Preparation of Block Copolymers of Polystyrene and Poly (*t*-butyl acrylate) of Various Molecular Weights and Architectures by Atom Transfer Radical Polymerization. *J. Polym. Sci., Part A: Polym. Chem.* **2000,** *38*, 2274–2283.

99. Kim, B.; Qiu, J.; Wang, J.; Taton, T. A., Magnetomicelles: Composite nanostructures from magnetic nanoparticles and cross-linked amphiphilic block copolymers. *Nano Lett.* **2005,** *5*, 1987-1991.

100. Joralemon, M. J.; O'Reilly, R. K.; Hawker, C. J.; Wooley, K. L., Shell Click-Crosslinked (SCC) Nanoparticles: A New Methodology for Synthesis and Orthogonal Functionalization. *J. Am. Chem. Soc.* **2005,** *127*, 16892-16899.

101. Huang, H.; Kowalewski, T.; Remsen, E. E.; Gertzmann, R.; Wooley, K. L., Hydrogel-Coated Glassy Nanospheres: A novel method for the synthesis of shell cross-linked knedels. *J. Am. Chem. Soc.* **1997,** *119*, 11653-11659.

102. Lehr, B.; Bristol, S.; Possolo, A., Oil Budget Calculator: Deepwater Horizon. Team, T. F. I. S. G. a. O. B. C. S. a. E., Ed. 2010.

103. Buchanan, G. W.; Munteanu, W.; Dawson, B. A.; Hodgson, D., Concerning the Origin of ^{19}F-^{19}F NMR COSY and NOESY Connections in the Spectra of Perfluorooctanoic Acid, R_f-palmitic Acid-F_{13} and Diethyl Perfluorosuberate. *Magn. Reson. Chem.* **2005,** *43*, 528-534.

104. Huang, T.; Brown, R.; Cong, R.; Yau, W.; Hazlitt, L.; deGroot, A. W., "True" Concentration Determination Using a Concentration and Composition Sensitive Infrared

Detector for Molecular Weight Characterization of Polyolefins. *Macromol. Symp.* **2012,** *312*, 20-26.

105. Usami, T.; Gotoh, Y.; Takayama, S., Determination of the Ring Concentration in Polyoctenamer. *Eur. Polym. J.* **1985,** *21*, 885-889.

106. Bajaj, H.; Sharma, V. K.; Kalonia, D. S., A High-Throughput Method for Detection of Protein Self-Association and Second Virial Coefficient Using Size-Exclusion Chromatography Through Simultaneous Measurement of Concentration and Scattered Light Intensity. *Pharm.. Res.* **2007,** *24*, 2071-2083.

107. Chu, Y.; Pan, Q., Three-Dimensionally Macroporous Fe/C Nanocomposites As Highly Selective Oil-Absorption Materials. *ACS Applied Materials & Interfaces* **2012,** *4* (5), 2420-2425.

108. Wu, L.; Li, L.; Li, B.; Zhang, J.; Wang, A., Magnetic, Durable, and Superhydrophobic Polyurethane@Fe3O4@SiO2@Fluoropolymer Sponges for Selective Oil Absorption and Oil/Water Separation. *ACS Appl. Mater. Inter.* **2015,** *7*, 4936-4946.

109. Palchoudhury, S.; Lead, J. R., A Facile and Cost-Effective Method for Separation of Oil–Water Mixtures Using Polymer-Coated Iron Oxide Nanoparticles. *Environmental Science & Technology* **2014,** *48* (24), 14558-14563.

110. Pavia-Sanders, A.; Zhang, S.; Flores, J. A.; Sanders, J. E.; Raymond, J. E.; Wooley, K. L., Robust Magnetic/Polymer Hybrid Nanoparticles Designed for Crude Oil Entrapment and Recovery in Aqueous Environments. *ACS Nano* **2013,** *7*, 7552-7561.

111. USEPA Oil Spill Response Techniques. http://www.epa.gov/swercepp/web/content/learning/oiltech.htm (accessed July 2015).

112. ZoBell, C. E., *Marine Microbiology: A monograph on hydrobacteriology*. Chronica Botanica Company: The University of California, 1946; Vol. 17, p 240.

113. Kunacheva, C., *et al.*, Worldwide Surveys of Perfluorooctane Sulfonate (PFOS) and Perfluorooctanoic Acid (PFOA) in Water Environment in Recent Years. *Water Sci. Technol.* **2012,** *66*, 2764-2771.

114. Deng, S.; Zheng, Y. Q.; Xu, F. J.; Wang, B.; Huang, J.; Yu, G., Highly Efficient Sorption of Perfluorooctane Sulfonate and Perfluorooctanoate on a Quaternized Cotton Prepared by Atom Transfer Radical Polymerization. *Chem. Eng. J.* **2012,** *193-194*, 154-160.

115. Flores, J. A.; Pavía-Sanders, A.; Chen, Y.; Pochan, D. J.; Wooley, K. L., Recyclable Hybrid Inorganic/Organic Magnetically Active Networks for the

Sequestration of Crude Oil from Aqueous Environments. *Chemistry of Materials* **2015,** *27* (10), 3775-3782.

116. Gu, L.; Fang, R. H.; Sailor, M. J.; Park, J.-H., In Vivo Clearance and Toxicity of Monodisperse Iron Oxide Nanocrystals. *ACS Nano* **2012,** *6* (6), 4947-4954.

117. Yalcin, S.; Khodadust, R.; Unsoy, G.; Ceren Garip, I.; Didem Mumcuoglu, Z.; Gunduz, U., Synthesis and Characterization of Polyhydroxybutyrate Coated Magnetic Nanoparticles: Toxicity Analyses on Different Cell Lines. *Synth. React. Inorg. Met.-Org. Chem.* **2014,** *45*, 700-708.

118. Borkar, S.; Jankova, K.; Siesler, H. W.; Hvilsted, S., New Highly Fluorinated Styrene-based Materials with Low Surface Energy Prepared by ATRP. *Macromolecules* **2004,** *37*, 788-794.

119. Chong, Y. K.; Moad, G.; Rizzardo, E.; Thang, S. H., Thiocarbonylthio End Group Removal from RAFT-Synthesized Polymers by Radical-Induced Reduction. *Macromolecules* **2007,** *40* (13), 4446-4455.

120. Willcock, H.; O'Reilly, R. K., End Group Removal and Modification of RAFT Polymers. *Polym. Chem.* **2010,** *1*, 149-157.

121. Cantrell, K. J.; Kaplan, D. I.; Weitsma, T. W., Zero-valent Iron for the *In Situ* Remediation of Selected Metals in Groundwater. *J. Hazard. Mater.* **1995,** *42*, 201-212.

122. Hoag, G. E. System for Soil and Water Remediation. 2008.

123. Calafat, A. M.; Wong, L. Y.; Kuklenyik, Z.; Reidy, J. A.; Needham, L. L., Polyfluoroalkyl Chemicals in the U.S. Population: Data from the National Health and Nutrition Examination Survey (NHANES) 2003–2004 and Comparisons with NHANES 1999–2000. *Environ Health Perspect* **2007,** *115*, 1596-1602.

124. D'eon, J. C.; Simpson, A. J.; Kumar, R.; Baer, A. J.; Mabury, S. A., Determining the Molecular Interactions of Perfluorinated Carboxylic Acids with Human Sera and Isolated Human Serum Albumin Using Nuclear Magnetic Resonance Spectroscopy. *Environ Toxicol Chem* **2010,** *29*, 1678-1688.

125. Zou, J.; Zhang, S.; Shrestha, R.; Seetho, K.; Donley, C. L.; Wooley, K. L., pH-Triggered Reversible Morphological Inversion of Orthogonally-addressable Poly(3-acrylamidophenylboronic acid)-block-poly(acrylamidoethylamine) Micelles and their Shell Crosslinked Nanoparticles. *Polym. Chem.* **2012,** *3*, 3146-3156.

126. Barron, M. G., Ecological Impacts of the Deepwater Horizon Oil Spill: Implications for Immunotoxicity. *Toxicol. Pathol.* **2012,** *40* (2), 315-320.

127. D'Andrea, M. A.; Reddy, G. K., Health Risks Associated with Crude Oil Spill Exposure. *Am. J. Med.* **2014,** *127*, 886.e889-886.e813.

128. Hansen, B. H., *et al.*, Reproduction Dynamics in Copepods Following Exposure to Chemically and Mechanically Dispersed Crude Oil. *Environ. Sci. Technol.* **2015,** *49*, 3822-3829.

129. Duan, B.; Gao, H.; He, M.; Zhang, L., Hydrophobic Modification on Surface of Chitin Sponges for Highly Effective Separation of Oil. *ACS Appl. Mater. Interfaces* **2014**.

130. Yang, Y.; Tong, Z.; Ngai, T.; Wang, C., Nitrogen-rich and Fire-resistant Carbon Aerogels for the Removal of Oil Contaminants from Water. *ACS Appl. Mater. Interfaces* **2014,** *6*, 6351-6360.

131. Chin, S. F.; Binti Romainor, A. N.; Pang, S. C., Fabrication of Hydrophobic and Magnetic Cellulose Aerogel with High Oil Absorption Capacity. *Mater. Lett.* **2014,** *115*, 241-243.

132. Gu, J.; Jiang, W.; Wang, F.; Chen, M.; Mao, J.; Xie, T., Facile Removal of Oils from Water Surfaces through Highly Hydrophobic and Magnetic Polymer Nanocomposites. *Appl. Surf. Sci.* **2014,** *301*, 492-499.

133. Zhu, J.; Zhang, S.; Zhang, K.; Wang, X.; Mays, J. W.; Wooley, K. L.; Pochan, D. J., Disk-Cylinder and Disk-Sphere Nanoparticles via a Block Copolymer Blend Solution Construction. *Nat. Commun.* **2013,** *4*.

134. Jang, S. G., *et al.*, Striped, Ellipsoidal Particles by Controlled Assembly of Diblock Copolymers. *J. Am. Chem. Soc.* **2013,** *135*, 6649-6657.

135. Pochan, D. J.; Chen, Z.; Cui, H.; Hales, K.; Qi, K.; Wooley, K. L., Toroidal Triblock Copolymer Assemblies. *Science* **2004,** *306*, 94-97.

136. Lee, N. S., *et al.*, Influence of Nanostructure Morphology on Host Capacity and Kinetics of Guest Release. *Small* **2011,** *7*, 1998-2003.

137. Geng, Y.; Discher, D. E., Visualization of Degradable Worm Micelle Breakdown in Relation to Drug Release. *Polymer* **2006,** *47*, 2519-2525.

138. Pochan, D. J.; Zhu, J.; Zhang, K.; Wooley, K. L.; Miesch, C.; Emrick, T., Multicompartment and Multigeometry Nanoparticle Assembly. *Soft Matter* **2011,** *7* (6), 2500-2506.

APPENDIX A

EXPLORATIONS INTO DIVERSE MORPHOLOGICAL ASSEMBLIES FOR NOVEL HYBRID SYSTEMS

A.1 Introduction

The use of petroleum is deeply ingrained in our society, as it accounts for a significant portion of energy generation. However, the transport, storage, and usage of crude oil and petroleum derivatives have led to increasing issues with environmental contamination. Oil spills, ranging from minor incidents to catastrophic events such as the Deepwater Horizon spill in 2010, pose severe threats to both human and environmental health.[126,127] To rapidly contain and recovery contaminants immediately following a spill, the initial stage of oil recovery involves the use of various mechanical techniques: booms, skimmers, and suction-based removal.[78,127] However, these methods applied during the bulk recovery phase are not effective for areas of low oil concentration. The removal of this residual oil, or sheen, remains a major barrier to the efficient remediation of oil spills. Moreover, current sheen recovery techniques are often labor-intensive and inefficient, as well as possibly toxic to present wildlife.[128]

In response to the lack of effective techniques for sheen removal, much interest has been placed on novel developments in nanotechnology. Many nanomaterials for applications in oil-water separation have been investigated, including fibers,[27] sponges,[26, 129] aerogels,[28, 130] and nanoparticles.[29-30] Materials with magnetic character, in particular, have attracted a considerable amount of interest, as these provide a facile means of recovery following pollutant collection. Among these materials, aerogels,[131]

sponges,[108] nanocomposites, [132] and nanoparticles[110,115] have been shown to be efficient in pollutant sequestration and recovery. However, these primarily hydrophobic materials are also limited in efficiency for field applications, as they fail to account for submerged oil, a crucial problem in oil spills.

Recently, our group has addressed these current limitations in nanotechnology through the development of a hybrid inorganic-organic magnetic shell crosslinked knedel-like (MSCK) nanoparticle system.[110] These MSCKs, comprised of amphiphilic diblock copolymers of poly(acrylic acid)$_{20}$-*block*-polystyrene$_{280}$ (PAA$_{20}$-*b*-PS$_{280}$), demonstrated the applicability of amphiphilic systems in oil removal, as compared to previously designed hydrophobic systems. Additionally, the magnetically-active cores of the MSCKs, achieved through the entrapment of iron oxide nanoparticles within the polymer framework, allowed for facile removal *via* magnetic force following oil sequestration. These well-defined spherical nanoparticles *ca*. 70 nm in diameter exhibited unprecedented oil uptake capacities that reach ten times their mass. The success of the MSCK system subsequently prompted investigations into the effect of morphological changes from the original core-shell structure on the efficiency of oil loading. Through the variation of the polymeric components, the co-assembly methods, or the degree of iron oxide incorporation, materials of different morphological assemblies can be produced. In recent years, several interesting micellar structures beyond traditional spheres have been explored, including vesicles,[75] disk-like micelles,[133] and ellipsoidal micelles.[134] For instance, the Pochan group has studied toroidal structures,[135] as well as numerous blended micellar structures, such as disk-

cylinder and disk-sphere micelles.[133] These interesting morphologies offer new alternatives for highly efficient nanoparticles for oil recovery.

Consequently, we investigated the development of cylindrical structures, as we anticipated that these hybrid nanoparticles would result in a higher degree of oil sequestration, as compared to the original MSCK system. Cylindrical micelles have been previously shown to result in increased loading of drug molecules, relative to analogous spherical morphology.[136-137] As an extension, cylindrical nanoparticles were expected to result in a higher degree of encapsulation of oil. However, rather than cylindrical structures, hybrid toroidal nanoparticles were synthesized following the co-assembly process and subsequent solvent exchange. Furthermore, by altering the co-assembly method for the same polymeric material, miniature MSCK nanoparticles *ca*. 40 nm in diameter were produced. Both the toroidal and miniature MSCK structures were tested against a complex crude oil to demonstrate their efficiency as environmental remediation agents, demonstrating that morphological changes can offer distinct improvements in oil sequestration capabilities.

A.2 Results and Discussion

Design of a new hybrid magnetic system. The polymeric component of PAA_{90}-*b*-PS_{120} (Scheme A.1) was chosen for development of this new hybrid system, as it has been shown to form cylindrical particles in the presence of 2,2'-(ethylenedioxy)bis(ethylamine) (EDDA).[138] Cylindrical structures were chosen due to their ideal volume-to-surface-area ratios which allow them to have a greater loading

capacity relative to spherical structures.[136] Hybrid magnetic magnetic structures are expected to have greater pollutant loading capabilities than their spherical counterparts. To test this hypothesis, hybrid spherical particles comprised of the same diblock copolymer were similarly synthesized to compare the oil loading capabilities of these two morphologies.

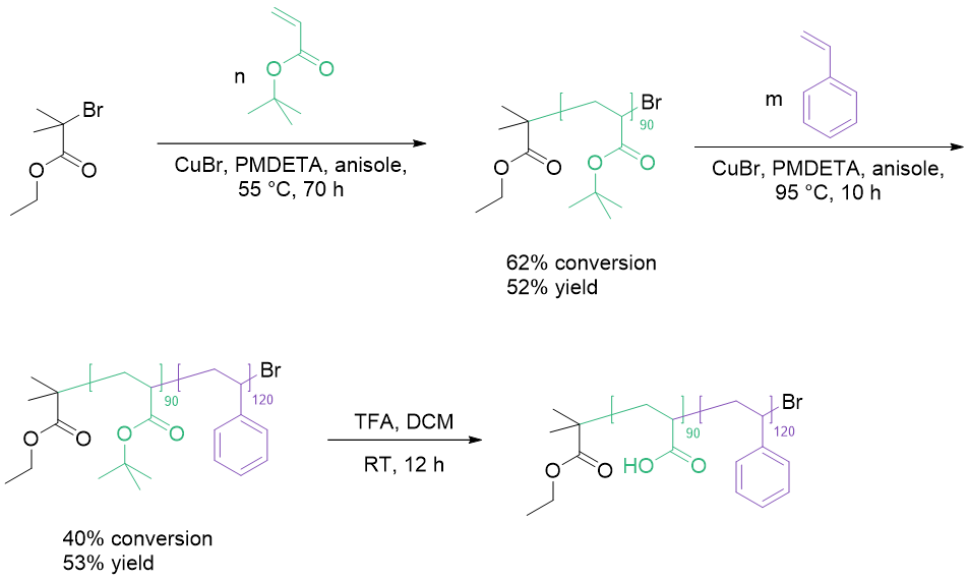

Scheme A.1. Synthesis of diblock copolymer PAA_{90}-*b*-PS_{120}.

Co-assembly and crosslinking of new hybrid magnetic system. Cylindrical structures were achieved using a modified method of a previously reported procedure. Briefly, an organic solution containing both the polymeric component and oleic acid-stabilized iron oxide nanoparticles at a concentration of 0.33 mg/mL was prepared. To this solution, 4× mass eq. of EDDA were added; EDDA interacts with the negatively charged PAA section of the diblock copolymer to form non-covalent bonds that drive the creation of cylindrical micelles. After homogeneity was achieved, 4.5 vol eq. of nanopure water were added to the stirring solution at a rate of 22.5 mL/h. Following an additional 24 hours of vigorous stirring to allow for the formation of the desired morphological structures, cylindrical micelles of varying lengths and an average diameter of 32 ± 4 nm were obtained. Due to the non-spherical nature of these structures, dynamic light scattering (DLS) characterization was not possible. The produced nanostructures were nominally crosslinked utilizing 25% of the acrylic acid groups present by the addition of 1-[3-(dimethylamino)propyl]-3-ethylcarbodiimide methiodide (EDCI). Following extensive dialysis against nanopure water for the removal of the organic solvent, a morphological change was observed to what is currently believed to be toroidal micelles (Figure A.1). AFM studies are ongoing in order to determine if the resulting particles are toroids or vesicles.

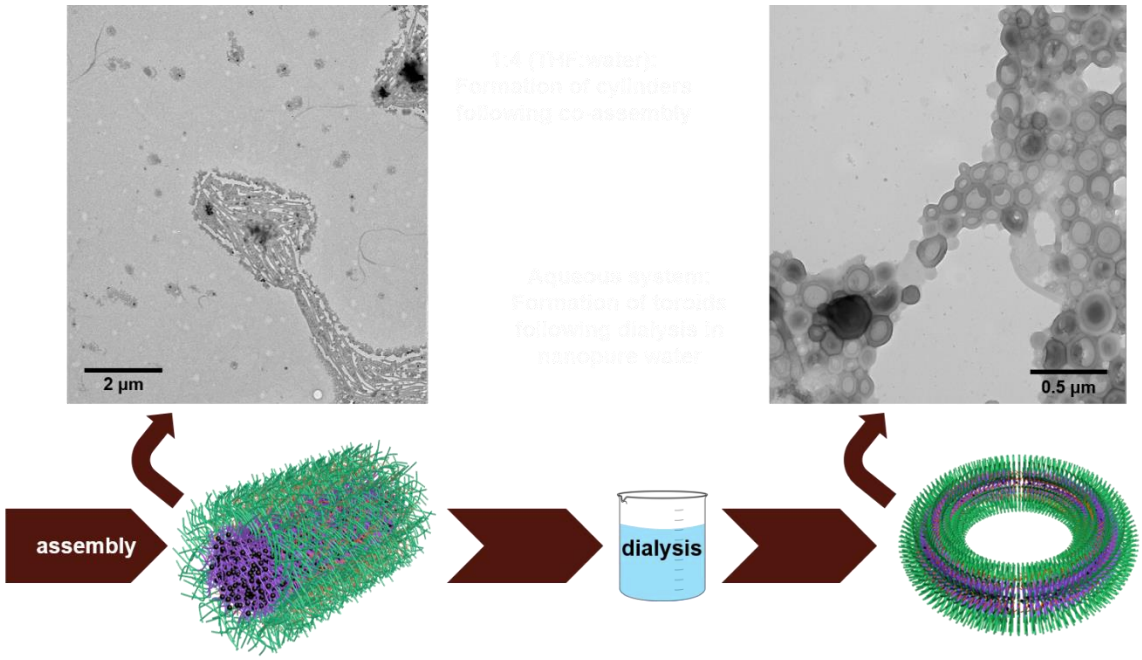

Figures A.1. TEM images showing the morphological change experienced by the cylindrical micelles following dialysis.

Micellar structure nominally crosslinked using 50% and 100% of the acrylic acid groups were also produces and the same morphological change was observed. The efficiency of crosslinking needs to be verified, and the experiment is ongoing.

Co-assembly and crosslinking of hybrid spherical nanoparticles. Spherical hybrid nanoparticles were obtained through a similar co-assembly method, without the presence of EDDA. Briefly, an organic solution containing both the polymeric component and oleic acid-stabilized iron oxide nanoparticles at a concentration of 0.33 mg/mL was prepared. After homogeneity was achieved, 4.5 vol eq. of nanopure water

were added to the stirring solution at a rate of 22.5 mL/h. The micellar hybrid structures were characterized by DLS and TEM. DLS analysis showed particles with hydrodynamic radii of 58 ± 15 nm and TEM characterization showed nanoparticles with diameters of 52 ± 7 nm (after counting over 50 micelles) (Fig. A.2). The obtained nanoparticles were subsequently crosslinked utilizing 25% of the acrylic acid groups present by the addition of EDDA in the presence of EDCI. Following extensive dialysis against nanopure water for the removal of the organic solvent, DLS analysis showed particles with hydrodynamic radii of 36 ± 10 nm, and TEM characterization showed nanoparticles with diameters of 41 ± 7 nm (after counting over 50 MSCKs) (Fig. A.3).

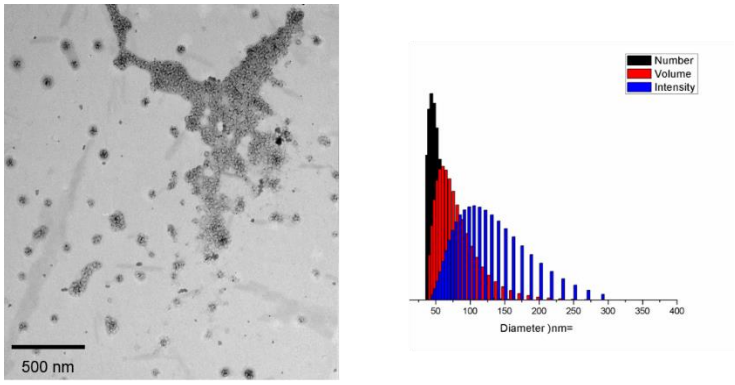

Figure A.2. TEM (left) and DLS (right) characterization of hybrid spherical micellar structures.

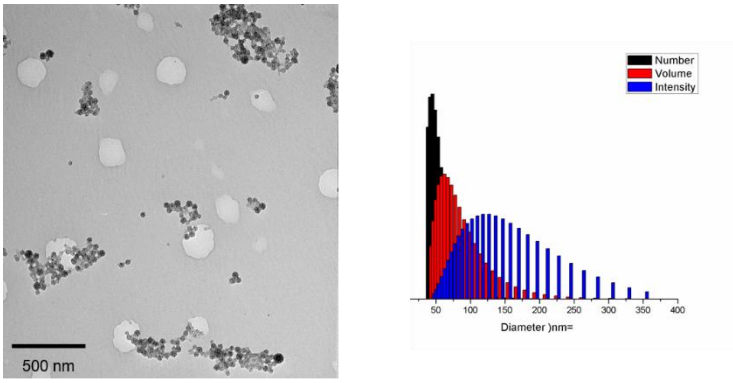

Figure A.3. TEM (left) and DLS (right) characterization of MSCK nanoparticles.

General oil sequestration and quantification. Weathered crude oil was added to deionized (DI) water in order to mimic contaminated water samples in 5 mL capped vials. The lyophilized powder samples of the hybrid nanoparticle systems were then added to the crude oil contaminated water at initial hybrid particle:oil weight ratios of 1:4.31, 1:6.31, 1:10.33, 1:15.12, and 1:20.33 (these rations are specific for the toroids/vesicles). With both the hybrid toroids/vesicles and MSCKs, a noticeable change in color was observed within seconds after addition to the crude-oil contaminated water. This change in color is attributed to oil sequestration by the hybrid systems and was used qualitatively to determine uptake. Following *ca.* 30 min, the hybrid systems were easily and quickly (in a matter of seconds) attracted to the external magnetic field of a neodymium magnet to allow for the decanting of the contaminated water. The weathered crude oil was then extracted from the water with the aid of chloroform to

allow for quantification of the pollutant through the use of the refractive index (RI) of the oil and a polystyrene (PS) standard (MW = 70,950 Da) using GPC. This PS internal standard was used as a means of normalizing the data obtained. The integration of the crude oil peaks (observed in the chromatogram as a broad band with high retention time) was performed by developing a mathematical relationship between the area under the peak and the mass of oil present. This relationship was achieved through the use of control groups to derive an empirical coefficient relating oil concentration to the integration value in the chromatogram. This co-efficient was later utilized to determine the unknown oil concentration left behind following nanoparticle deployment and removal.

Remediation results. A mass analysis of the hybrid toroids/vesicles was performed as a means of determining the magnetic efficiency of the material. It was found that only *ca.* 70% of the material was magnetically active and responsive to the external magnetic field during decanting. As such, the oil recovery capabilities of this material are reported as mg of oil removed per mg of the magnetically active material; the reason for this is that the non-magnetically-active material would have been present during the chloroform washings and therefore the oil encapsulated by it would have been in the samples injected through the GPC during quantification. For the trials of 1:4.31, 1:6.31, 1:10.33, 1:15.12, and 1:20.33, the sorption limit were found to be, 1:1.47, 1:3.38, 1:4.91, 1:8.48, and 1:8.94, respectively. The percentage oil recovery was also determined (Fig. A.4). Through these experiments, the maximum loading capability of this material was determined to be *ca.* 1:13.

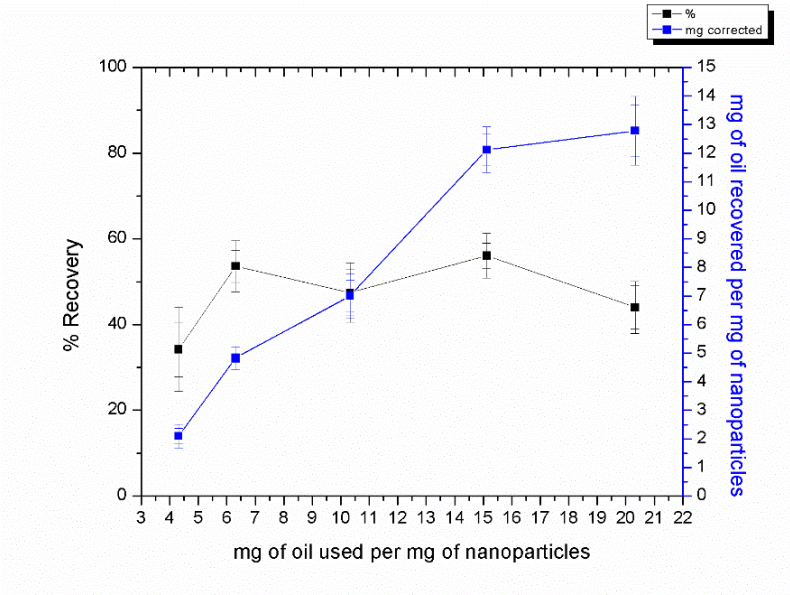

Figure A.4. Oil recovery data for hybrid toroids/vesicles. Percentage recovery in black. Mass recovered in blue.

A mass analysis of the magnetic responsivity of the MSCK nanoparticles showed a magnetic recovery of over 98%. This result is not surprising considering that the TEM analysis of these MSCKs showed a high incorporation of the iron oxide nanoparticles, whereas the toroid/vesicle structures showed very little incorporation of the iron oxide nanoparticles. A series of oil sequestration trials with initial MSCK:oil ratios of 1:6.43, 1:10.37, 1:15.47, and 1:19.83 were performed. The sorption limits of these experiments were determined to be 1:1.72, 1:2.61, 1:4.49, and 1:4.75, respectively (Fig. A.5). The maximum loading capability of this material was determined to be *ca.* 1:5; this loading is almost a third of that achieved by the toroids/vesicles.

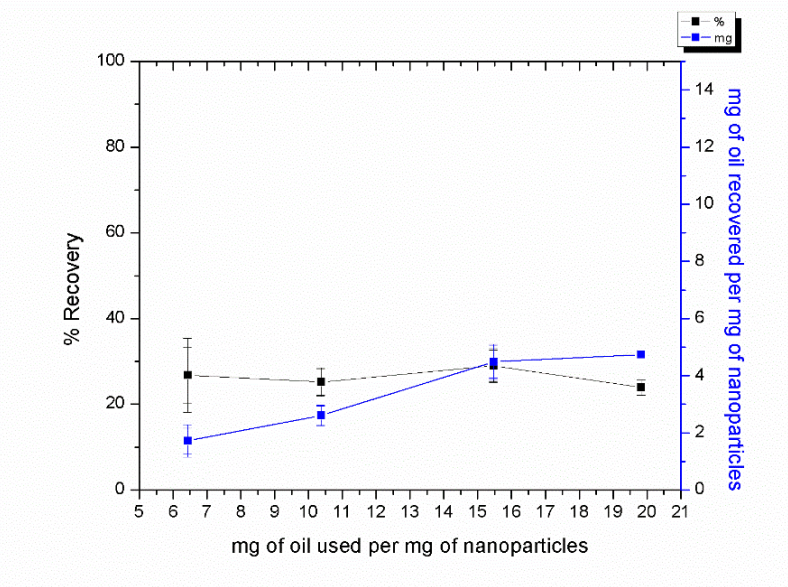

Figure A.5. Oil recovery data for MSCKs. Percentage recovery in black. Mass recovered in blue.

A.3 Conclusions

Although further research is needed in order to determine the true morphological nature of the hybrid toroid/vesicle nanoparticles produced and the extent of crosslinking, if any, these nanoparticles have shown super oil recovery capabilities, having a loading capacity of almost 3× that shown by their MSCK counterparts. Ongoing and future work is needed to better characterize the hybrid nanoparticles obtained following crosslinking and dialysis. However, these preliminary results indicate that the development of hybrid systems with interesting morphological structures are potential

candidates for oil spill remediation with higher loading capacities than those previously reported by our group.[110,115]

A.4 Materials and Methods

Materials. All chemicals were purchased from Aldrich Chemical Co. and used without further purification unless otherwise noted. *tert*-Butyl acrylate and styrene monomers were purified through an alumina plug to remove stabilizer. Iron(III) acetyl-acetonate was purchased from Strem Chemicals, Inc. Nanopure water (18 MΩ·cm) was acquired by means of a Milli-Q water filtration system, Millipore Corp. (Bedford, MA). Neodymium magnet (90 lb pull) was purchased from magnets4less.com. Crude oil for this research was generously donated by Enbridge Energy Partners, L.P.

Characterization techniques. ^{1}H NMR and ^{13}C NMR spectra were recorded on an Inova 300 or Mercury 300 spectrometer interfaced to a UNIX computer using VnmrJ software. Samples were prepared as solutions in $CDCl_3$ or THF-d_8, and solvent protons were used as internal standard. IR spectra were recorded on an IR Prestige 21 system (Shimadzu Corp., Japan). A small amount of sample was placed to cover the ATR crystal for IR measurements. Data were analyzed using IRsolution software. Differential scanning calorimetry studies were performed on a Mettler Toledo DSC822 (Mettler-Toledo, Inc., Columbus, OH) calibrated according to the standard procedures using indium. The heating rates were 10 °C min^{-1} and cooling rates were 10 °C min^{-1} with a temperature range of – 100 to 150 °C. Thermogravimetric analysis was performed under Ar atmosphere using a Mettler Toledo model TGA/DSC1 with a

heating rate of 10 °C/min. Measurements were analyzed using Mettler Toledo STAR^e software v 10.00. THF gel permeation chromatography (GPC) was performed on a system equipped with Waters chromatography, Inc. (Milford, MA) model 1515 isocratic pump and a model 2414 differential refractometer with a three-column set of Polymer Laboratories, Inc. (Amherst, MA) Styragel columns (PL_{gel} 5 μm Mixed C, 500 Å, and 10^4 Å, 300 7.5 mm columns) and a guard column (PL_{gel} 5 μm, 50 7.5 mm). The system was equilibrated at 40 °C in THF, which served as the polymer solvent an eluent (flow rate set to 1.00 mL/min). The differential refractometer was calibrated with Polymer Laboratories, Inc., polystyrene standards (300 – 467,000 Da0. Polymer solutions were prepared at a concentration of *ca*. 3 mg/mL with 0.05% vol toluene as a flow rate marker. An injection volume of 200 μL was used. Data were analyzed using Empower Pro software from Waters Chromatography, Inc. Chloroform GPC for oil quantification was conduction on a system equipped with a Tosoh Corporation (Tokyo, Japan) model HLC-8320 EcoSEC system with a two-column set of TOSOH Bioscience columns. The system was equilibrated at 30 °C in chloroform, which served as the polymer solvent and eluent (flow rate set to 0.600 mL/min). The differential refractometer was calibrated with Polymer Laboratories, Inc. polystyrene standards (580 – 370,000 Da). Polymer solutions were prepared at a concentration of *ca.* 3 mg/mL and an injection volume of 200 μL was used. Dynamic light scattering (DLS) measurements were conducted using Delsa Nano C from Beckman Coulter, Inc. (Fullerton, CA) equipped with a laser diode operating at 658 nm. Size measurements were made in water (n = 1.3329, η = 0.890 cP at 25 ± 1 °C; n = 1.3293, η = 0.547 cP at 50 ± 1 °C; n =

1.3255, η = 0.404 cP at 70 ± 1 °C). Scattered light was detected at 165° angle and analyzed using a log correlator over 70 accumulations for a 0.5 mL of sample in a glass sizing cell (0.9 mL capacity). The photomultiplier aperture and the attenuator were automatically adjusted to obtain a photon counting rate of *ca*. 10 kcps. The calculations of the particle size distribution and distribution averages were performed using CONTIN particle size distribution analysis routines. Prior to analysis, the samples were filtered through a 0.45 μm Whatman nylon membrane filter (Whatman, Inc.). The samples in the glass sizing cell were equilibrated at the desired temperature for 5 min before measurements were made. The peak average of histograms from intensity, volume, or number distributions out of 70 accumulations was reported as the average diameter of the particles.

Synthesis of poly(*tert*-butyl acrylate) (P*t*BA$_{90}$) *via* ATRP. A flame-dried 25-mL Schlenk flask equipped with a magnetic stir bar was charged with PMDETA (1.1 equiv, 51.7 mg, 0.3 mmol), *t*BA (150 equiv, 4.9892 g, 38.9 mmol), ethyl α-bromoisobutyrate (1 equiv, 50.8 mg, 0.3 mmol), and anisole (5 mL). The flask was sealed with a rubber septum, and the reaction mixture was degassed by three freeze–pump–thaw cycles. Then, the CuBr (1.1 equiv, 40.9 mg, 0.3 mmol) was added under a nitrogen flow to the frozen mixture. Following three additional freeze–pump–thaw cycles, the reaction mixture was allowed to return to room temperature and to stir for 5 min to ensure homogenous mixing. The flask was then immersed into a preheated oil bath at 55 °C to start the polymerization. The polymerization was monitored by analyzing aliquots collected at predetermined times by ^{1}H NMR spectroscopy. When

the expected monomer conversion was reached, *ca.* 66 h, the polymerization was quenched by quick immersion of the reaction flask into liquid N_2 and exposure to air. THF (20 mL) was added to the reaction flask, and the polymer was purified by filtration through an alumina plug followed by subsequent precipitation into 500 mL of a methanol/ice mixture (3×). The precipitant was collected and dried under vacuum overnight to yield 1.19 g of P*t*BA$_{90}$ as an off-white solid, giving 40% yield of the 60% conversion polymerization. $M_{n(NMR)}$ = 9,900 Da, $M_{n(GPC)}$ = 14,300 Da, PDI = 1.04. IR: 2978, 2931, 2870, 1720, 1473, 1450, 1381, 1365, 1249, 1141, 1033, 918, 840, 795, 748 cm^{-1}. ^{1}H NMR (300 MHz, $CDCl_3$) δ 4.08 (q, *J* = 7 Hz, 2H), 2.37 – 2.09 (br, 90H), 1.94 – 1.72 (br, 42H), 1.69 – 1.28 (m, br, 915H), 1.28 – 1.19 (m, 17H) 1.16 – 1.09(m, 6H) ppm. ^{13}C NMR (75 MHz, THF) characterization ongoing. DSC: T_g = 50 °C. TGA: T_{onset} = 216 °C, $T_{decomposition}$ = (216 – 452 °C) 76% mass loss; 24% mass remaining.

Synthesis of poly(*tert*-butyl acrylate)$_{90}$-*b*-polystyrene$_{120}$ (P*t*BA$_{90}$-*b*-PS$_{120}$) *via* ATRP. A flame-dried 25-mL Schlenk flask equipped with a magnetic stir bar was charged with PMDETA (1.1 equiv, 8.5 mg, 0.05 mmol), styrene (300 equiv, 1.2962 g, 12.5 mmol), P*t*BA$_{90}$ (1 equiv, 500.5 mg, 0.04 mmol), and anisole (5 mL). The flask was sealed with a rubber septum, and the reaction mixture was degassed by three freeze–pump–thaw cycles. Then, the CuBr (1.1 equiv, 36.6 mg, 0.05 mmol) was added under a nitrogen flow to the frozen mixture. Following three additional freeze–pump–thaw cycles, the reaction mixture was allowed to return to room temperature and to stir for 5 min to ensure homogenous mixing. The flask was then immersed into a preheated oil bath at 95 °C to start the polymerization. The polymerization was monitored by

analyzing aliquots collected at predetermined times by ^{1}H NMR spectroscopy. When the expected monomer conversion was reached, after *ca.* 127 h, the polymerization was quenched by quick immersion of the reaction flask into liquid N_2 and exposure to air. THF (10 mL) was added to the reaction flask, and the polymer was purified through filtration by an alumina plug and precipitation into 500 mL of a methanol/ice mixture (3×). The precipitants were collected and dried under vacuum overnight to afford P*t*BA$_{90}$-*b*-PS$_{120}$ as an off-white solid, giving 53% yield of the 47% conversion polymerization. $M_{n(NMR)}$ = 22,400 Da, $M_{n(GPC)}$ = 32,700 Da, PDI = 1.12. IR: 3070, 3024, 2970, 2924, 28541314, 2067, 1982, 1859, 1728, 1597, 1489, 1450, 1381, 1365, 1249, 1149, 1033, 910, 756, 694 cm^{-1}. ^{1}H NMR (300 MHz, $CDCl_3$) δ 7.26 – 6.87 (m, br, 326H), 6.86 – 6.25 (m, br, 226H), 4.08 (q, *J* = 7 Hz, 2H), 2.37 – 2.11 (br, 90H), 2.10 – 1.72 (br, 142H), 1.67 – 1.16 (m, br, 1104H), 1.16 – 1.19 (m, 17H) 1.16 – 1.09(m, 16H) ppm. ^{13}C NMR (75 MHz, THF) characterization ongoing. DSC: T_g = 60 °C. TGA: T_{onset} = 237 °C, $T_{decomposition}$ = (237 – 246 °C) 11% mass loss; (382 – 438°C) 78% mass loss; 11% mass remaining.

Synthesis of poly(acrylic acid)$_{90}$-*b*-polystyrene$_{120}$ (PAA$_{90}$-*b*-PS$_{120}$). P*t*BA$_{90}$-*b*-PS$_{120}$ (1 equiv, 250.0 mg) was dissolved in dichloromethane (2 mL). Trifluoroacetic acid (TFA) (100 equiv, 6.75 mL) was added. The reaction mixture was left stirring vigorously overnight. After evaporation of the solvent and TFA, THF was added to redissolve the polymer, which was then dialyzed for three days against nanopure water using (MWCO 12–14 kDa). The precipitate was lyophilized to yield a white solid. IR: 3690 – 2408, 3070, 3060, 3027, 2961, 2919, 2852, 1982, 1940, 1878, 1789, 1726, 1599,

1493, 1452, 1390, 1364, 1256, 1151, 1080, 1019, 903, 842, 798, 755, 697 cm^{-1}. NMR characterization ongoing. TGA: T_{onset} = 237 °C, $T_{decomposition}$ = (352 – 438 °C) 43% mass loss; 57% mass remaining.

Co-assembly and crosslinking of PAA_{90}-*b*-PS_{120} and Fe_3O_4 NPs for toroid formation. An organic solution was prepared by mixing 3.3 mg of PAA_{90}-*b*-PS_{120} and 0.33 mL of a 10 mg/mL solution of iron oxide nanoparticles in THF. The total volume of the polymer/iron oxide nanoparticle mixture was adjusted to 10 mL by addition of THF. To this organic solution was added 12.9 mg of EDDA. The solution was allowed to stir vigorously for 30 min to ensure homogeneity prior to dropwide addition of 45 mL of nanopure water at a rate of 22.5 mL/h. The mixture was kept stirring for an additional 24 h prior to crosslinking. TEM characterization of the produced nanoparticles showed cylindrical structures of *ca*. 30 nm in diameter and varying lengths. AFM characterization is ongoing. The resulting micelles were crosslinked to nominally 25% based on acrylic acid units (1 mol equiv., 1.52 10^{-5} mol) with the aid of EDCI (0.25 mol equiv., 3.80 10^{-6} mol, 1.13 mg). TEM, and AFM characterization of the produced nanoparticles showed cylindrical structures of 32 ± 4 nm in diameter and varying lengths. Dialysis against nanopure water (MWCO 12-14 kDa) was employed in order to remove the organic solvents and byproducts present in the nanoparticle solution. Following dialysis, TEM analysis showed a morphological change into toroidal/vesicular nanoparticles with widths of 32 ± 3 nanometers and diameters of 138 ± 36 nm. AFM characterization is ongoing to determine the true morphological structure.

Co-assembly of PAA_{90}-*b*-PS_{120} and Fe_3O_4 NPs for miniature MSCK formation. An organic solution was prepared by mixing 3.3 mg of PAA_{90}-*b*-PS_{120} and 0.33 mL of a 10 mg/mL solution of iron oxide nanoparticles in THF. The total volume of the polymer/iron oxide nanoparticle mixture was adjusted to 10 mL by addition of THF. The solution was allowed to stir vigorously for 30 min to ensure homogeneity prior to dropwise addition of 45 mL of nanopure water at a rate of 22.5 mL/h. The mixture was kept stirring for an additional 24 h prior to crosslinking. DLS analysis showed nanoparticles with hydrodynamic radii of 58 ± 15 nm. TEM characterization showed nanoparticles with diameters of 52 ± 7 nm. The resulting micelles were crosslinked to nominally 25% based on acrylic acid units (1 mol equiv., 1.52 10^{-5} mol) with the aid of EDDA (0.125 mol equiv., 1.91 10^{-6} mol, 0.282 mg) and EDCI (0.25 mol equiv., 3.80 10^{-6} mol, 1.13 mg). DLS analysis showed nanoparticles with hydrodynamic radii of 36 ± 10 nm. TEM characterization showed nanoparticles with diameters of 41 ± 8 nm.

Representative procedure for oil sequestration. Weathered crude oil originating from the Texas-Oklahoma pipeline (light sweet crude) was added to a vial containing DI water, and the weight of the oil was recorded. To each testing vial were added nanoparticles (either toroidal or spherical depending on the trial) in the form of powder (1.4 mg). After approximately 30 min with little to no agitation, the loaded nanoparticles were attracted by an external magnetic field to allow for decantation of the oil-containing water for oil extraction. The vial was then washed three times with water

to maximize the removal of oil from the vial. The oil was extracted through chloroform washings. The combined organic fractions containing crude oil were spiked with a solution of polystyrene of 70,950 Da molecular weight to serve as an internal standard for comparative studies with the control group. Oil was similarly extracted from the contaminated water in the control groups using chloroform, and the combined fractions were likewise spiked. The spiked samples were examined using a chloroform GPC. Oil recovery was determined by chromatogram comparison with data from the control group. Experiments were conducted in triplicate.

Quantification through GPC analysis. To account for the behavior and RI response of the crude material through the columns, the spiked samples from the control groups were analyzed through chloroform GPC. With the use of the known mass of oil present in the control samples, a relationship between the areas under the chromatogram peaks and oil mass was established; this was mathematically accomplished through the use of coefficient *k*.

$$k \cdot \frac{\int_{soil}}{\int_{spike}} = \frac{M_{oil}}{M_{spike}}$$

The use of this coefficient was validated by the low percent variation of this number within a sample set (1 - 17%). This k value was subsequently used in the tested samples to determine the unknown oil mass in the samples (M_{oil}).